

**Water saturation phase of
the buffer and backfill in the
KBS-3V concept**

**Special emphasis given to the influence of
the backfill on the wetting of the buffer**

Lennart Börgesson, Billy Fälth
Clay Technology AB

Jan Hernelind, 5T Engineering AB

August 2006

Svensk Kärnbränslehantering AB

Swedish Nuclear Fuel
and Waste Management Co
Box 5864

SE-102 40 Stockholm Sweden

Tel 08-459 84 00

+46 8 459 84 00

Fax 08-661 57 19

+46 8 661 57 19



Water saturation phase of the buffer and backfill in the KBS-3V concept

**Special emphasis given to the influence of
the backfill on the wetting of the buffer**

Lennart Börgesson, Billy Fälth
Clay Technology AB

Jan Hernelind, 5T Engineering AB

August 2006

Keywords: Bentonite, Buffer, Backfill, Unsaturated, Hydraulic, Rock.

This report concerns a study which was conducted for SKB. The conclusions and viewpoints presented in the report are those of the authors and do not necessarily coincide with those of the client.

A pdf version of this document can be downloaded from www.skb.se

Abstract

The wetting and rate of saturation of the buffer and backfill materials in a KBS-3V repository from the rock fractures and the rock matrix have been investigated by a large number of different finite element models and calculations. For most models the FE-code ABAQUS has been used but for investigation of the influence of trapped air in the backfill FE-code Code Bright was used.

Both codes include completely coupled THM models, which have been used, but for some calculations it has been sufficient to limit the models to only use the hydraulic or thermo-hydraulic parts of the models.

The following analyses have been made:

1. The influence of the backfill properties and wetting conditions on the water saturation phase of the buffer has been investigated with the old FEM-model used in earlier wetting calculations for SR-97. The old calculations have been updated regarding the influence of the backfill. The model is 2-dimensional with axial symmetry around the axis of the deposition hole.

These calculations show that there is strong influence of wetting from the backfill if the rock is rather dry ($K_{rock} \leq 10^{-13}$ m/s), while the influence is low if the rock is rather wet ($K_{rock} \geq 10^{-12}$ m/s). At $K_{rock} = 10^{-13}$ m/s the time to saturation decreases with a factor 2 in the absence of fractures and with a factor 1.5 with two fractures intersecting the hole when water is supplied from the backfill (30/70) compared to when no water is available.

A completely dry rock yields very long time to saturation and of course decisive influence of the water supply from the backfill. If water is freely available at a water pressure of 5 MPa in the backfill it takes 250–500 years to reach full saturation of the buffer. If the water available in the backfill is limited to the initial amount (completely dry rock also around the tunnel and thus no addition of water from the rock in the tunnel) it will take several thousands years to reach some kind of equilibrium with a degree of saturation in the buffer of $> 98\%$. When very dry Friedland Clay is installed as backfill the backfill will dry the buffer.

2. The influence of the rock conditions on the wetting phase of the backfill in the deposition tunnels has been investigated for three different backfill types. The model is 2D axial symmetric around the tunnel axis.

A large number of calculations have been performed. The fracture frequency, the fracture transmissivity and the backfill type have been primary variations and the rock matrix hydraulic conductivity, the distance to the water supplying boundary and the existence of a highly permeable zone at the rock surface have been secondary variations.

The time to complete saturation varies according to these calculations from 0.5 years for 30/70 backfill and 1 m between fractures to more than 150 years for Friedland Clay and 24 m between the fractures (300 years for the sandwich backfill).

The influence of backfill type on the wetting rate is strong due to the difference in hydraulic conductivity of the different backfill types, which seems to control the wetting rate. The difference in time to full saturation of Friedland Clay is about 10 times longer than for 30/70 backfill.

The influence of fracture frequency is strong since very little water is transported in the rock matrix at the hydraulic conductivity 10^{-13} m/s. The time to full saturation is almost proportional to the fracture distance.

The influence of transmissivity is insignificant except for the combination of the lowest transmissivity ($T = 10^{-11}$ m²/s) and 30/70 backfill, since the transmissivity is high enough

compared to the hydraulic conductivity of the backfill to yield a high water pressure in the fracture/backfill interface and the water inflow thus hindered by the backfill and not the fracture.

The influence of high matrix permeability (10^{-12} m/s instead of 10^{-13} m/s) is not very strong for the 30/70 and Friedland Clay (a factor 1–2 faster) since the average hydraulic conductivity including the fractures is not affected very much and the hydraulic conductivity of the backfills are still much higher than the hydraulic conductivity of the rock matrix.

In situ compacted Friedland clay with low density is assumed. If pre-compacted blocks are used the density will be higher, the hydraulic conductivity lower and the time to full saturation considerably longer.

3. The influence on the wetting phase of having entrapped air in the backfill in the deposition tunnels has been investigated with Code Bright calculations in 2D with a material model that includes the gas phase.

If there are no escape routes for the air hosted in the initially unsaturated backfill other than through the rock, the trapped air will have an impact on the saturation process. The trapped air forms a “bubble”, which holds back the inflowing water and delays the saturation. This effect is more important the more permeable the rock is. When the water supply from the rock is high, the gas diffusion rate will rule the water saturation process.

4. Finally complete hydraulic interaction between rock, buffer and backfill has been modelled with a 3D model that simulates an infinite repository intersected by rock fractures. Four rock fracture configurations have been modelled and the results show how the buffer, backfill, rock matrix and rock fractures interact during the wetting process. The results largely confirm the results from the earlier 2D calculations.

Sammanfattning

Den hastighet med vilken bufferten och återfyllnadsmaterialen beväts från bergmatrisen och vattenförande bergsprickor i ett KBS-3V-förvar har undersökts med ett stort antal olika finita elementmodeller och beräkningar. För de flesta modellerna har FE-koden ABAQUS använts, men vid undersökningen av påverkan av instängd luft i återfyllnaden användes FE-koden Code Bright.

Båda koderna har kompletta och kopplade THM-modeller, som har använts, men för vissa beräkningar har det varit tillräckligt att begränsa modellerna till att enbart använda de hydrauliska eller termo-hydrauliska delarna av modellerna.

Följande analyser har gjorts:

1. Inverkan av återfyllningsegenskaperna och bevättningsförhållandena på vattenmättnadsfasen hos bufferten har undersökts med hjälp av den gamla FEM-model som använts i tidigare bevättningsberäkningar för SR-97. De äldre beräkningarna har uppdaterats vad gäller påverkan av återfyllnaden. Modellen är tvådimensionell med axiell symmetri runt förvarshålets axel.

Dessa beräkningar visar att bevätning från återfyllnaden har stor påverkan om berget är tämligen torrt ($K_{rock} \leq 10^{-13}$ m/s), medan påverkan är liten om berget är ganska blött ($K_{rock} \geq 10^{-12}$ m/s). Vid $K_{rock} = 10^{-13}$ m/s minskar tiden till mättnad med en faktor 2 när det inte finns några sprickor, och med en faktor 1,5 om två sprickor skär genom hålet när vatten kommer från återfyllnaden (30/70), jämfört med när vatten inte är tillgängligt.

Ett helt torrt berg ger en mycket lång tid till mättnad, och självfallet har vattentillförseln från återfyllnaden stor betydelse. Om vatten är fritt tillgängligt vid ett vattentryck på 5 MPa i återfyllnaden tar det 250–500 år att uppnå full mättnad i bufferten. Om vatteninnehållet i återfyllnaden är begränsat till den ursprungliga mängden (dvs helt torrt berg även runt tunneln och således ingen påfyllnad av vatten från berget), kommer det att ta åtskilliga tusen år för att uppnå något slags jämvikt med en mättnadsgrad i bufferten på > 98 %. Om mycket torr Friedland lera installerats som återfyllnad kommer återfyllnaden att torka ut bufferten.

2. Hur bergsförhållandena påverkar bevättningsfasen hos återfyllnaden i förvarstunnlarna har undersökts för tre olika återfyllnadstyper. Modellen är 2D axiellt symmetrisk runt tunnelaxeln.

Ett stort antal beräkningar har gjorts varvid sprickfrekvens, spricktransmissivitet och återfyllnadstyp har varierats i första hand och bergsmatrisens hydrauliska konduktivitet, avståndet till vattenförsörjningsgränsen samt närvaron av en mycket genomsläpplig zon vid bergytan har varierats i andra hand.

Enligt dessa beräkningar varierar tiden till total mättnad från 0,5 år för 30/70 återfyllnaden med 1 m mellan sprickorna till mer än 150 år för Friedland lera and 25 m mellan sprickorna (300 år för sandwich-conceptet).

Återfyllnadsmaterialets påverkan på bevätningstakten är ganska stor beroende på skillnaden i hydraulisk konduktivitet hos de olika återfyllnadstyperna, vilket tycks kontrollera bevättningshastigheten. Skillnaden i tid för att uppnå full vattenmättnad hos Friedland lera är ca 10 gånger längre än för 30/70-återfyllningen.

Påverkan av sprickfrekvens är stor eftersom väldigt lite vatten transporteras i bergmatrisen vid en hydraulisk konduktivitet på 10^{-13} m/s. Tiden för att uppnå full vattenmättnad är nästan proportionell mot sprickavståndet.

Påverkan av transmissiviteten är obetydlig, förutom vid en kombination av lägsta transmissivitet ($T=10^{-11}$ m²/s) och 30/70 återfyllnad, eftersom transmissiviteten är tillräckligt hög

jämfört med den hydrauliska konduktiviteten i återfyllnaden för att ge ett högt vattentryck i sprick/återfyllnadsgränsytan och eftersom inflödet av vatten således hindras av återfyllnaden och inte av sprickan.

Påverkan av hög matrispermeabilitet (10^{-12} m/s istället för 10^{-13} m/s) är inte särskilt stor för 30/70 och Friedland lera (en faktor 1–2 gånger snabbare) eftersom den genomsnittliga hydrauliska konduktiviteten inklusive sprickorna inte påverkas särskilt mycket, och den hydrauliska konduktiviteten i återfyllnaden är fortfarande mycket högre än i bergmatrisen.

In situ packad Friedland lera med låg densitet har antagits. Om förkompakterade block används istället kommer densiteten att vara högre, hydrauliska konduktiviteten lägre och tiden till full mättnad avsevärt längre.

3. Påverkan av att ha instängd luft i återfyllnaden i tunnlarna under bevättningsfasen har undersökts med Code Bright beräkningar i 2D med en materialmodell som inkluderar gasfasen.

Om inga utloppsvägar finns för luften i den ursprungliga omättade återfyllnaden annat än genom det omgivande berget så kommer den instängda luften att påverka mättnadsprocessen. Den instängda luften bildar då en ”bubbla”, som hindrar inflödande vatten och försenare vattenmättnaden. Denna effekt blir viktigare ju högre permeabilitet berget har. När vattentillflödet från berget är stort kommer gasdiffusionshastigheten att styra vattenmättnadsprocessen.

4. Slutligen har det totala hydrauliska samspelet mellan berg, buffert och återfyllnad modellerats i en 3D-modell som simulerar ett oändligt förvar som genomskärs av bergsprickor. Fyra bergsprickskonfigurationer har modellerats och resultaten visar buffert, återfyllning, berg matris och bergsprickor samverkar under bevättningsprocessen. Resultaten bekräftar i huvudsak resultaten från de tidigare 2D-beräkningarna.

Contents

1	Introduction	9
2	Calculations	11
3	Codes and material models	13
3.1	General	13
3.2	ABAQUS	13
3.2.1	General	13
3.2.2	Hydro-mechanical analyses in ABAQUS	13
3.2.3	Uncoupled heat transfer analysis	15
3.2.4	Coupling of thermal and hydro-mechanical solutions	16
3.3	Material properties of the buffer material in the ABAQUS calculations	17
3.3.1	Reference material	17
3.3.2	Thermal properties	17
3.3.3	Hydraulic properties	18
3.3.4	Mechanical properties	20
3.4	Code Bright	21
3.4.1	General	21
3.4.2	Equations for moisture and gas transport	22
4	Influence of backfill conditions on the wetting of the buffer	25
4.1	General	25
4.2	Element mesh and material properties	25
4.3	Results	27
4.4	Conclusions	31
5	Influence of rock and backfill properties on the water saturation phase of the backfill	37
5.1	General	37
5.2	Geometry	37
5.3	Material properties, initial conditions and boundary conditions	39
5.3.1	General	39
5.3.2	Rock properties and boundary conditions	39
5.3.3	Backfill properties	40
5.4	Results	44
5.4.1	General	44
5.4.2	Primary variations	47
5.4.3	Secondary variations	54
5.5	Conclusions	58
6	Code_Bright analysis of trapped air in backfill	61
6.1	General	61
6.2	Initial- and boundary conditions	61
6.3	Governing equations and parameter values	61
6.4	Models	63
6.5	Results	64
6.6	Conclusions	71
7	3D-model of the tunnel and a deposition hole	73
7.1	General	73
7.2	Geometry	73
7.3	Material properties and initial conditions	74
7.3.1	General	74

7.3.2	Buffer material	74
7.3.3	Backfill material	75
7.3.4	Rock	75
7.3.5	Canister	76
7.4	Boundary conditions	77
7.5	Calculations	77
7.5.1	General	77
7.5.2	Calculation sequence	78
7.6	Results	78
7.6.1	General	78
7.6.2	Summary of results	79
7.6.3	Temperature	80
7.6.4	Case 4, main case with two fractures	80
7.6.5	Cases 1–3	82
7.6.6	Mechanical results	85
7.7	Conclusions	94
8	Comments and conclusions	95
	References	97

1 Introduction

At installation of the buffer and backfill materials they are only partly water saturated and after installation there is a considerable space of unfilled pores and voids in the deposition hole and tunnel. After installation 30–50% of the pore volume available is unfilled and will be filled with water before the pore water pressure in the repository can return to hydrostatic and the buffer and backfill have been homogenized. This means filling of about 3 m³ unfilled pore space in the buffer in each deposition hole and about 3.8 m³ unfilled pore space in the backfill per meter tunnel (for 30/70 bentonite/sand mixture).

The water saturating the buffer mainly comes from rock fractures but a substantial part of the water may also come from the rock matrix and the backfill if the fracture frequency or transmissivity is rather low. The influence of the rock properties on the wetting rate of the buffer in a KBS-3V deposition hole has been studied by FE-modelling and reported earlier for SR-97 /1-1/. However, in that study the hydraulic interaction with the backfill was in principle excluded in the sense that the backfill was modelled to be water saturated from start. In order to widen the study and include the wetting of the backfill as well as the full hydraulic interaction between buffer and backfill the presented study has been performed.

2 Calculations

The water saturation phase of the backfill and the water saturation phase of the buffer interact in a coupled way. This is a 3D problem that has completely coupled THM-processes. The problem also includes influence of a large number of parameters regarding mainly the hydraulic conditions in the rock and includes also two-phase flow conditions. In order to structure and simplify the calculations the problem has been treated in four different models using two different codes. The following sub-investigations have been made:

1. Investigation of the influence of the backfill properties and wetting conditions on the water saturation phase of the buffer with the old FEM-model used in earlier wetting calculations for SR-97. The old calculations have been updated regarding the influence of the backfill. 2D rotational symmetry was used in these calculations.
2. Influence of the rock conditions on the wetting phase of the backfill in the deposition tunnels for three different backfill types. 2D rotational symmetry was used in these calculations.
3. Influence of having entrapped air on the wetting phase of the backfill in the deposition tunnels. These calculations have been done with Code Bright with a material model that includes the air phase (2D rotational symmetry).
4. Examples of complete interaction between buffer and backfill with a 3D model. Four different fracture configurations were modelled and the results compared to the results of the 2D-calculations.

3 Codes and material models

3.1 General

Two different codes have been used. Most calculations have been done with the code ABAQUS. Since ABAQUS cannot handle the gas-phase and there is a risk of having entrapped air in the backfill, some calculations have also been made with Code Bright. This chapter includes brief descriptions of those two codes.

3.2 ABAQUS

3.2.1 General

The finite element code ABAQUS contains a capability of modelling a large range of processes in many different materials as well as complicated three-dimensional geometry.

The code includes special material models for rock and soil and ability to model geological formations with infinite boundaries and in situ stresses by e.g. the own weight of the medium. It also includes capability to make substructures with completely different finite element meshes and mesh density without connecting all nodes. Detailed information of the available models, application of the code and the theoretical background is given in the ABAQUS Manuals /3-1/.

3.2.2 Hydro-mechanical analyses in ABAQUS

The hydro-mechanical model consists of porous medium and wetting fluid and is based on equilibrium, constitutive equations, energy balance and mass conservation using the effective stress theory.

Equilibrium

Equilibrium is expressed by writing the principle of virtual work for the volume under consideration in its current configuration at time t :

$$\int_V \boldsymbol{\sigma} : \delta \boldsymbol{\varepsilon} dV = \int_S \mathbf{t} \cdot \delta \mathbf{v} dS + \int_V \hat{\mathbf{f}} \cdot \delta \mathbf{v} dV, \quad (3-1)$$

where $\delta \mathbf{v}$ is a virtual velocity field, $\delta \boldsymbol{\varepsilon} = \text{sym}(\partial \delta \mathbf{v} / \partial \mathbf{x})$ is the virtual rate of deformation, $\boldsymbol{\sigma}$ is the true (Cauchy) stress, \mathbf{t} are the surface tractions per unit area, and $\hat{\mathbf{f}}$ are body forces per unit volume. For our system, $\hat{\mathbf{f}}$ will often include the weight of the wetting liquid,

$$\mathbf{f}_w = S_r n \rho_w \mathbf{g}, \quad (3-2)$$

where S_r is the degree of saturation, n the porosity, ρ_w the density of the wetting liquid and \mathbf{g} is the gravitational acceleration, which we assume to be constant and in a constant direction (so that, for example, the formulation cannot be applied directly to a centrifuge experiment unless the model in the machine is small enough that \mathbf{g} can be treated as constant). For simplicity we consider this loading explicitly so that any other gravitational term in $\hat{\mathbf{f}}$ is only associated with the weight of the dry porous medium. Thus, we write the virtual work equation as

$$\int_V \boldsymbol{\sigma} : \delta \boldsymbol{\varepsilon} dV = \int_S \mathbf{t} \cdot \delta \mathbf{v} dS + \int_V \mathbf{f} \cdot \delta \mathbf{v} dV + \int_V S_r n \rho_w \mathbf{g} \cdot \delta \mathbf{v} dV, \quad (3-3)$$

where \mathbf{f} are all body forces except the weight of the wetting liquid.

The simplified equation used in ABAQUS for the effective stress is:

$$\bar{\boldsymbol{\sigma}}^* = \boldsymbol{\sigma} + \chi u_w \mathbf{I}. \quad (3-4)$$

where $\boldsymbol{\sigma}$ is the total stress, u_w is the pore water pressure, χ is a function of the degree of saturation (usual assumption $\chi = S_r$), and \mathbf{I} the unitary matrix.

Energy balance

The conservation of energy implied by the first law of thermodynamics states that the time rate of change of kinetic energy and internal energy for a fixed body of material is equal to the sum of the rate of work done by the surface and body forces. This can be expressed as (not considering the thermal part, which is solved as uncoupled heat transfer; cf Equation 3-15):

$$\frac{d}{dt} \int_V \left(\frac{1}{2} \rho \mathbf{v} \cdot \mathbf{v} + \rho U \right) dV = \int_S \mathbf{v} \cdot \mathbf{t} dS + \int_V \mathbf{f} \cdot \mathbf{v} dV \quad (3-5)$$

where

ρ is the current density,

\mathbf{v} is the velocity field vector,

U is the internal energy per unit mass,

\mathbf{t} is the surface traction vector,

\mathbf{f} is the body force vector, and

Constitutive equations

The constitutive equation for the solid is expressed as:

$$d\boldsymbol{\tau}^c = \mathbf{H} : d\boldsymbol{\varepsilon} + \mathbf{g} \quad (3-6)$$

where $d\boldsymbol{\tau}^c$ is the stress increment, \mathbf{H} the material stiffness, $d\boldsymbol{\varepsilon}$ the strain increment and \mathbf{g} is any strain independent contribution (e.g. thermal expansion). \mathbf{H} and \mathbf{g} are defined in terms of the current state, direction for straining, etc, and of the kinematic assumptions used to form the generalised strains.

The constitutive equation for the liquid (static) in the porous medium is expressed as:

$$\frac{\rho_w}{\rho_w^0} \approx 1 + \frac{u_w}{K_w} - \varepsilon_w^{\text{th}}, \quad (3-7)$$

where ρ_w is the density of the liquid, ρ_w^0 is its density in the reference configuration, $K_w(T)$ is the liquid's bulk modulus, and

$$\varepsilon_w^{\text{th}} = 3\alpha_w (T - T_w^0) - 3\alpha_w|_{T^I} (T^I - T_w^0) \quad (3-8)$$

is the volumetric expansion of the liquid caused by temperature change. Here $\alpha_w(T)$ is the liquid's thermal expansion coefficient, T is the current temperature, T^I is the initial temperature at this point in the medium, and T_w^0 is the reference temperature for the thermal expansion. Both u_w/K_w and $\varepsilon_w^{\text{th}}$ are assumed to be small.

Mass conservation

The mass continuity equation for the fluid combined with the divergence theorem implies the pointwise equation:

$$\frac{1}{J} \frac{d}{dt} (J \rho_w S_r n) + \frac{\partial}{\partial \mathbf{x}} \cdot (\rho_w S_r n \mathbf{v}_w) = 0. \quad (3-9)$$

where J is the determinant of the Jacobian matrix of the skeleton motion and \mathbf{x} is position. The constitutive behaviour for pore fluid is governed by Darcy's law, which is generally applicable to low fluid velocities. Darcy's law states that, under uniform conditions, the volumetric flow rate of the wetting liquid through a unit area of the medium, $S_r n \mathbf{v}_w$, is proportional to the negative of the gradient of the piezometric head:

$$S_r n \mathbf{v}_w = -\hat{\mathbf{k}} \frac{\partial \phi}{\partial \mathbf{x}}, \quad (3-10)$$

where $\hat{\mathbf{k}}$ is the permeability of the medium and ϕ is the piezometric head, defined as:

$$\phi \stackrel{def}{=} z + \frac{\mathbf{u}_w}{g \rho_w} \quad (3-11)$$

where z is the elevation above some datum and g is the magnitude of the gravitational acceleration, which acts in the direction opposite to z . $\hat{\mathbf{k}}$ can be anisotropic and is a function of the saturation and void ratio of the material. $\hat{\mathbf{k}}$ has units of velocity (length/time). [Some authors refer to $\hat{\mathbf{k}}$ as the hydraulic conductivity and define the permeability as

$$\hat{\mathbf{K}} = \frac{\nu}{g} \hat{\mathbf{k}} \quad (3-12)$$

where ν is the kinematic viscosity of the fluid.]

We assume that g is constant in magnitude and direction, so

$$\frac{\partial \phi}{\partial \mathbf{x}} = \frac{1}{g \rho_w} \left(\frac{\partial \mathbf{u}_w}{\partial \mathbf{x}} - \rho_w \mathbf{g} \right) \quad (3-13)$$

Vapour flow

Vapour flow is modelled as a diffusion process driven by a temperature gradient (coded as UEL user supplied routine with stiffness and flow).

$$\mathbf{q}_v = -D_{T_v} \frac{\partial T}{\partial \mathbf{x}} \quad (3-14)$$

where \mathbf{q}_v is the vapour flux and D_{T_v} the thermal vapour diffusivity.

3.2.3 Uncoupled heat transfer analysis

Energy balance

The basic energy balance is (neglecting mechanical contribution; cf Equation 3-5)

$$\int_v \rho \dot{U} dV = \int_s q dS + \int_v r dV \quad (3-15)$$

where V is a volume of solid material, with surface area S ; ρ is the density of the material; \dot{U} is the material time rate of the internal energy; q is the heat flux per unit area of the body, flowing into the body; and r is the heat supplied externally into the body per unit volume.

It is assumed that the thermal and mechanical problems are uncoupled in the sense that $U = U(T)$ only, where T is the temperature of the material, and q and r do not depend on the strains or displacements of the body. For simplicity a Lagrangian description is assumed, so "volume" and "surface" mean the volume and surface in the reference configuration.

Constitutive definition

The relationship is usually written in terms of a specific heat, neglecting coupling between mechanical and thermal problems:

$$c(T) = \frac{dU}{dT} \quad (3-16)$$

Heat conduction is assumed to be governed by the Fourier law.

$$\mathbf{f}_q = -\mathbf{k} \frac{\partial T}{\partial \mathbf{x}} \quad (3-17)$$

where \mathbf{f}_q is the heat flux and \mathbf{k} is the heat conductivity matrix, $\mathbf{k} = \mathbf{k}(T)$. The conductivity can be fully anisotropic, orthotropic, or isotropic.

3.2.4 Coupling of thermal and hydro-mechanical solutions

In ABAQUS thermal coupling is solved through a “staggered solution technique” as sketched in Figure 3-1 and below.

1. First a thermal analysis is performed where heat conductivity and specific heat are defined as functions of saturation and water content. In the first analysis these parameters are assumed to be constant and in the subsequent analyses they are read from an external file.
2. The hydromechanical model calculates stresses, pore pressures, void ratios, degree of saturation etc as function of time. Saturation and void ratio histories are written onto an external file.
3. The material parameters update module reads the file with saturation and void ratio data and creates a new file containing histories for saturation and water content.
4. The saturation and water content histories are used by the thermal model in the following analysis.
5. Steps 1-3 are repeated if parameter values are found to be different compared to those of the previous solution.

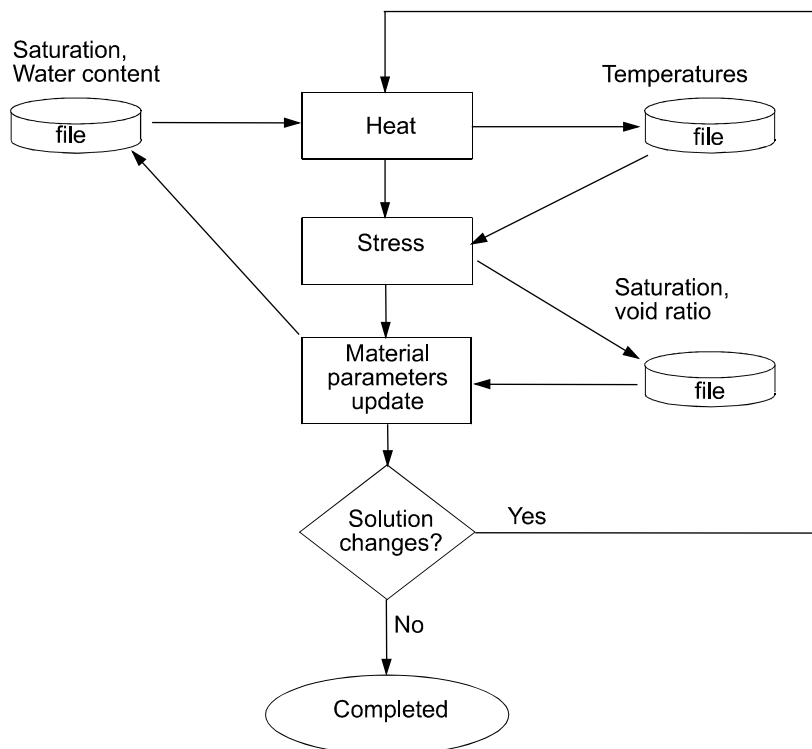


Figure 3-1. In ABAQUS, heat transfer calculations and hydro-mechanical calculations are decoupled. By using the iteration procedure schematically shown above, the effects of a fully coupled THM model are achieved.

3.3 Material properties of the buffer material in the ABAQUS calculations

3.3.1 Reference material

The reference material is Volclay sodium bentonite MX-80. Results from laboratory tests on this material are described by Börgesson et al. /3-2, 3-3/. The initial conditions vary a little between the laboratory tests, but the following values correspond regarding density to the planned average dry density of the buffer in the Prototype Repository deposition hole and regarding water content to the planned water ratio in the bentonite blocks after compaction.

- dry density: $\rho_d = 1.67 \text{ g/cm}^3$ and
- water ratio: $w = 0.17$

which yield

- void ratio: $e = 0.77$ and
- degree of saturation: $S_r = 0.61$.

The water ratio at water saturation is for this void ratio $w = 0.277$.

3.3.2 Thermal properties

The thermal conductivity has been measured as a function of the degree of saturation /3-3/. The parameter values for the ABAQUS model are shown in Table 3-1 (linear interpolation between the values).

The specific heat has been calculated as the weight average of the specific heat of water and particles according to Equation 3-18.

$$c = 800/(1+w)+4,200w/(1+w) \quad (3-18)$$

Equation 3-18 yields the input parameters shown in Table 3-2 (linear interpolation).

Table 3-1. Thermal conductivity λ of the buffer material as a function of the degree of saturation S_r .

S_r	λ W/m, K
0	0.3
0.2	0.3
0.3	0.4
0.4	0.55
0.5	0.75
0.6	0.95
0.7	1.1
0.8	1.2
0.9	1.25
1.0	1.3

Table 3-2. Heat capacity c of the buffer material as a function of the water ratio w .

w	c Ws/m, kg
0	800
0.1	1,109
0.2	1,367
0.3	1,585
1.0	2,500

3.3.3 Hydraulic properties

The hydraulic conductivity has been measured at different temperatures and void ratios /3-2/. Table 3-3 shows the values in the model.

The influence of the degree of saturation is governed by the parameter δ in Equation 3-19.

$$k_p = S_r^\delta k \quad (3-19)$$

where

K_p = hydraulic conductivity of partly saturated soil (m/s).

K = hydraulic conductivity of completely saturated soil (m/s).

δ = parameter (usually between 3 and 10).

For the reference material the standard value.

$$\delta = 3.$$

has been found to be satisfactory according to the calibration and validation calculations /1-1/.

Table 3-3. Hydraulic conductivity K as a function of void ratio e and temperature T .

T °C	e	K m/s
20	0.4	$0.035 \cdot 10^{-13}$
20	0.6	$0.2 \cdot 10^{-13}$
20	0.8	$0.65 \cdot 10^{-13}$
20	1.0	$1.75 \cdot 10^{-13}$
40	0.4	$0.05 \cdot 10^{-13}$
40	0.6	$0.31 \cdot 10^{-13}$
40	0.8	$1.0 \cdot 10^{-13}$
40	1.0	$2.75 \cdot 10^{-13}$
60	0.4	$0.07 \cdot 10^{-13}$
60	0.6	$0.44 \cdot 10^{-13}$
60	0.8	$1.45 \cdot 10^{-13}$
60	1.0	$3.85 \cdot 10^{-13}$
80	0.4	$0.1 \cdot 10^{-13}$
80	0.6	$0.55 \cdot 10^{-13}$
80	0.8	$1.8 \cdot 10^{-13}$
80	1.0	$4.9 \cdot 10^{-13}$

The thermal vapour flow diffusivity D_{Tv} and the parameters a and b according to Equations 3-20 to 3-22 have been determined with calibration calculations of moisture redistribution tests.

$$D_{Tv} = D_{Tvb} \quad 0.3 \leq S_r \leq 0.7 \quad (3-20)$$

$$D_{Tv} = D_{Tvb} \cdot \cos^a \left(\frac{S_r - 0.7}{0.3} \cdot \frac{\pi}{2} \right) \quad S_r \geq 0.7 \quad (3-21)$$

$$D_{Tv} = D_{Tvb} \cdot \sin^b \left(\frac{S_r}{0.3} \cdot \frac{\pi}{2} \right) \quad S_r \leq 0.3 \quad (3-22)$$

The following values were chosen /1-1/:

$$D_{Tvb} = 0.7 \cdot 10^{-11} \text{ m}^2/\text{s}, \text{ K}$$

$$a = 6$$

$$b = 6$$

The water retention curve has been determined from measurements of the total suction, the matric suction and the swelling pressure. The measurements have been converted to degree of saturation for the reference density. Figure 3-2 shows the relation used in the model /1-1/. The retention curve of the rock is also shown.

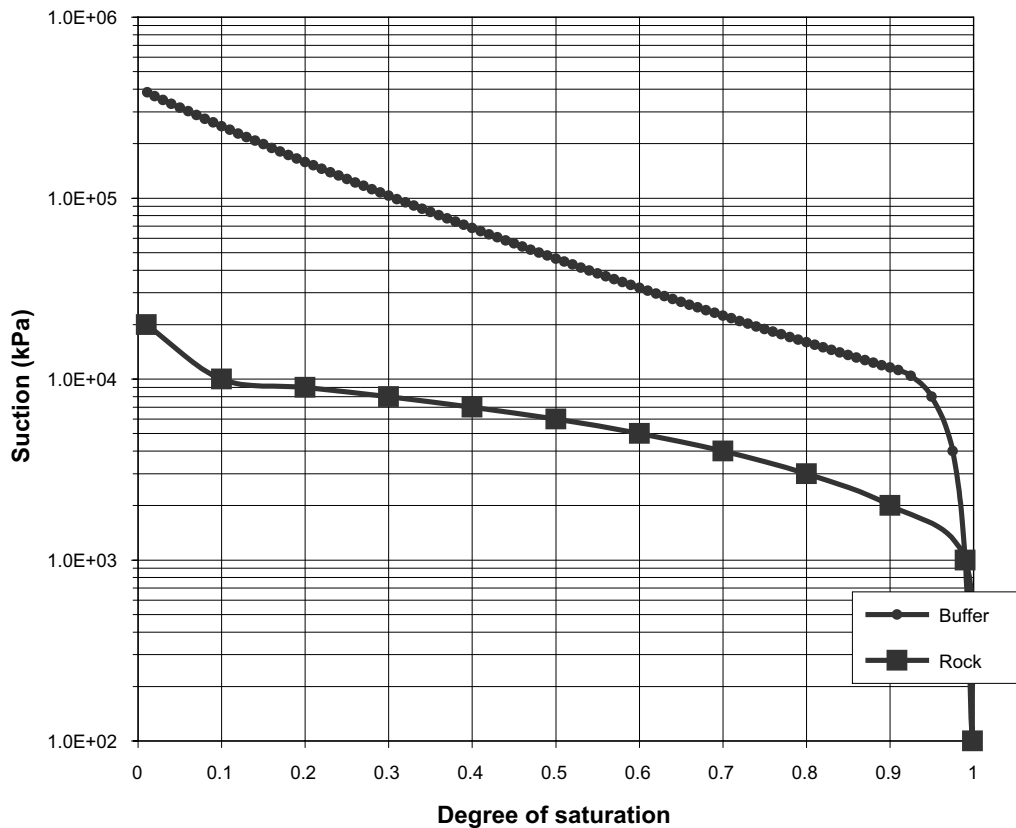


Figure 3-2. Relation between suction and degree of saturation used in the material models of the buffer material and the rock

3.3.4 Mechanical properties

The following data has been used for the Porous Elastic model:

$$\kappa = 0.20$$

$$\nu = 0.4$$

The value of κ has been derived from oedometer and swelling pressure tests /3-2/. The following data was used for the Drucker Prager Plasticity model

$$\beta = 17^\circ$$

$$d = 100 \text{ kPa}$$

$$\psi = 2^\circ$$

The friction angle in the q-p plane and the dilation angle were taken from triaxial test results /3-2/ with the curved failure line approximated to a straight line.

The following standard values have been used for the properties of the water and solid phases:

$$B_w = 2.1 \cdot 10^6 \text{ kPa (bulk modulus of water).}$$

$$B_s = 2.1 \cdot 10^8 \text{ kPa (bulk modulus of solids).}$$

$$\alpha_w = 3.0 \cdot 10^{-4} \text{ (coefficient of thermal volumetric expansion of water).}$$

$$\alpha_s = 0 \text{ (coefficient of thermal expansion of solids).}$$

$$\rho_w = 1,000 \text{ kg/m}^3 \text{ (density of water).}$$

$$\rho_s = 2,780 \text{ kg/m}^3 \text{ (density of solids).}$$

The parameters used for calculating the effective stress are χ in Equation 3-4 and the moisture swelling data:

$$\chi = S_r$$

The data for the moisture swelling procedure is taken from calibration tests and includes a long list of volumetric strain corrections $\Delta\epsilon_v$. Table 3-5 shows a selection of values from this table.

Table 3-4. Yield function.

q (kPa)	ϵ_{pl}
1	0
50	0.005
100	0.02
150	0.04
200	0.1

Table 3-5. Change in volumetric strain ϵ_v as a function of the degree of saturation S_r used in the "moisture swelling" procedure (selection of curtailed data).

S_r	$\Delta\epsilon_v$
0	-0.2
0.1	-0.01
0.2	0.02
0.3	0.03
0.4	0.02
0.5	0.01
0.6	0
0.7	-0.02
0.8	-0.03
0.88	-0.04
0.94	-0.06
0.97	-0.11
0.99	-0.24
1.0	-0.81

3.4 Code Bright

3.4.1 General

Code_Bright v2.2 /3-4/ is a 3-D finite element program designed to handle thermo-hydro-mechanical (THM) coupled problems in geological media. The code was developed at the Technical University of Catalonia (UPC) in the beginning of the 1990s /3-5/. The theoretical approach consists of a set of governing equations, a set of constitutive laws and a special computational approach. The code is written in FORTRAN and is composed of several subroutines. The program does not use external libraries. The code was originally developed on the basis of a new general theory of saline media, hence the name: *CO*upled *DE*formation, *BR*ine, *G*as and *H*eat *T*ransport problems.

Code_Bright solves in the most general case an Initial Boundary Value Problem consisting in a set of five governing equations (stress equilibrium, water mass balance, air mass balance, energy balance and balance of conservative solute). A Newton-Raphson iterative scheme is used to solve the non-linear system of equations.

The inclusion of a gas phase enables the explicit representation of water in both liquid and vapor form. In the same way, gas is represented both in a gas phase and as dissolved in the liquid phase.

The code includes completely coupled THM processes, but only the moisture and gas parts were used for the modelling described in Chapter 6 so the T and M processes are omitted in this description.

The parameter data for the material properties are given in Chapter 6.

3.4.2 Equations for moisture and gas transport

The van Genuchten retention model used in the Code_Bright model is given by Equation 2-23.

$$S_r = \left\{ 1 + \left[\frac{P_g - P_l}{P_0 \cdot \left(\frac{\sigma}{\sigma_0} \right)} \right]^{\frac{1}{1-m}} \right\}^{-m} \quad (3-23)$$

where P_l is the pore pressure and P_g is the gas pressure. P_0 is a reference pressure and λ a shape parameter. The quantity $P_g - P$ is usually referred to as suction and (σ/σ_0) is a built-in temperature dependent surface tension ratio. The default value of σ_0 is 0.072.

There are two main transport modes that were considered for gas and moisture, respectively.

Moisture:

- Moisture moves in water form driven by pore pressure gradients, obeying the Darcy law.

Gas:

- Gas moves driven by gas pressure gradients, obeying Darcy's law.
- Gas dissolved in the liquid phase moves driven by mass fraction gradients, obeying laws of molecular diffusion. If there is advective liquid transport, there will also be advective flux of gas.

The Darcy flux q_a is given by

$$q_a = -\frac{k k_{ra}}{\mu_a} (\nabla P_a - \rho_a \mathbf{g}) \quad (3-24)$$

where k , k_{ra} , μ_a , P_a and ρ_a are the intrinsic permeability, the relative permeability, viscosity, pressure and density, respectively, for the phase α . Non-advective fluxes are driven by mass fraction gradients according to

$$\mathbf{i}_\alpha^i = -(\phi S_\alpha \rho_\alpha D_m^i \mathbf{I}) \nabla \omega_\alpha^i, \quad (3-25)$$

where ϕ is the porosity, S_α is phase degree of saturation, ω_α^i is mass fraction and D_m^i is the diffusion coefficient of species i in phase α .

The liquid pressures P_l (and liquid pressure gradients ∇P_l) are calculated from Equation 3-23 (retention dependence). The liquid density is controlled by the relation

$$\rho_l = \rho_{l0} \exp \left[\beta (P_l - P_{l0}) + \gamma \omega_l^g \right] \quad (3-26)$$

The parameter values used are Code_Bright default values and are presented in Table 3-6.

The relative liquid permeability k_{rl} was assumed to depend on the water saturation S , according to

$$k_{rl} = S_r^{\delta_l} \quad (3-27)$$

The gas phase relative permeability is computed by

$$k_{rg} = 1 - k_{rl} \quad (3-28)$$

Gas, which is dissolved into the liquid phase moves driven by mass fraction gradients, obeying laws of molecular diffusion. The gas diffusivity is given by

$$D_m^{gas} = \tau \cdot D_g \exp\left(\frac{-24530}{R(273.15 + T)}\right) \quad (3-29)$$

where τ is the tortuosity factor, D_g a diffusion coefficient and R is the gas constant. The solubility of air in the liquid phase is controlled by Henry's law:

$$\omega_l^g = \frac{P'_g M_g}{H M_w} \quad (3-30)$$

where ω_l^g is the mass fraction of dissolved air in the liquid, P'_g is the partial pressure of the dry air, H is Henry's constant (10,000 MPa for air) and M_g (0.02895 kg/mol) and M_w (0.018 kg/mol) are the molecular masses of air and water respectively. The dry air partial pressure is computed by means of the law of ideal gases.

Table 3-6. Parameter values used in Equation 3-26.

Parameter	Value
P_{io} = reference pressure	0.1
ρ_{io} = the reference density	–
β = water compressibility	$4.5 \cdot 10^{-3} \text{ MPa}^{-1}$
γ = solute variation	0.6923
ω_l^g = air dissolved mass fraction	c.f. Equation 3–30

4 Influence of backfill conditions on the wetting of the buffer

4.1 General

In the calculations for SR-97 /1-1/ the influence of the backfill was not studied in detail. Almost all calculations were performed with the assumption that the backfill was water saturated from start and that the buffer could suck water without limitations from the backfill. In reality the supply of water depends both on the initial conditions of the backfill and on the supply of water to the backfill i.e. the wetting rate of the backfill.

In order to investigate the influence of a limited water supply from the backfill a number of supplementary calculations have been done. In these calculations the old model was used and all material parameters were the same as in the old model, with exception of the backfill. The following three types of variations were done:

1. Wetting from only the rock. In eight new calculations the backfill has been assumed to not supply any water at all to the buffer. By comparing the results with the old calculations where unlimited water was supplied, the influence of the backfill can be evaluated.
2. Wetting from only the backfill. In six new calculations the extreme case that no water at all is supplied by the rock has been considered. Three types of supply from the backfill has been modelled one of them being that only the water in the backfill at the initial water ratio is available. Two backfill types (30/70 bentonite/crushed rock and Friedland Clay) were considered.

In one additional calculation (*Stress_2ar*) the extreme situation in calculation *Stress_2a*, where all rock and backfill were assumed to have a hydraulic conductivity of $K = 10^{-14}$ m/s, was changed to free supply of water from only the backfill.

In order to simplify the work only hydraulic calculations were performed in this series. The thermal results were taken from the results derived in /1-1/ and mechanically the nodes were locked so that no displacements could occur.

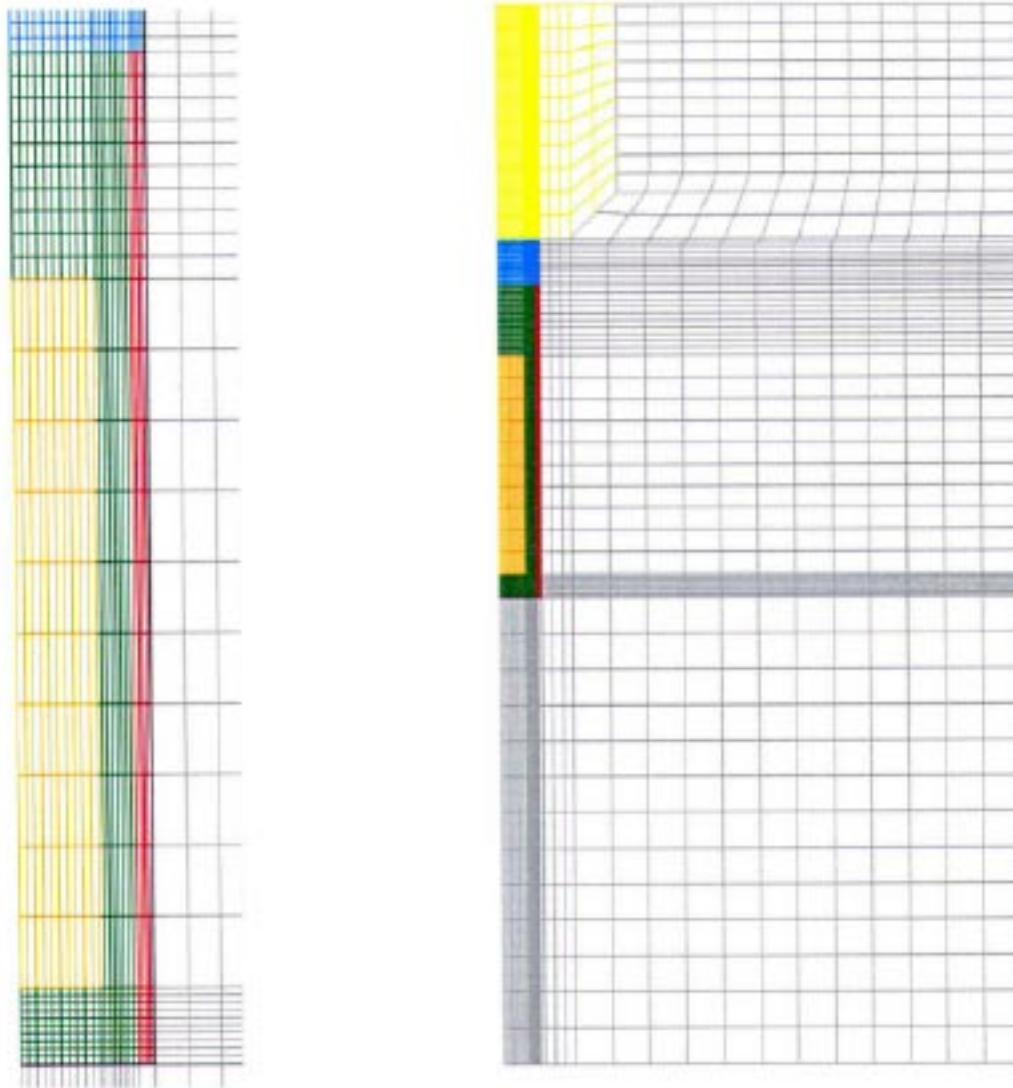
4.2 Element mesh and material properties

The old mesh is shown in Figure 4-1. The elements are 2D axial symmetric with the symmetry axis in the centre of the deposition hole. The backfill material, the buffer material, the canister, the rock matrix, and the damaged zone of the rock around the deposition hole are modelled. In some calculations two horizontal fractures are included in the model. One of them intersects the deposition hole in the middle of the canister. The other fracture intersects the deposition hole at the bottom. The damaged zone has the thickness 1 cm. The fractures are modelled as porous material with the thickness 1 cm. The properties of the fractures are described in /1-1/.

The mesh is 24 m high and has the radius 11 m. The number of elements is about 2,600.

Buffer material

The material properties and initial conditions of the buffer material are identical to the ones used in the earlier calculations. They are described in Chapter 3 with the difference that the buffer is divided into two parts with the following initial conditions:



Rock: grey
 Backfill: yellow and blue
 Buffer: green and red
 Canister: yellow
 Disturbed zone: black line

Figure 4-1. Element mesh of the old model. Entire mesh and an enlargement of the deposition hole (axial symmetry).

The average void ratio of the buffer is used for the entire buffer. However, the inhomogeneous water ratio distribution caused by filling the pellets slot with water is simulated by distributing the surplus water in the 5 cm wide slot over a 10 cm wide zone in the periphery. By starting with a 10 cm zone that is water saturated, the right total amount of water is used. Thus the buffer is divided into two materials (*buffer 1* and *buffer 2*) with the same void ratio but different initial degree of saturation:

Buffer 1

A 10 cm thick zone in the periphery of the deposition hole with the following initial conditions:

$$e = 0.77 \text{ (void ratio)}$$

$$S_r = 1.0 \text{ (degree of saturation)}$$

which yields

$$w = 0.277 \text{ (water ratio)}$$

$$\rho_d = 1.57 \text{ (dry density)}$$

$$\rho_m = 2.01 \text{ (density at saturation)}$$

Buffer 2

The rest of the buffer with the following initial conditions:

$$e = 0.77 \text{ (void ratio)}$$

$$S_r = 0.61 \text{ (degree of saturation)}$$

which yields

$$w = 0.169 \text{ (water ratio)}$$

$$\rho_d = 1.57 \text{ (dry density)}$$

$$\rho_m = 2.01 \text{ (density at saturation)}$$

Backfill materials

In the six calculations where water was only available from the initial water content in the backfill the backfill was modelled with material models of unsaturated clays. The same material models of 30/70 backfill and Friedland Clay were used for these calculations as for the calculations of the wetting of only the backfill described in Chapter 5.

The mesh, the properties, boundary conditions and calculation sequences are described in more detail by Börgesson et al. /1-1/.

4.3 Results

The results of the new calculations with the old mesh are summarised in Table 4-1. All new calculations were done with zero hydraulic conductivity of the backfill, i.e. no water came from the backfill. The first part (Table 4-1a) concerns calculations without activating the fractures, while the second part (Table 4-1b) concerns calculations with activated fractures. The table shows the new calculations with the letter r added to the name and marked in red and the difference in properties between the old and new comparative calculations marked bold.

Table 4-1a. Parameter variation and time until completed saturation of the buffer material. The new calculations are marked red.

(1) Calc. No	(2) K (rock) m/s	(3) K (EDZ) m/s	(4) K (T) (fract.) m/s (m ² /s)	(5) K (backf.) m/s	(6) Water pressure kPa	(7) Unsaturated rock	(8) Time to S _r > 99% at canister lid Years	(9) Time to S _r > 95% at canister lid Years	(10) Time to S _r > 99% at canister periphery Years	(11) Time to S _r > 95% at canister periphery Years
Stress_1	10 ⁻¹⁰	10 ⁻¹⁰	10 ⁻¹⁰	2·10 ⁻¹⁰	0	No	10.5	6.7	7.6	2.4
Stress_1r	10 ⁻¹⁰	10 ⁻¹⁰	10 ⁻¹⁰	0	0	No	10.5	6.7	2.9 ¹⁾	1.5 ¹⁾
Stress_1b	10 ⁻¹⁰	10 ⁻¹⁰	10 ⁻¹⁰	2·10 ⁻¹⁰	5,000	No	6.0	5.0	2.9	1.5
Stress_2a	10 ⁻¹⁴	10 ⁻¹⁴	10 ⁻¹⁴	10 ⁻¹⁴	0	No	>>32	>>32	>>32	>>32
Stress_2ar	10 ⁻¹⁴	10 ⁻¹⁴	10 ⁻¹⁴	u = 0	0	No	>64	>64	>64 ²⁾	>64 ²⁾
Stress_2b	10 ⁻¹⁴	10 ⁻¹⁴	10 ⁻¹⁴	10 ⁻¹⁴	5,000	No	>>32	>>32	>>32	>>32
Stress_2br	10 ⁻¹⁴	10 ⁻¹⁴	10 ⁻¹⁴	0	5,000	No	>>32	>>32	>>32	>>32
Stress_3a	10 ⁻¹³	10 ⁻¹³	10 ⁻¹³	2·10 ⁻¹⁰	0	No	24	13.6	20.3	11.1
Stress_3b1	10 ⁻¹³	10 ⁻¹³	10 ⁻¹³	2·10 ⁻¹⁰	5,000	No	12.4	10.6	11.4	7.5
Stress_3b2	10 ⁻¹³	10 ⁻¹¹	10 ⁻¹³	2·10 ⁻¹⁰	5,000	No	10.8	9.4	10.1	7.3
Stress_3a_o	10 ⁻¹³	10 ⁻¹³	10 ⁻¹³	2·10 ⁻¹⁰	0	Yes	~35	20.3	~35	20.6
Stress_3a_or	10 ⁻¹³	10 ⁻¹³	10 ⁻¹³	0	0	Yes	~54	~42	~48	~38
Stress_3b1_o	10 ⁻¹³	10 ⁻¹³	10 ⁻¹³	2·10 ⁻¹⁰	5,000	Yes	15.0	12.2	14.4	11.3
Stress_3b1_or	10 ⁻¹³	10 ⁻¹³	10 ⁻¹³	0	5,000	Yes	26	20	21	17
Stress_3b1_or2	10 ⁻¹²	10 ⁻¹²	10 ⁻¹²	0	5,000	Yes	7.6	6.3	2.9	2.5
Stress_3b2_o	10 ⁻¹³	10 ⁻¹¹	10 ⁻¹³	2·10 ⁻¹⁰	5,000	Yes	11.9	10.1	11.5	8.2
Stress_3b2_or	10 ⁻¹³	10 ⁻¹¹	10 ⁻¹³	0	5,000	Yes	23	18	20	15.2

¹⁾ Evaluated at different parts of the canister surface (centric instead of at the lid).

²⁾ After 64 years S_r = 85%.

Table 4-1b. Parameter variation and time until completed saturation of the buffer material (cont.). The new calculations are marked red.

(1) Calc. No	(2) K (rock) m/s	(3) K (EDZ) m/s	(4) K (T) (fract.) m/s (m ² /s)	(5) K (backf.) m/s	(6) Water pressure kPa	(7) Unsaturated rock	(8) Time to S _r > 99% Years	(9) Time to S _r > 95% at canister lid Years	(10) Time to S _r > 99% at canister periphery Years	(11) Time to S _r > 95% at canister periphery Years
Stress2_3b1	10 ⁻¹³	10 ⁻¹³	10 ⁻⁸ (10 ⁻¹⁰)	2·10 ⁻¹⁰	5,000	No	10.8	9.5	9.8	7.3
Stress2_3b2	10 ⁻¹³	10 ⁻¹¹	10 ⁻⁸ (10 ⁻¹⁰)	2·10 ⁻¹⁰	5,000	No	9.2	8.2	7.6	5.4
Stress2_3b1_o	10 ⁻¹³	10 ⁻¹³	10 ⁻⁸ (10 ⁻¹⁰)	2·10 ⁻¹⁰	5,000	Yes	12.0	10.8	11.2	9.1
Stress2_3b2_o	10 ⁻¹³	10 ⁻¹¹	10 ⁻⁸ (10 ⁻¹⁰)	2·10 ⁻¹⁰	5,000	Yes	9.4	8.6	8.2	5.9
Stress2_3b2_or	10 ⁻¹³	10 ⁻¹¹	10 ⁻⁸ (10 ⁻¹⁰)	0	5,000	Yes	16	12.4	9.5 ¹⁾	6.0 ¹⁾
Stress2_3b1_oa	10 ⁻¹³	10 ⁻¹³	10 ⁻⁷ (10 ⁻⁹)	2·10 ⁻¹⁰	5,000	Yes	12.0	10.8	11.2	9.1
Stress2_3b1_ob	10 ⁻¹³	10 ⁻¹³	10 ⁻⁹ (10 ⁻¹¹)	2·10 ⁻¹⁰	5,000	Yes	12.0	10.8	11.2	9.1

¹⁾ Evaluated at different parts of the canister surface (centric instead of at the lid).

Wetting from only the rock

The influence of not having water supplied from the backfill is illustrated in Figures 4-2 and 4-3. They refer to calculations *Stress_3b1_o*/*Stress_3b2_o* and *Stress_3b1_or*/*Stress_3b2_or*. The suffixes *b1_o* and *b2_o* stand for a model with $K_{rock} = 10^{-13}$ m/s, the water pressure 5 MPa at the rock boundaries and possibility to de-saturate the rock. The first one has no disturbed zone (*b1_o*) and the other one (*b2_o*) has a 1 cm thick disturbed zone in the deposition hole with $K_{rock} = 10^{-11}$ m/s. The suffix *r* relates to the new revised calculations, where no water is supplied by the backfill in contrary to the old calculations.

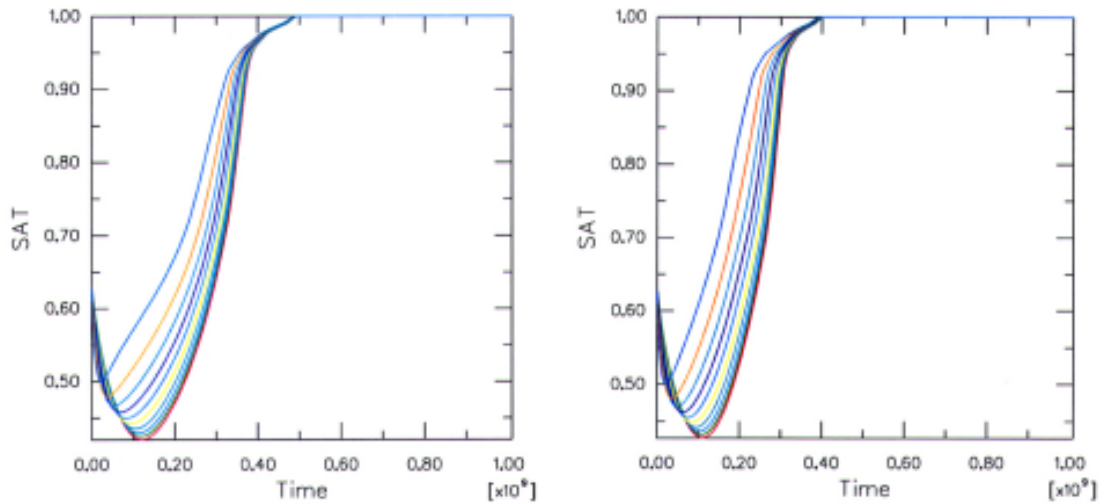


Figure 4-2. *Stress_3b1_o* (left) and *Stress_3b2_o*. Degree of saturation in the buffer at equidistant points along a radial line on top of the canister as a function of time (s) without damaged zone (left) and with damaged zone. Old calculations with water supply from the backfill.

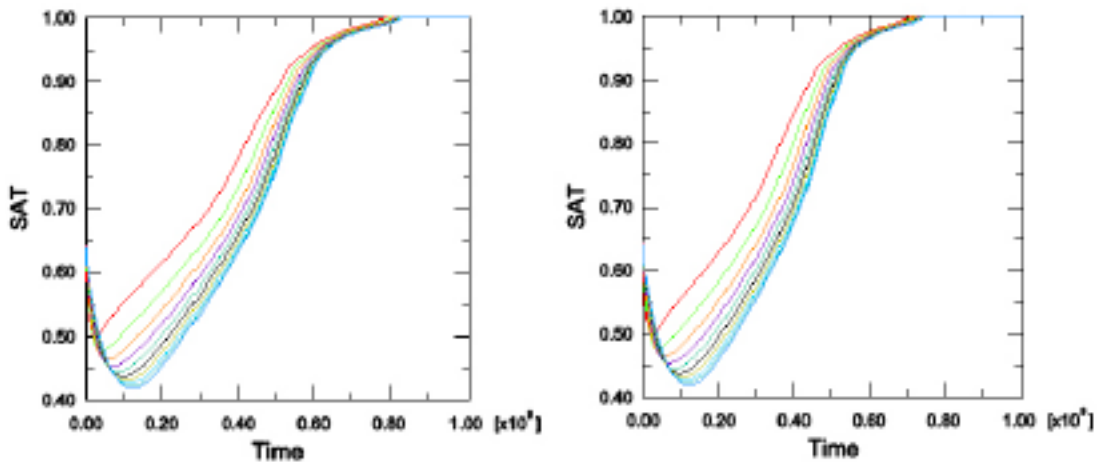


Figure 4-3. *Stress_3b1_or* (left) and *Stress_3b2_or*. Degree of saturation in the buffer at equidistant points along a radial line on top of the canister as a function of time (s) without damaged zone (left) and with damaged zone. New calculations without water supply from the backfill.

Figure 4-2 shows the evolution with time of the degree of saturation on the lid of the canister in the old calculations and shows that it takes $0.49 \cdot 10^9$ seconds or 15.5 years with no disturbed zone and $0.40 \cdot 10^9$ seconds or 12.7 years with a disturbed zone until complete saturation (100%). Figure 4-3 shows corresponding curves according to the new calculations with no water available at the backfill interface. This figure shows that it takes $0.82 \cdot 10^9$ seconds or 26.0 years with no disturbed zone and $0.75 \cdot 10^9$ seconds or 23.8 years with disturbed zone until complete saturation. Thus, the influence of the backfill implies for those examples a reduction in time to saturation with 40–50% if water is freely available in the backfill compared to if there is no water available.

Looking at Table 4-1a one finds similar results when comparing calculation *Stress_3a_or* and *Stress_3a_o*, which concerns the case with 0 kPa water pressure at the boundary instead of 5 MPa, while calculations *Stress_2br* and *Stress_2b* with low permeable rock ($K_{rock} = 10^{-14}$ m/s) were not run long time enough to yield a comparable difference (see also calculation *Stress_4c*, which relates to completely dry rock). Calculations *Stress_1r* and *Stress_1* with highly permeable rock ($K_{rock} = 10^{-10}$ m/s) yielded no difference due to the fast wetting through the rock. A new calculation *Stress_3b1_or2* with 10 times higher rock permeability ($K_{rock} = 10^{-12}$ m/s) than the “standard value” was also done for reviewing the influence of the rock permeability. The result was a rather fast wetting that differed very much from the results of the calculation *Stress_3b1_or*, but did not differ much from the results of calculation *Stress_1b* with $K_{rock} = 10^{-10}$ m/s, which confirms the old observation that the influence of the rock on then wetting time is insignificant at rock a hydraulic conductivity higher than about $K_{rock} = 10^{-12}$ m/s.

One new calculation, with fractures activated (*Stress2_3b2_or*) and no water available at the backfill interface, was also done. The results were similar with a reduced saturation time of 30–40% when water is available in the backfill although the reduction was slightly smaller than for the cases with no fractures due to the assistance in wetting from the fractures.

Wetting from only the backfill

Table 4-2 shows the results of the calculations of the extreme cases with no water available from the rock. The two backfill materials 30/70 mixtures and Friedland Clay have been modelled. Three different backfill conditions have been assumed, namely

1. that only the initial water content of the backfill is available (12% for 30/70 and 8% for Friedland Clay), i.e. no water inflow from the rock to the backfill takes place,
2. that the backfill is water saturated very early (21% for 30/70 and 26% for Friedland Clay) and no additional water is available,
3. that the backfill is water saturated at all times and a water pressure of 5 MPa is supplied through the backfill.

Figures 4-4 to 4-6 show as example the results of the calculation with condition 1 (30/70 and initial water content 12%) as contour plots of the degree of saturation at three different times. Figure 4-4 shows that after 16 years there is not much wetting received from the backfill and the buffer has still dried on top of the canister. It also shows that some water has been supplied and that the backfill in the deposition hole has dried from the initial degree of saturation 58% to 34% in the contact zone with the buffer. Figure 4-5 shows the state after 256 years. The wetting has gone rather far above the canister (> 85%) while it is still below 60% just below the canister. The drying has at that time spread about 1.5 m up into the tunnel backfill. After 2030 years (Figure 4-6) the buffer is close to equilibrium ($S_r > 95\%$) while the backfill still has a gradient in degree of saturation of 2%. The final degree of saturation in the buffer is 98.5% and 52.5% in the backfill.

Table 4-2. Time to equilibrium in the case of dry rock for different backfill materials and conditions.

(1) Calc. No	(2) Conditions	(3) K (backfill) m/s	(4) Time to equilibrium Years	(5) Degree of saturation (S_r) at equilibrium %	
				Buffer	Backfill
Stress_4	Dry rock, 30/70, $w_o = 12\%$	$0.5 \cdot 10^{-10}$	~2,000	98.5	52.5
Stress_4b	Dry rock, 30/70, $w_o = 21\%$	$0.5 \cdot 10^{-10}$	500–1,000	99.9	94.3
Stress_4c	Dry rock, 30/70, $u = 5,000$ kPa	$0.5 \cdot 10^{-10}$	250–500	100	100
Stress_5	Dry rock, Friedland Clay, $w_o = 8\%$	$0.7 \cdot 10^{-11}$	4,000–8,000	~50 (dries)0	30
Stress_5b	Dry rock, Friedland Clay, $w_o = 26\%$	$0.7 \cdot 10^{-11}$	1,000–2,000	99.6	95
Stress_5c	Dry rock, Friedland Clay, $u = 5,000$ kPa	$0.7 \cdot 10^{-11}$	250–500	100	100

The calculation with the early water saturated backfill (condition 2) yields for 30/70 that it takes 500 to 1,000 years to equilibrium with a degree of saturation of 99.9% in the buffer and 94.3% in the backfill while the calculation assuming an early water pressure of 5 MPa supplied through the backfill (condition 3) yields a halving of that time.

The calculations with Friedland Clay are also summarised in Table 4-2. The improbable case of no water supplied at all and an initial water content of 8% of the backfill yields that the buffer dries because of the low initial water content in the backfill, which yields a high initial suction in the backfill. The result implies that a backfill with very high initial suction probably should be avoided in very dry rock.

Examples of results from the Friedland Clay calculations are shown in Figure 4-7. History plots of the degree of saturation along a section located on the lid of the canister and a contour plot of the degree of saturation in the buffer after 1,024 years are shown. The calculation refers to condition 2 of Friedland Clay with early water saturation (*Stress_5b*). The figure shows that drying of the buffer takes place close to the canister but it ends after $2 \cdot 10^8$ seconds or 3 years. The figure also shows that 95% degree of saturation in the driest point is reached after $5 \cdot 10^9$ seconds or 150 years and that the final saturation is very slow and ends at 99.6% degree of saturation after $3 \cdot 10^{10}$ seconds or 950 years. The figure also shows that after 1,024 years there is still a small gradient in degree of saturation of 0.4%.

4.4 Conclusions

These calculations show that there is a significant influence of wetting from the backfill if the rock is very dry ($K_{rock} \leq 10^{-13}$ m/s), while the influence is low if the rock is less dry ($K_{rock} \geq 10^{-12}$ m/s). At $K_{rock} = 10^{-13}$ m/s the time to saturation decreases with a factor 2 in the absence of fractures and a little less when two fractures are intersecting the hole when water is supplied from the backfill (30/70) compared to when no water is available.

A completely dry rock yields very long time to saturation and of course strong influence of the water supply from the backfill. If water is freely available at a water pressure of 5 MPa in the backfill it takes 250–500 years to reach full saturation of the buffer. If the water available in the backfill is limited to the initial amount (no addition from the rock in the tunnel) it will take several thousands years to reach some kind of equilibrium with a degree of saturation in the buffer of > 98%. When very dry Friedland Clay is installed the backfill will dry the buffer.

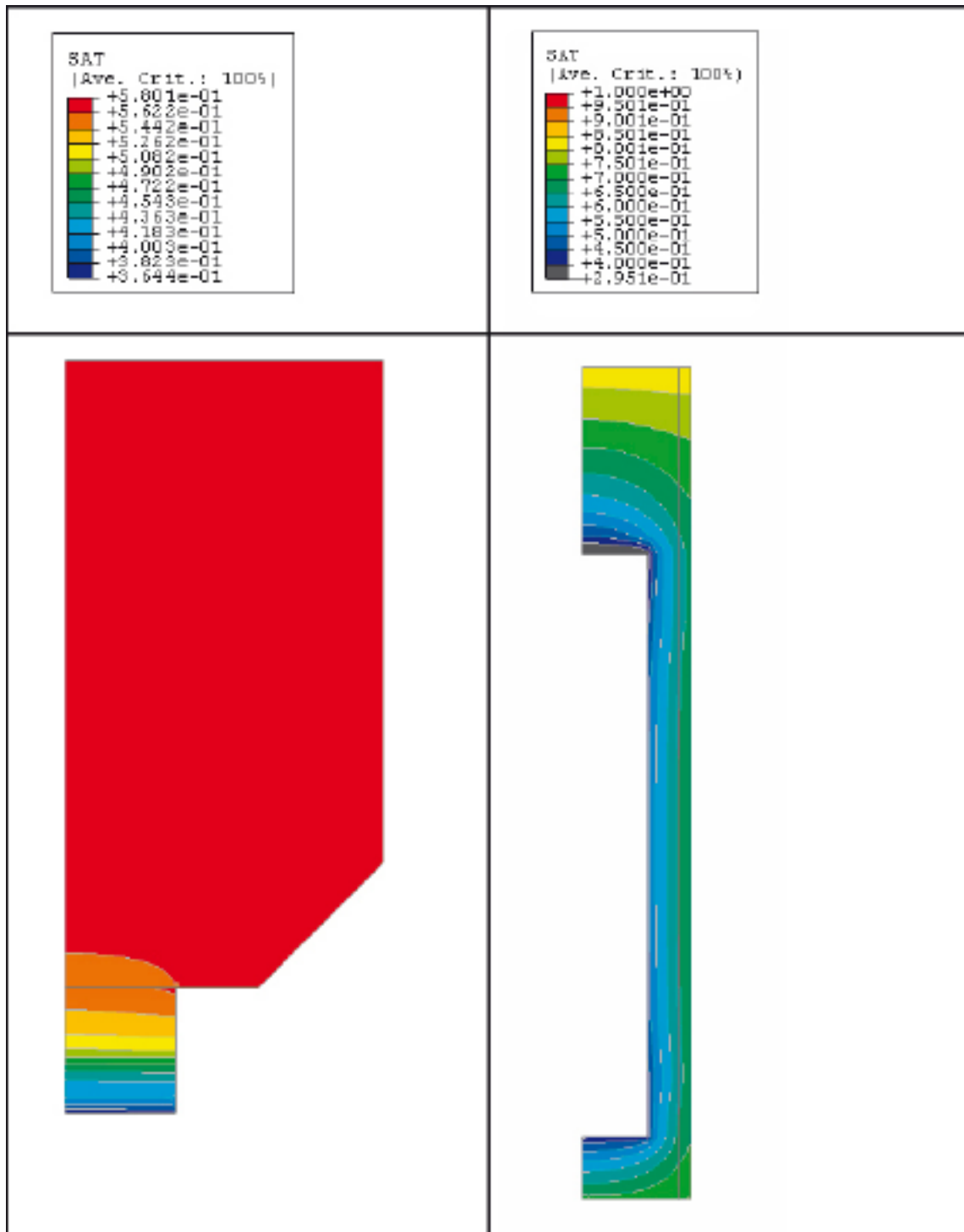


Figure 4-4. Stress_4. Dry rock and water supplied only by the initial water content 12% in 30/70. Degree of saturation in the backfill (left) and buffer after 16 years.

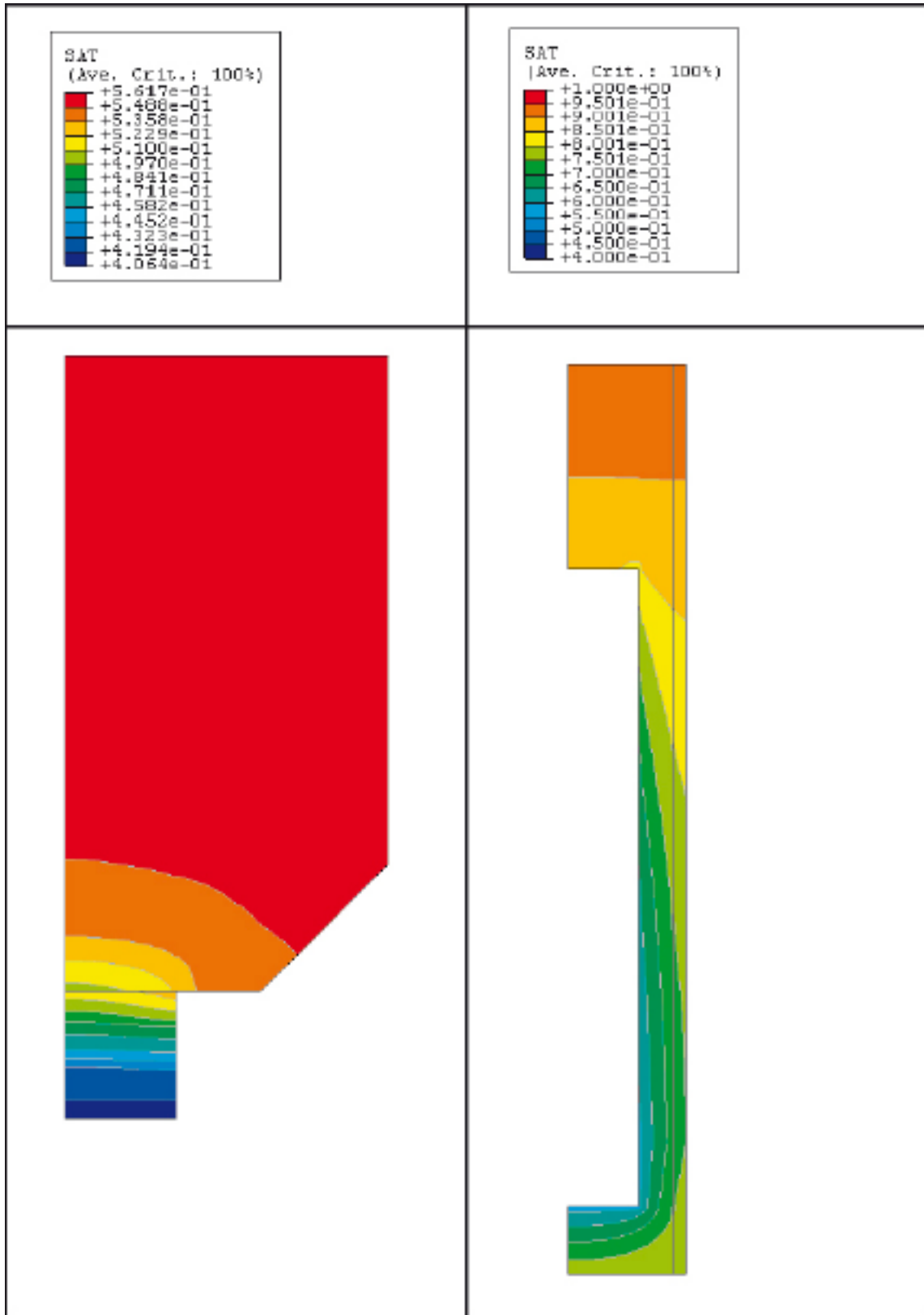


Figure 4-5. Stress_4. Dry rock and water supplied only by the initial water content 12% in 30/70. Degree of saturation in the backfill (left) and buffer after 510 years.

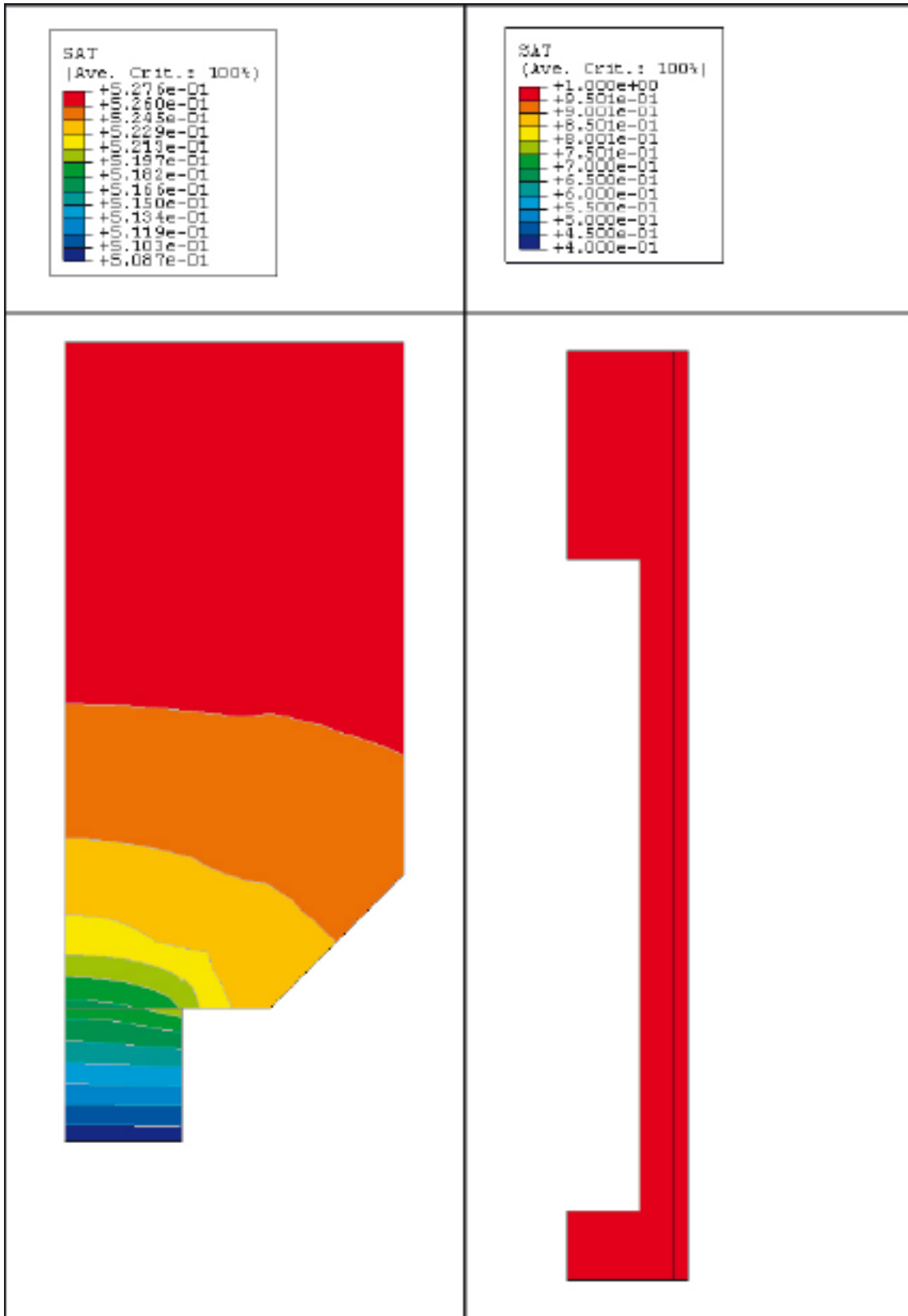


Figure 4-6. Stress_4. Dry rock and water supplied only by the initial water content 12% in 30/70. Degree of saturation in the backfill (left) and buffer after 2,030 years.

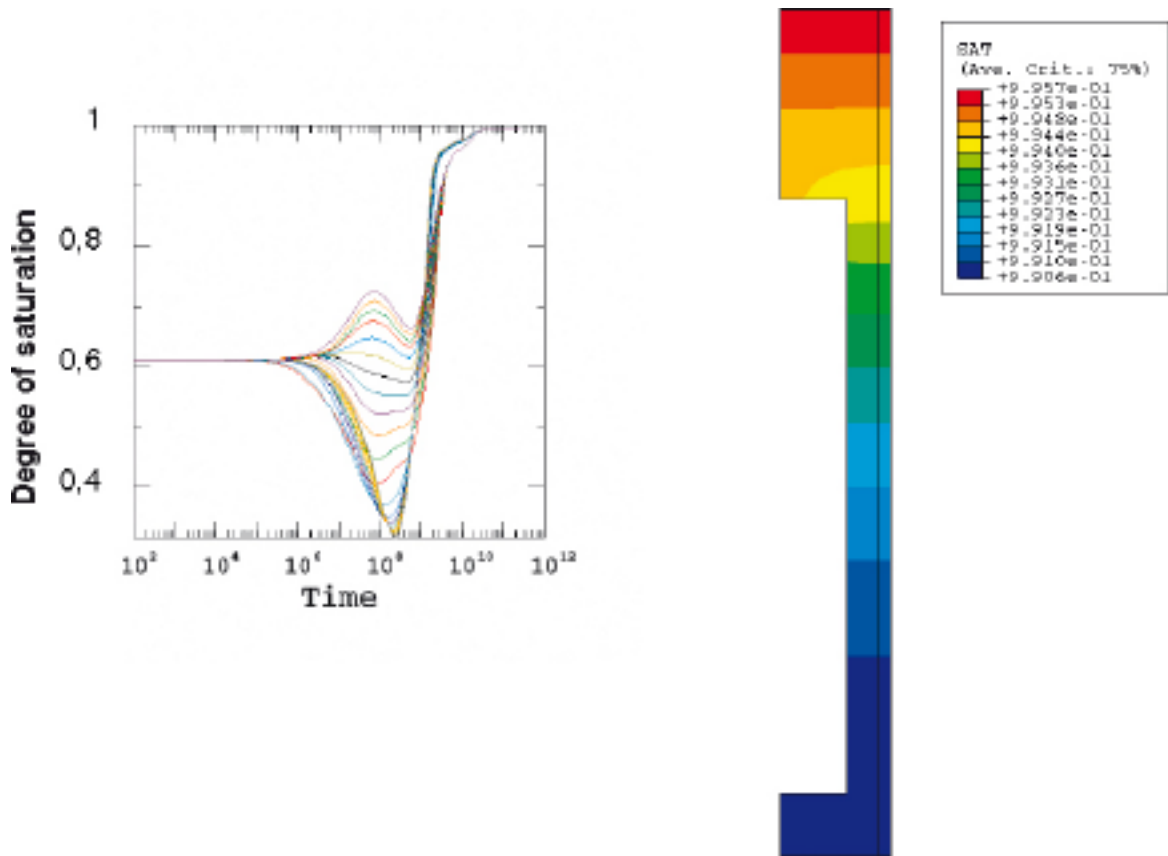


Figure 4-7. *Stress_5b. Dry rock and backfill material of initially water saturated Friedland Clay. Left: Degree of saturation of the buffer material as a function of time (s) for equidistant points in a radial section through the deposition hole on top of the canister. Lower: Degree of saturation of the buffer after 1,024 years.*

5 Influence of rock and backfill properties on the water saturation phase of the backfill

5.1 General

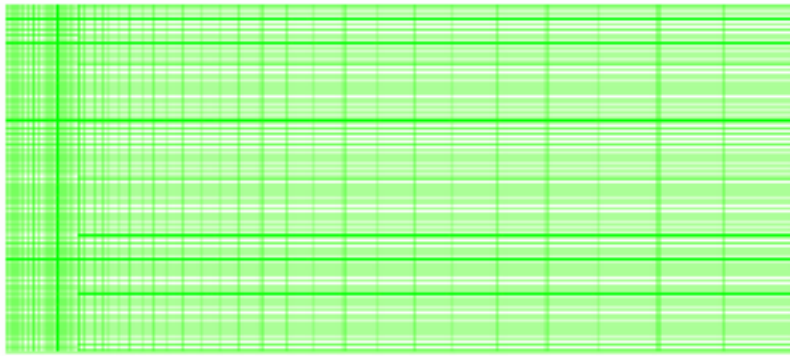
The additional new calculations of the saturation phase of the buffer with varying backfill water supply, which were described in Chapter 4, showed that the backfill has a major influence on the wetting when the rock matrix hydraulic conductivity is lower than 10^{-12} m/s. The backfill conditions and the rate of backfill wetting are thus vital for understanding the buffer wetting at those conditions. Consequently a number of calculations of the wetting rate of different backfill types at different rock conditions have been performed. The following variations have been done:

- Three different backfill materials: 30/70 crushed rock/bentonite, Friedland Clay and the so called Sandwich concept.
- Fracture distance (1–24 m between the fractures).
- Rock matrix hydraulic conductivity ($K = 10^{-13}$ – 10^{-12} m/s).
- Fracture transmissivity ($T = 5 \cdot 10^{-8}$ – $5 \cdot 10^{-11}$ m²/s).
- With and without EDZ.
- Distance to water supplying hydraulic boundary (25–100 m).

The finite element code ABAQUS has been used for these calculations.

5.2 Geometry

Figure 5-1 shows the geometry and the element mesh. The mesh is 2D axial symmetric. The tunnel diameter is 5 m and the length of the tunnel 12 m. The length corresponds thus to two sections with two deposition holes provided that the distance between two deposition holes is 6 m. The tunnel is surrounded by a 0.3 m zone that can have different properties in order to model either a disturbed zone or a piping induced zone between the rock surface and the backfill. The tunnel is intersected by fractures with the individual distance 1 m. All fractures can have separate properties. The axial boundaries are set to be symmetry planes so that the tunnel section models an infinite tunnel. The outer boundary is 25 m from the tunnel centre and has a constant water pressure, thus modelling a water supplying fractured zone.



000: 1.830E1_02_001_000 ARAGRE/21000000 0.0-1.0 000 000 00 00 11 144000 00000000. 0000000 0000
 Stage: Stage-1
 Time: 000 End Time = 1.70733E04

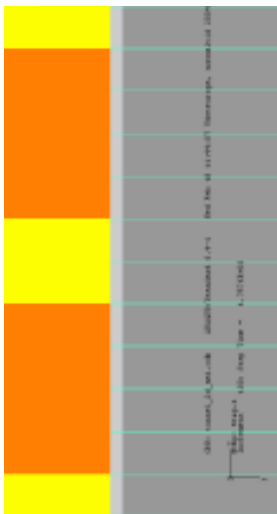


Figure 5-1. Geometry used for the backfill calculations seen from above. The upper picture shows the entire mesh and the central picture shows the property limits. The mesh is axially symmetric with the tunnel center at the left boundary. The lower picture is an enlargement of the tunnel (yellow and orange). The disturbed zone and the fractures are also seen. For the sandwich concept the yellow part is bentonite and the orange is crushed rock.

5.3 Material properties, initial conditions and boundary conditions

5.3.1 General

Only hydraulic modelling has been made. Thus no mechanical or thermal modelling is included. The properties have been divided into primary and secondary cases. The primary cases correspond to the calculations with a complete variation of the following properties:

- Three different backfill materials.
- Five different fracture frequencies.
- Three different fracture transmissivities.

The secondary cases are variations in properties with only a few examples that are done to illustrate the influence of factors such as the rock matrix hydraulic conductivity, additional fracture transmissivities, a fracture free rock, the existence of an EDZ and the distance to the hydraulic boundary.

5.3.2 Rock properties and boundary conditions

Rock matrix

Primary case: $K = 10^{-13}$ m/s.

Secondary case: $K = 10^{-12}$ m/s.

Rock fractures

Primary cases: $T = 5 \cdot 10^{-9}$ m²/s; $T = 5 \cdot 10^{-10}$ m²/s; $T = 5 \cdot 10^{-11}$ m²/s.

Secondary case: $T = 5 \cdot 10^{-8}$ m²/s.

The fracture transmissivity $T = 5 \cdot 10^{-9}$ m²/s corresponds to a theoretical inflow at steady state into an open tunnel of 0.431 l/min from that fracture with the hydraulic boundary 5 MPa at 25 m radius.

Fracture frequency

Primary cases: 1 m, 2 m, 6 m, 12 m and 24 m between fractures.

Secondary case: No fractures at all.

“EDZ”

No EDZ is included in the primary cases. In the secondary cases an EDZ with the thickness of 0.3 m and a hydraulic conductivity of $K = 10^{-6}$ m/s that yield a corresponding transmissivity of $T = 3 \cdot 10^{-7}$ m²/s. The intention of the secondary case is actually not to simulate an EDZ but to simulate a scenario where the backfill cannot withstand the pressure of from the water in the fractures but will respond with piping and thus form a hydraulically very permeable zone between the rock surface and the backfill. The consequence will of course be similar to the existence of a real EDZ although the transmissivity of an EDZ is a couple of orders of magnitude lower.

Boundary conditions

Primary case: 5 MPa constant water pressure at the outer boundary located at the radius 25 m.

Secondary case: The outer boundary located at the radius 100 m.

5.3.3 Backfill properties

Three backfill materials have been simulated.

Mixture of 30% bentonite and 70% crushed rock (30/70).

Composition

The properties of the backfill have been taken from the calculations for the Backfill and Plug Test /5-1/ and the Prototype Repository /5-2/. A mixture of 30% bentonite and 70% crushed TBM-muck is assumed to be backfilled in the tunnel and compacted to an average degree of compaction of 90% modified Proctor. According to compaction tests 90% Proctor corresponds to the following initial properties:

$\rho_d = 1.75 \text{ t/m}^3$ (dry density).

$e = 0.57$ (void ratio).

$w_m = 20.7 \%$ (water ratio at saturation).

Hydraulic parameters

The hydraulic conductivity of the water unsaturated backfill is modelled to be a function of the degree of saturation S_r , raised to a factor δ multiplied with the hydraulic conductivity at saturation K according to Equation 5-1 (identical to Equation 3-19).

$$k_p = S_r^\delta k \quad (5-1)$$

where

K_p = hydraulic conductivity of partly saturated soil (m/s).

K = hydraulic conductivity of completely saturated soil (m/s).

δ = parameter (usually between 3 and 10).

K is strongly dependent on the salt content in the water added and taken up by the backfill. In the calculations done for the Prototype Repository the salt content has been assumed to be 1.2%. The following values of K and δ in Equation 5-1 have been obtained from calibration tests /5-1/.

$K = 0.5 \cdot 10^{-10} \text{ m/s}$

$\delta = 10$

The relation between matrix suction s_w and water ratio of the backfill material is also required in the model. It has been measured (Figure 5-2) and transformed to degree of saturation. The relation shown in Table 5-1 has been used /5-1/:

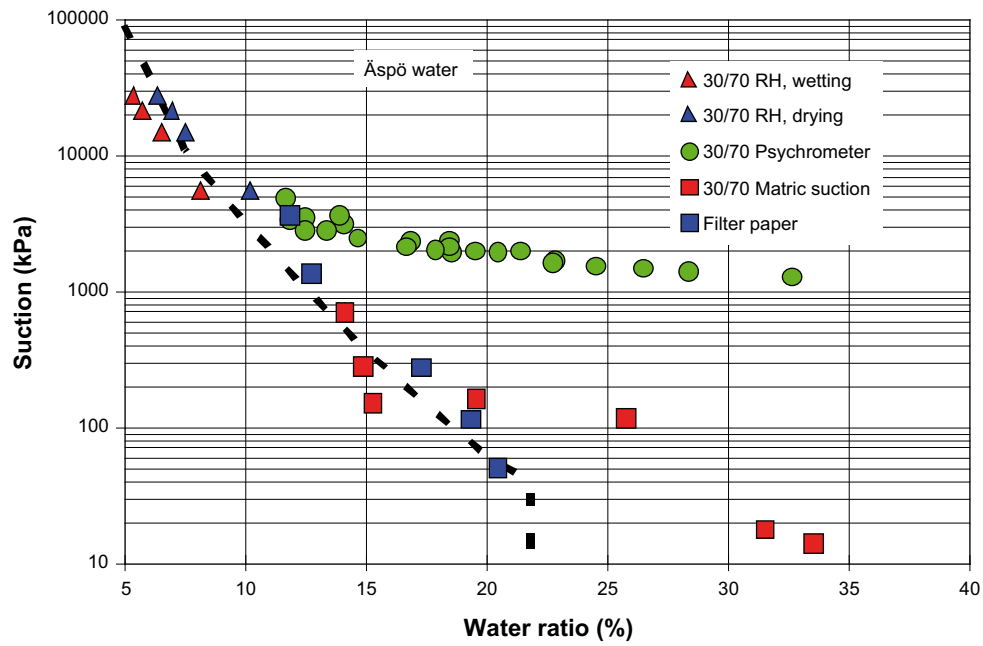


Figure 5-2. Measured relation between suction and water ratio for 30/70 backfill with 1.2% salt in the added water. The matric suction relation marked with the dashed line has been used in the calculations.

Table 5-1. Relation between suction s_w and degree of saturation S_r .

S_r	s_w kPa
0.01	400,000
0.28	50,000
0.33	20,000
0.40	12,000
0.43	5,000
0.48	3,000
0.58	1,050
0.67	500
0.77	230
0.87	110
0.92	80
0.97	50
0.995	40
1.0	0

Initial conditions

The following initial conditions in the backfill are specified:

$$e_0 = 0.57$$

$$S_{r0} = 0.58 \text{ (degree of saturation)}$$

$$u_0 = -1,050 \text{ kPa (pore water pressure)}$$

Friedland Clay

Friedland Clay is a German natural smectitic clay with good sealing and swelling properties. Its properties have been investigated in two laboratory series /5-3, 5-4/. Friedland Clay is in these calculations assumed to be backfilled in the tunnel and compacted to an average degree of compaction of 90% modified Proctor. If precompacted blocks are used the properties will be quite different. According to compaction tests 90% Proctor corresponds to the following initial properties:

$$\rho_d = 1.59 \text{ t/m}^3 \text{ (dry density)}$$

$$e = 0.70 \text{ (void ratio)}$$

$$w_m = 25.9\% \text{ (water ratio at saturation)}$$

Hydraulic parameters

The hydraulic conductivity of the water unsaturated backfill is modelled according to Equation 5-1 in the same way as the buffer and the 30/70 mixture. The following value of K has been obtained in laboratory tests as shown in Figure 5-3:

$$K = 0.7 \cdot 10^{-11} \text{ m/s}$$

The value of δ has not been determined but the same value as for MX-80 has been used.

$$\delta = 3$$

Retention curve:

The relation between matrix suction s_w and water ratio of Friedland Clay has recently been measured and transformed to degree of saturation. The relation was originally derived from the swelling pressure relation and a comparison between the derived (and used) relation and the measured values are shown in Figure 5-3.

Initial conditions

$$e_0 = 0.70$$

$$S_{r0} = 0.3 \text{ (degree of saturation)}$$

$$u_0 = -43,100 \text{ kPa (pore water pressure)}$$

Sandwich

The backfill named sandwich consists of 30% bentonite MX-80 and 70% crushed rock just as the 30/70 mixture but in the sandwich backfill they are not mixed but applied separately. The design is suggested to be as presented in Figure 5-4, with pure bentonite for about 30% of the distance between two deposition holes and crushed rock for the remaining 70%, which means that 30% of the tunnel volume is filled with bentonite compacted to blocks with the same properties as the buffer material. The crushed rock is intended to be compacted in layers with the inclination 35° as shown in Figure 5-4. In the element model the inclination is not modelled, due to the axial symmetry used. Instead the limits between the materials are assumed to be vertical as was shown in Figure 5-1.

Bentonite part

The bentonite part is modeled with identical properties and initial conditions as the buffer material described in Chapter 3.

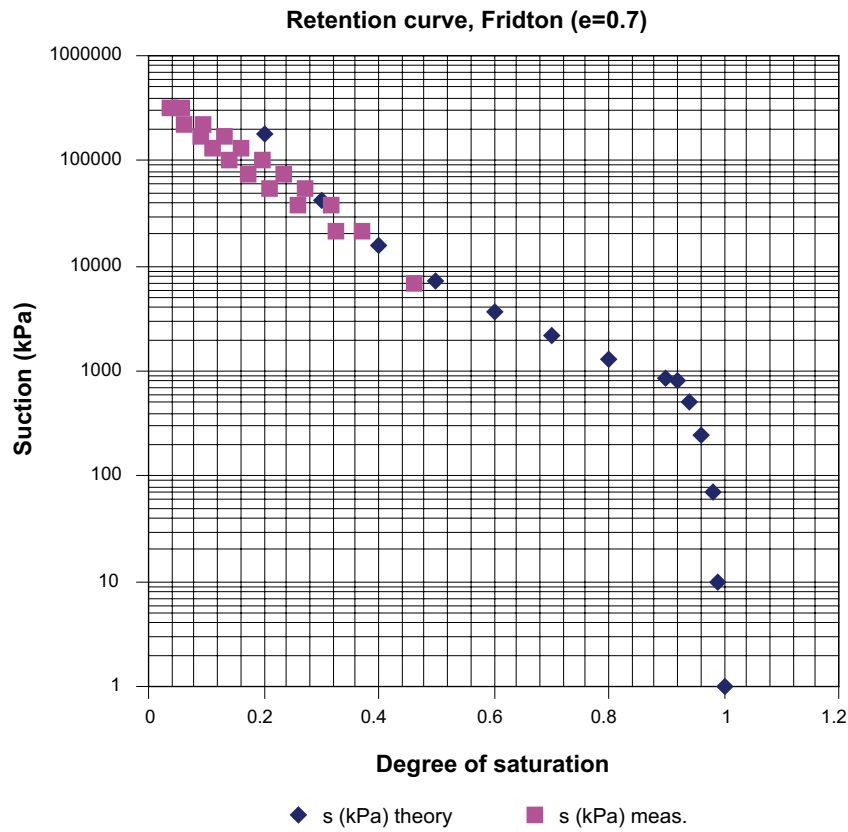
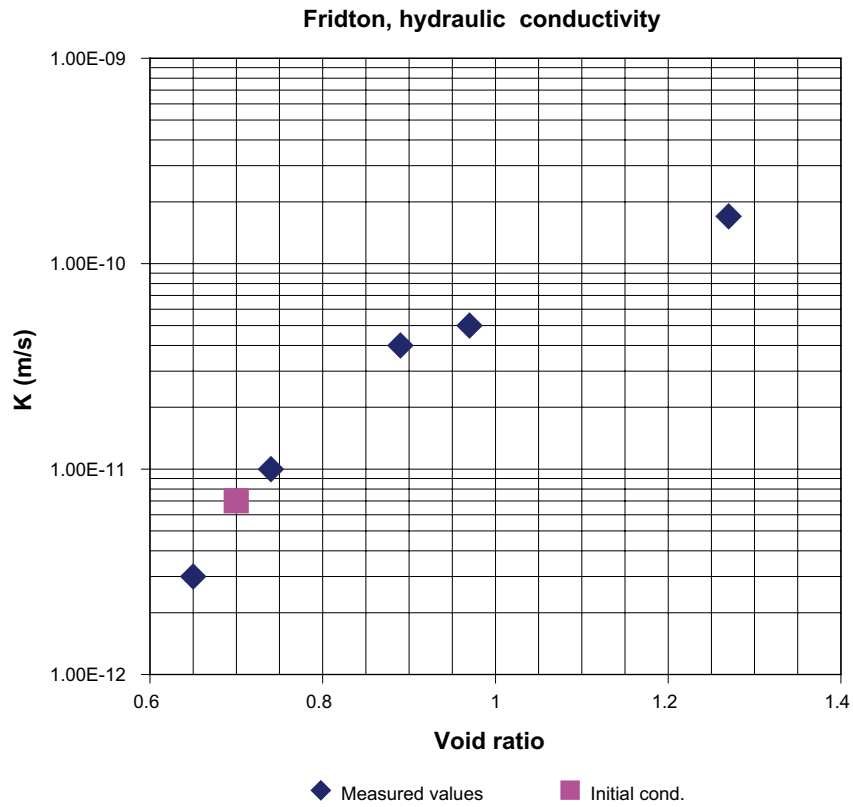


Figure 5-3. Hydraulic conductivity relation and retention curve for Friedland Clay

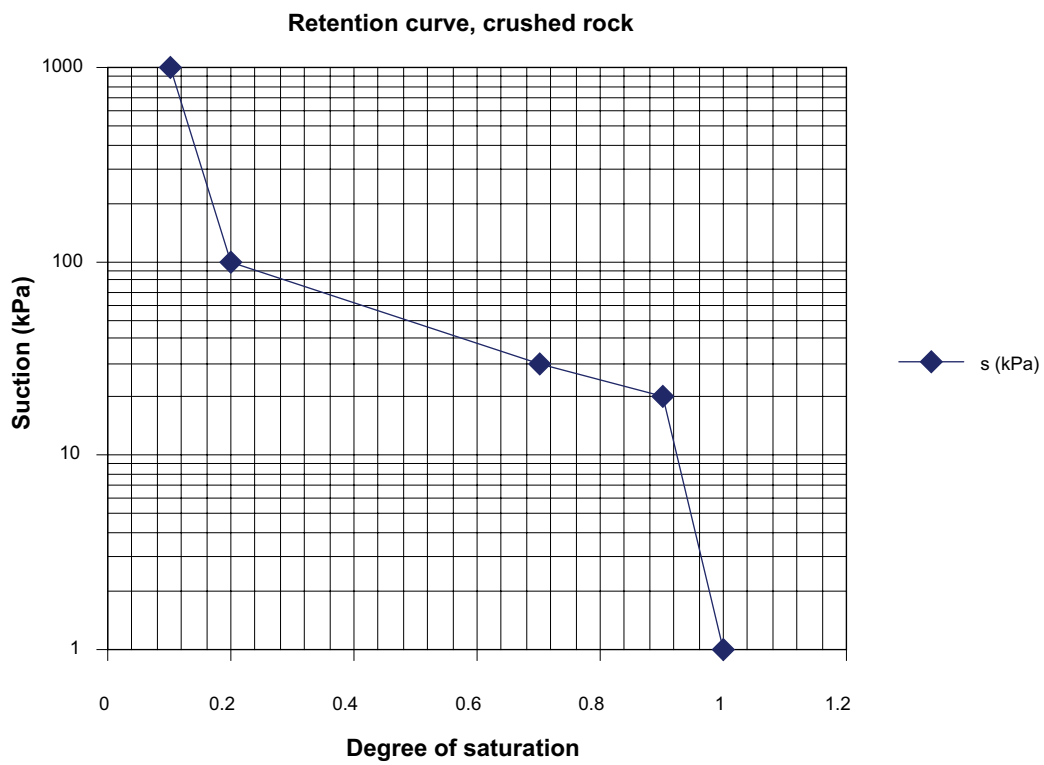
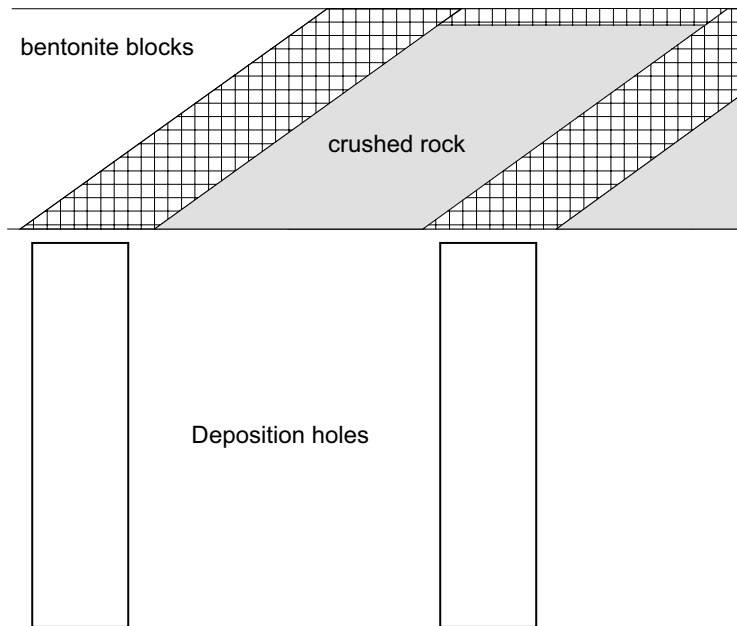


Figure 5-4. Layout of the sandwich concept (upper) and the retention curve used for the crushed rock in the sandwich concept.

Crushed rock part

The crushed rock is assumed to be compacted to the same high density as reached in field.

$$\rho_d = 2.1 \text{ t/m}^3 \text{ (dry density)}$$

$$e = 0.23 \text{ (void ratio)}$$

$$w_m = 8.5\% \text{ (water ratio at saturation)}$$

Hydraulic parameters

Bentonite part

The same as for the buffer.

Crushed rock part

The hydraulic conductivity of the water unsaturated backfill is modelled according to Equation 5-1 in the same way as the other backfill materials.

$$K = 1.0 \cdot 10^{-6} \text{ m/s}$$

The standard value of δ has been used.

$$\delta = 3$$

The relation between matrix suction s_w and water ratio of the crushed rock that has been used in the calculations is shown in Figure 5-4.

Initial conditions

Bentonite part

The same as for the buffer.

Crushed rock part

$$e_0 = 0.23$$

$$S_{r0} = 0.7 \text{ (degree of saturation)}$$

$$u_0 = -30 \text{ kPa (pore water pressure)}$$

5.4 Results

5.4.1 General

In all 69 calculations have been performed. 45 of them concern the primary cases with full variation of fracture frequency and fracture transmissivity for the three backfill-types, while 24 calculations concern the secondary cases with occasional variations in some parameters. All calculations and the most relevant results are summarized in Tables 5-2 and 5-3.

Table 5-2. Compilation of calculation results for the primary cases.

Case	Boundary <i>u</i> (kPa)	Rock matrix <i>K</i> (m/s)	"EDZ" <i>K</i> (m/s)	Fracture dist. <i>d</i> (m)	Fracture <i>K</i> (m/s)	Average rock <i>K</i> (m/s)	Q into empty tunnel (l/min,m)	Time until saturation (years)			Remarks
								30/70	F. Clay	Sandwich	
aa1	5,000	1E-13	1E-13	24	2.5E-7	2.1E-10	0.017	17.4-18.4 ³⁾	120	270	$T_f = 5E-9^5)$
aa2	5,000	1E-13	1E-13	12	2.5E-7	4.2E-10	0.034	5.4-15.9	44	149	"
aa3	5,000	1E-13	1E-13	6	2.5E-7	8.3E-10	0.069	2.2-2.4	19	101	"
aa4	5,000	1E-13	1E-13	2	2.5E-7	2.5E-9	0.206	0.78-0.95	6.5	25	"
aa5	5,000	1E-13	1E-13	1	2.5E-7	5.0E-9	0.413	0.52	4.3	24.4	"
ab1	5,000	1E-13	1E-13	24	2.5E-8	2.1E-11	0.0017	20.6-79	130	273	$T_f = 5E-10^5)$
ab2	5,000	1E-13	1E-13	12	2.5E-8	4.2E-11	0.0034	6.9-9.5	46	147	"
ab3	5,000	1E-13	1E-13	6	2.5E-8	8.3E-11	0.0069	3.0-(5.3)	20	99	"
ab4	5,000	1E-13	1E-13	2	2.5E-8	2.5E-10	0.0206	1.2-1.5	6.7	24-27 ³⁾	"
ab5	5,000	1E-13	1E-13	1	2.5E-8	5.0E-10	0.0413	0.63(-0.87)	4.3	24-25 ³⁾	"
ac1	5,000	1E-13	1E-13	24	2.5E-9	2.1E-12	0.00017	44-120	149-178	317	$T_f = 5E-11^5)$
ac2	5,000	1E-13	1E-13	12	2.5E-9	4.2E-12	0.00034	19-86	63-79	158	"
ac3	5,000	1E-13	1E-13	6	2.5E-9	8.3E-12	0.00069	9.5-79	31-33	105	"
ac4	5,000	1E-13	1E-13	2	2.5E-9	2.5E-11	0.00206	3.4-5.1	10.6	25	"
ac5	5,000	1E-13	1E-13	1	2.5E-9	5.0E-11	0.00413	1.9-2.0	6.0	24-25 ³⁾	"

1) 1 m on each side of the fracture.

2) Transmissivity of the "disturbed zone" that simulates piping along the rock surface.

3) First number: Time until $u = 0$. Second number: Time until $u = 5,000$ kPa.

4) Fracture(s) intersect(s) only the crushed rock part.

5) Transmissivity of fractures (m²/s).

Table 5-3. Compilation of calculation results for the secondary cases. The deviations from the primary cases are marked in bold

Case	Boundary <i>u</i> (kPa)	Rock <i>K</i> (m/s)	"EDZ" <i>K</i> (m/s)	Fracture dist. <i>d</i> (m)	Fracture <i>K</i> (m/s)	Average rock <i>K</i> (m/s)	Q into empty tunnel (l/min,m)	Time until saturation (years)			Remarks
								30/70	F. Clay	Sandwich	
ad2	5,000	1E-13	1E-13	12	2.5E-6	4.2E-9	0.34	4.0-6.3			$T_f = 5E-8^5)$
ad4	5,000	1E-13	1E-13	2	2.5E-6	2.5E-8	2.05	0.75-0.78			$T_f = 5E-8^5)$
ac2-K	5,000	1E-12	1E-12	12	2.5E-9	5.2E-12	0.00043	14.0-22.2	36	33	$T_f = 5E-11^5)$
ab2-K	5,000	1E-12	1E-12	12	2.5E-8	4.3E-11	0.0035	6.3-8.9	25	32	$T_f = 5E-10^5)$
aa0-K	5,000	1E-12	1E-12	-	-	1.0E-12	0.00043	70-823)	84-893)		
aa0	5,000	1E-13	1E-13	-	-	1.0E-13	0.000043			400-500 ³⁾	
aa4-r	5,000	1E-13	1E-13	2	2.5E-7	2.5E-9	0.206	0.79			$r_2 = 100$ m
ac2-r	5,000	1E-13	1E-13	12	2.5E-9	4.2E-12	0.00034	32.7			$r_2 = 100$ m
aa1-p	5,000	1E-13	1E-6¹⁾	24	2.5E-7	2.1E-10	0.017			35	$T_z = 3E-7^2)$
aa3-p	5,000	1E-13	1E-6¹⁾	6	2.5E-7	8.3E-10	0.069	0.74-0.78	3.1	27	$T_z = 3E-7^2)$
aa5-p	5,000	1E-13	1E-6¹⁾	1	2.5E-7	5.0E-9	0.413	0.30-0.34	2.76	24.4	$T_z = 3E-7^2)$
ab5-p	5,000	1E-13	1E-6¹⁾	1	2.5E-8	5.0E-10	0.0413			23.5-24.7 ³⁾	$T_z = 3E-7^2)$
ac3-p	5,000	1E-13	1E-6¹⁾	6	2.5E-9	8.3E-12	0.00069			30	$T_z = 3E-7^2)$
aa6	5,000	1E-13	1E-13	6/18⁴⁾	2.5E-7	4.2E-10	0.034			184-195 ³⁾	$T_f = 5E-9^5)$
aa7	5,000	1E-13	1E-13	6⁴⁾	2.5E-7	8.3E-10	0.069			28-29 ⁴⁾	$T_f = 5E-9^5)$

1) 1 m on each side of the fracture.

2) Transmissivity (m²/s) of the "disturbed zone" that simulates piping along the rock surface.

3) First number: Time until $u = 0$. Second number: Time until $u = 5,000$ kPa.

4) Fracture(s) intersect(s) only the crushed rock part of the sandwich backfill.

5) Transmissivity of fractures (m²/s).

The tables show the basic data of the different calculations and the results regarding the time until full saturation. Full saturation is reached when the pore pressure is higher than 0 kPa in all the backfill. Since the outer pressure is set to 5,000 kPa there is still some time until equilibrium is reached and additional water will enter the backfill until full pressure is reached. Both figures are given for some of the calculations (noted with ³⁾). For some calculation the last time steps have been too large, which yielded that the exact time cannot be evaluated. The possible time span is given for those cases.

The tables also show the average hydraulic conductivity of the rock along the entire tunnel section and the corresponding average inflow that the rock and boundary conditions yield at equilibrium before the backfill is applied (in litres per minute and meter tunnel length). This data is calculated according to Equations 5-1 and 5-2.

The average rock hydraulic conductivity K_{ra} is calculated according to Equation 5-1 in the case of fractures intersecting the tunnel perpendicular to the tunnel axis.

$$K_{ra} = K_{rm} \frac{(d - \delta)}{d} + K_f \frac{\delta}{d} \quad (5-2)$$

where

K_{rm} = rock matrix hydraulic conductivity (m/s).

K_f = fracture hydraulic conductivity (m/s).

d = distance between fractures (m).

δ = fracture width (0.02 m).

The inflow into an empty tunnel is calculated according to Equation 5-2.

$$Q_f = 2\pi K_{ra} (h_2 - h_1) / \ln(r_2/r_1) \quad (5-3)$$

where

Q_f = total inflow into the empty tunnel per meter tunnel (m^3/s , m).

K_{ra} = average rock hydraulic conductivity (m/s).

$h_2 - h_1$ = pressure drop between the radial boundary and the tunnel (mwh).

r_2 = outer radius of the rock (m).

r_1 = radius of the tunnel (m).

5.4.2 Primary variations

The results of the primary variations with different fracture distances (1–24 m) and different fracture transmissivities ($5 \cdot 10^{-9}$ – $5 \cdot 10^{-11}$ m^2/s) are shown in Figure 5-5 as time until saturation plotted as a function of the fracture distance for all three backfill types.

The results show that the dependence on both the fracture distance and the backfill type is very strong, while the influence of the fracture transmissivity is less important. In fact only the 30/70 mixture is influenced and only when fracture transmissivity changes from $5 \cdot 10^{-10}$ to $5 \cdot 10^{-11}$ m^2/s .

Figures 5-6 to 5-8 show as example the development of the water pressure in the backfill and rock for 30/70 and the high fracture transmissivity ($5 \cdot 10^{-9}$ m^2/s). The two extremes of 1 and 24 m between fractures are chosen. Figure 5-6 shows for the case of 24 m between fractures that the water pressure in the fracture very early (18 days) reaches almost 5 MPa in the contact with the backfill due to the high hydraulic conductivity in the fracture. There is thus very early a high hydraulic gradient in the backfill and the low hydraulic conductivity of the backfill then controls the wetting rate (in combination with the geometry). The wetting mainly takes place axially in the tunnel due to the long distance between the fractures and the low hydraulic conductivity of the rock matrix.

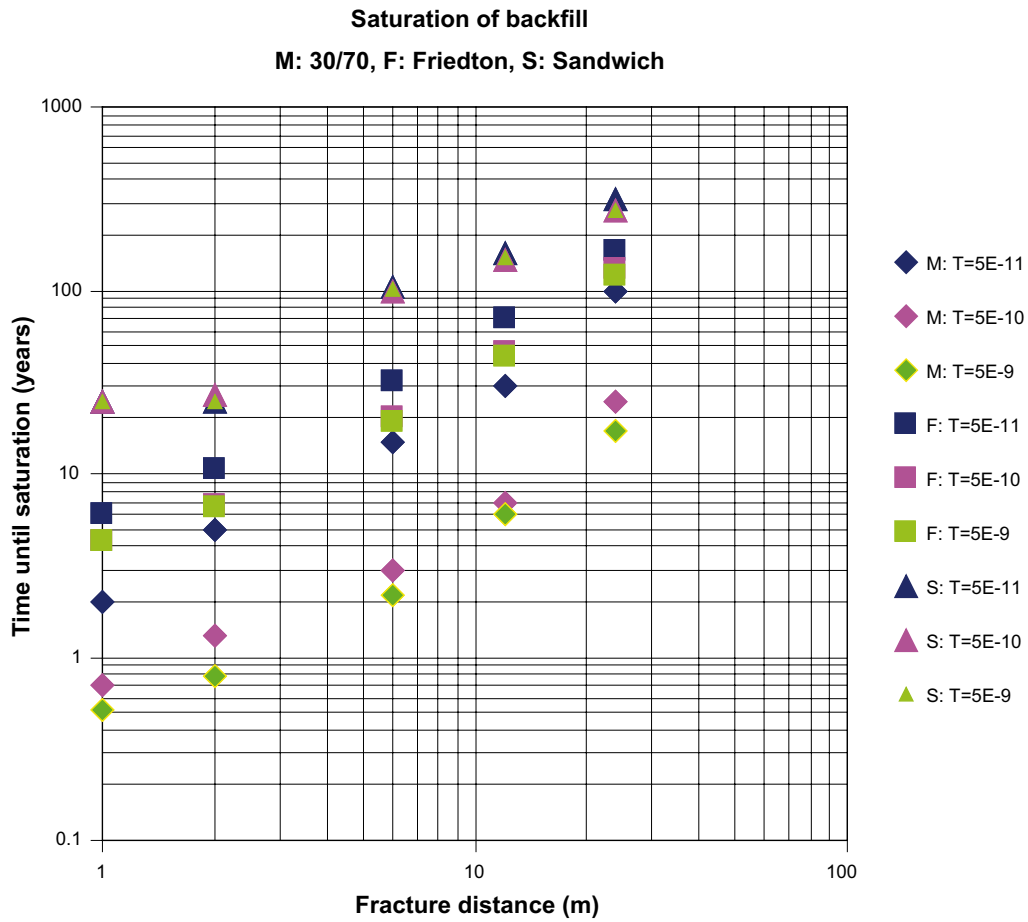
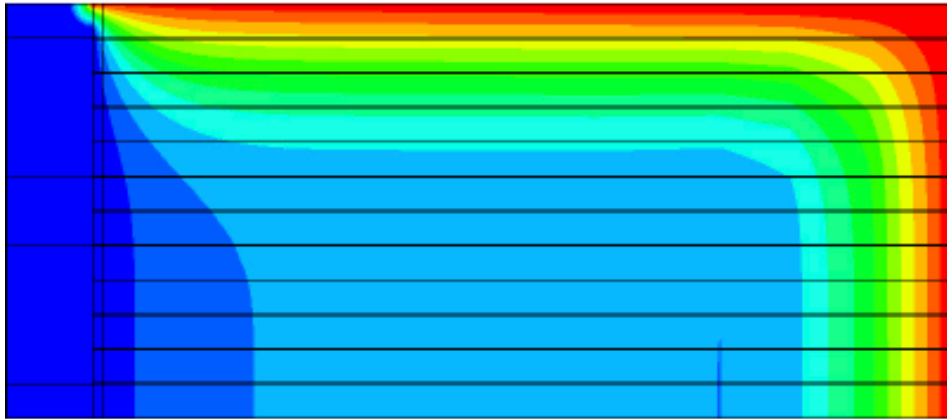
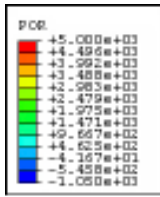
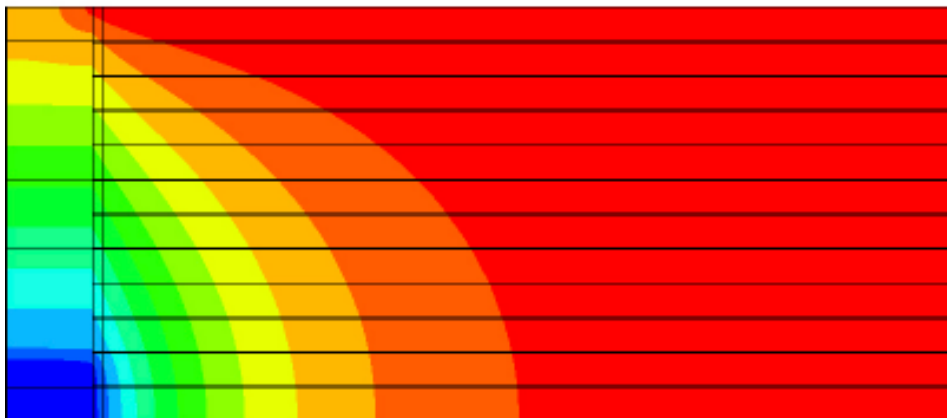


Figure 5-5. Primary cases. Time until water saturation of the three backfill concepts as function of the distance between fractures intersecting the deposition tunnel.



2 ODB: tunnel_2d_aa1.odb ABAQUS/Standard 6.4-2 Tue Apr 06 18:22:02 Västerteuropa, somstartid 2004
 3 Step: Step-1
 Increment: 100: Step Time = 2.2031E+06
 Primary Var: POF



2 ODB: tunnel_2d_aa1.odb ABAQUS/Standard 6.4-2 Tue Apr 06 18:22:02 Västerteuropa, somstartid 2004
 3 Step: Step-1
 Increment: 1000: Step Time = 4.1287E+08
 Primary Var: POF

Figure 5-6. Primary case of 30/70 with fracture distance 24 m and fracture transmissivity $5 \cdot 10^{-9} \text{ m/s}^2$ (aa1). Water pressure (kPa) in the rock and backfill after 18 days (upper) and 13 years.

Figure 5-7 shows for the case of only 1 m between fractures the same early high water pressure but also that after some time that the wetting is rather evenly distributed along the rock surface and that the gradient as well as the wetting is radial. The behaviour is similar to the expected behaviour of a rock with high matrix conductivity and no fractures. The behaviour at a fracture frequency of about one fracture per meter is thus for the tunnel similar to a permeable rock without fractures.

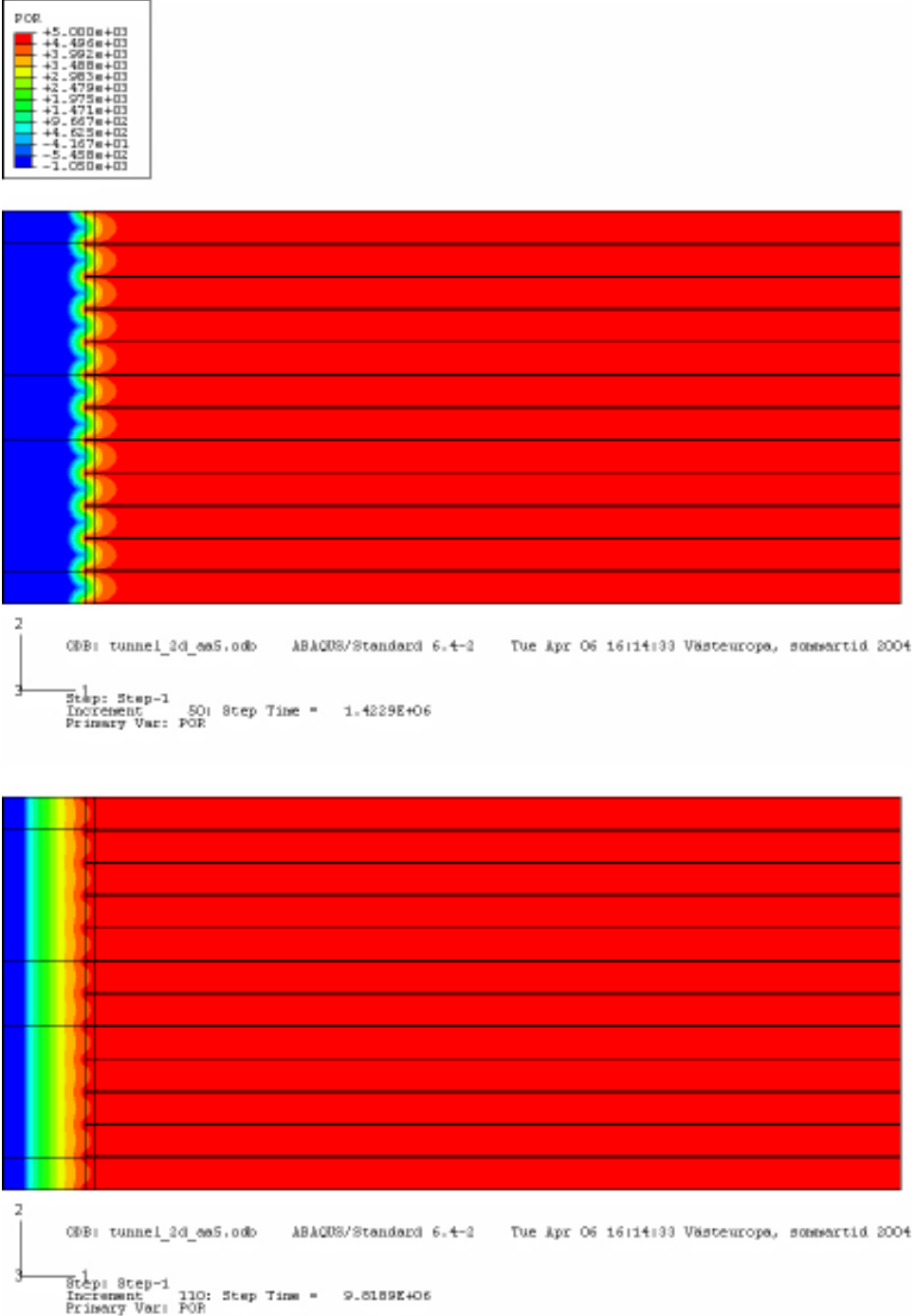


Figure 5-7. Primary case of 30/70 with fracture distance 1 m and fracture transmissivity $5 \cdot 10^{-9} \text{ m/s}^2$ (aa5). Water pressure (kPa) in the rock and backfill after 16 days (upper) and 114 days.

Figure 5-8 illustrates the water pressure in equidistant points (0.5 m) along the central axis of the backfill as a function of time for the same two cases. The difference is obvious. While all points in the case with frequent fractures have identical behaviour and is very fast (about half a year) the opposite can be seen for the case with only one fracture. It is also interesting to note for the latter case that after full saturation (pore water pressure $u \geq 0$ kPa) there is still a about another year until full water pressure is reached because of the compressibility of the water that requires an additional amount of water to flow into the backfill.

The same examples but for Friedland Clay are shown in Figures 5-9 and 5-10. The behaviour is similar but the time to saturation is about 10 times longer due to the difference in hydraulic conductivity. The same case for the sandwich backfill with 24 m between fractures is shown in Figure 5-11. The strong delay in saturation caused by the bentonite sections with very low hydraulic conductivity is clearly seen.

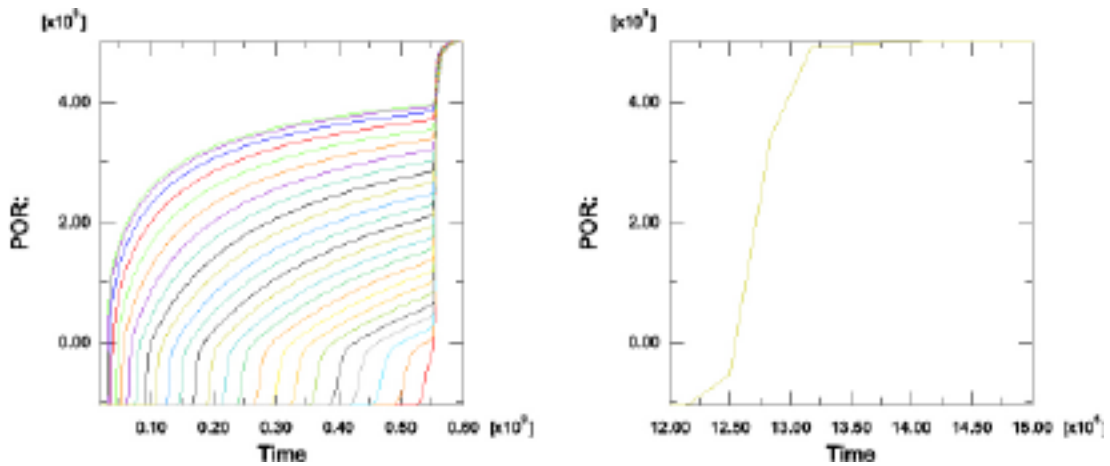


Figure 5-8. Primary case of 30/70 with fracture distance 24 m and fracture transmissivity $5 \cdot 10^{-9} \text{ m/s}^2$ (aa1). Water pressure (kPa) in the rock and backfill after 18 days (upper) and 13 years.

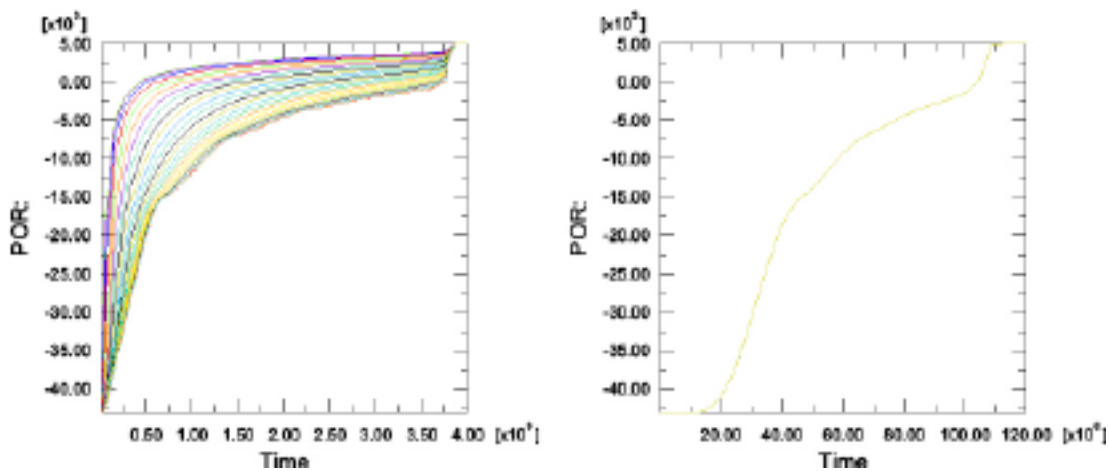
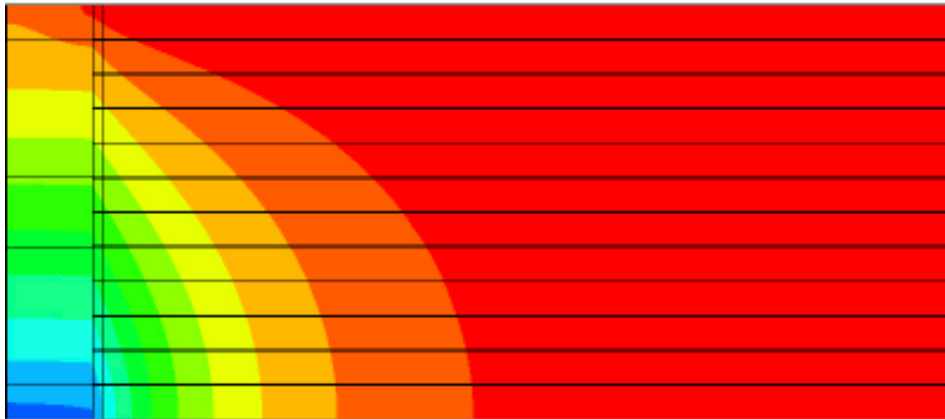
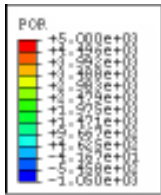


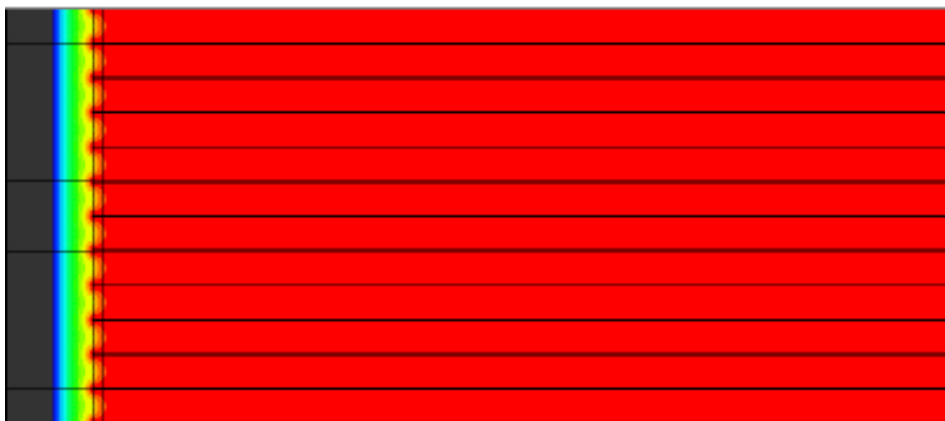
Figure 5-9. Primary case of 30/70 with fracture transmissivity $5 \cdot 10^{-9} \text{ m/s}^2$ and fracture distance 24 m (left) and 1 m (aa5). Water pressure (kPa) in equidistant points (0.5 m) along the central axis of the backfill as a function of time (s).



2
 1
 3

ODB: tunnel_2d_fridton_aa1.odb ABAQUS/Standard 6.4-2 Thu Mar 18 08:38:52 Warteuropa, normalti

Step: Step-1
 Increment: 800; Step Time = 3.7465E+09
 Primary Var: POR

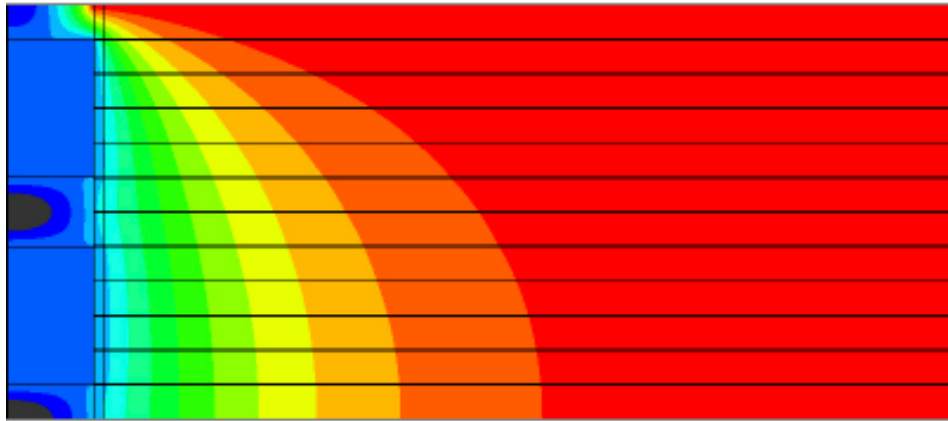
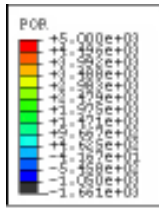


2
 1
 3

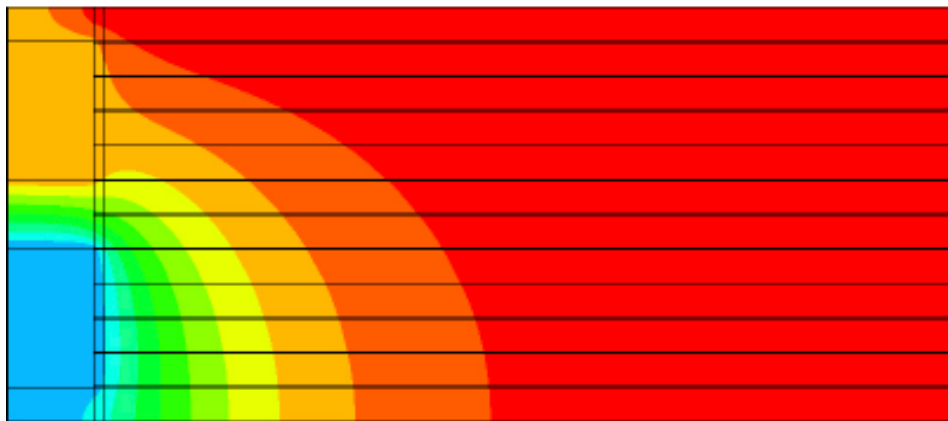
ODB: tunnel_2d_fridton_aa5.odb ABAQUS/Standard 6.4-2 Thu Apr 08 08:33:46 Warteuropa, normalti

Step: Step-1
 Increment: 140; Step Time = 6.0496E+07
 Primary Var: POR

Figure 5-10. Primary case of Friedland Clay with fracture transmissivity $5 \cdot 10^{-9} \text{ m}^2/\text{s}$ and 1 m (aa5). Water pressure (kPa) after 119 years with the fracture distance 24 m (upper) and after 1.9 year with the fracture distance 1 m.



2
 ODB: tunnel_2d_sandwich_wal.odb ABAQUS/Standard 6.4-2 Sun Mar 21 18:58:38 Västereuropa, normalt
 3
 Step: Step-1
 Increment: 60; Step Time = 1.3098E+09
 Primary Var: POR



2
 ODB: tunnel_2d_sandwich_wal.odb ABAQUS/Standard 6.4-2 Sun Mar 21 18:58:38 Västereuropa, normalt
 3
 Step: Step-1
 Increment: 90; Step Time = 7.3098E+09
 Primary Var: POR

Figure 5-11. Primary case of sandwich backfill with fracture distance 24 m and fracture transmissivity $5 \cdot 10^{-9} \text{ m}^2/\text{s}$ (a1). Water pressure (kPa) in the rock and backfill after 41 years (upper) and 231 years.

The reasons for the strong influence from the type backfill concept used and from the fracture distance and the low influence from the fracture transmissivity on the wetting time are thus

- the low hydraulic conductivity of the rock matrix which makes almost all flow go in the fractures,
- the high hydraulic transmissivity of the fractures compared to the hydraulic conductivity of the backfill that causes a fast water pressure build-up in the fractures and in the intersection between the fractures and the backfill.

The only exceptions are the calculations with 30/70 backfill and fractures with low transmissivity ($5 \cdot 10^{-11}$ m/s²) as shown in the example in Figure 5-12. The low transmissivity in combination with the relatively high hydraulic conductivity of the backfill (in relation to the other backfill concepts) makes the water pressure in the fracture to be rather low. Figure 5-12 shows that the water pressure in the fracture/backfill intersection is only a few hundred kPa.

5.4.3 Secondary variations

The results of the secondary variations are summarized in Figures 5-13 to 5-15.

Influence of higher transmissivity

Two calculations with 10 times higher fracture transmissivity ($T = 5 \cdot 10^{-8}$ m/s²) were done with the 30/70 backfill (cases ad2 and ad4). The results showed insignificantly shorter times to saturation compared to the primary cases, which confirm the conclusions that there is no influence of transmissivity at transmissivities higher than about $T = 10^{-10}$ m/s².

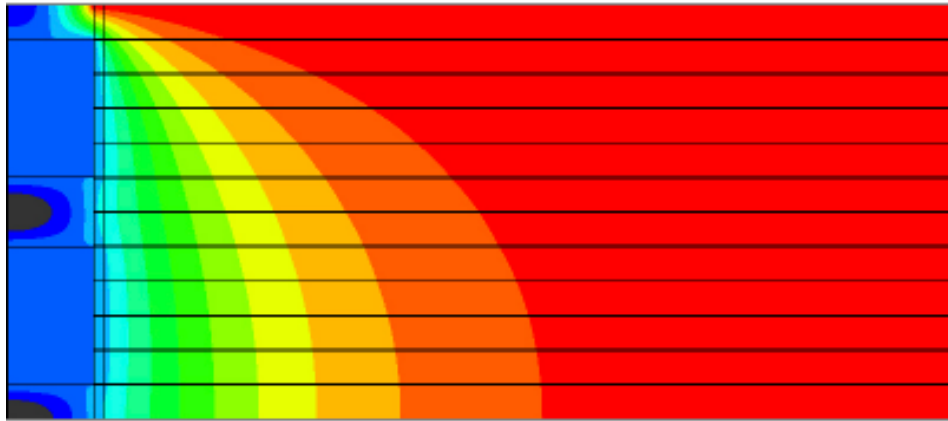
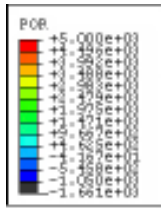
Influence of higher rock matrix hydraulic conductivity

Nine calculations with an order of magnitude higher hydraulic conductivity of the rock matrix (3 on each concept) were performed. $K = 10^{-12}$ m/s were used instead of $K = 10^{-13}$ m/s (cases ac2-K, ab2-K and aa0-K). The results show that the influence is not very strong for 30/70 and Friedland Clay, since the average hydraulic conductivity of the rock is not affected very much due to the high transmissivity of the fractures. For the sandwich backfill, however, the influence is rather strong at the fracture distance 12 m since the water can enter the crushed rock through the rock matrix and thus start wetting the bentonite part early.

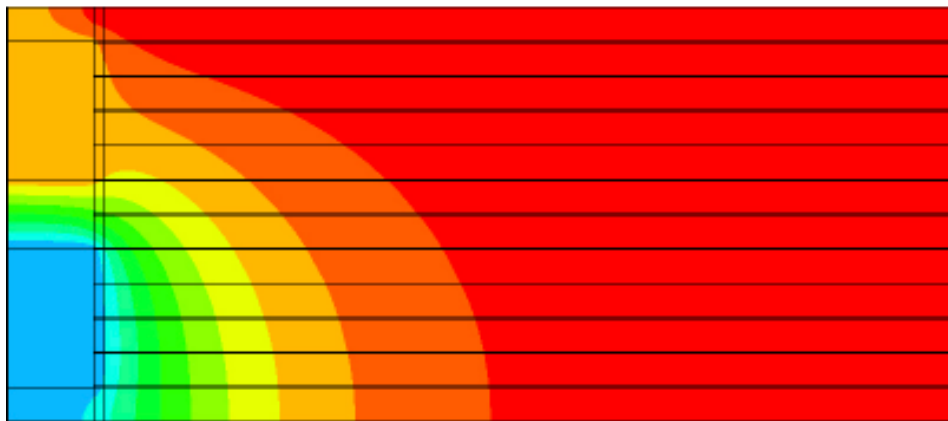
All three concepts were also studied with no fractures at all but only the rock matrix conductivity $K = 10^{-12}$ m/s for 30/70 and Friedland Clay and $K = 10^{-13}$ m/s for the sandwich concept. The results are marked in the figures as the fracture distance 100 m in order to include them in the diagrams. $K = 10^{-12}$ m/s and no fractures yield very little difference in saturation time between 30/70 and Friedland Clay, which is due to the low hydraulic conductivity of the rock compared to the backfill.

Influence of distance to the hydraulic boundary

Two calculations (aa4-r and ac2-r) were done with 100 m distance to the hydraulic boundary instead of 25 m. The results show that the difference in rock boundary distance is small and the reason is that there is only an influence if the rock determines the saturation process and the inflow rate into an open tunnel is only reduced with a factor 1.5 if the distance is 100 m instead of 25 m (see Equation 5-2).

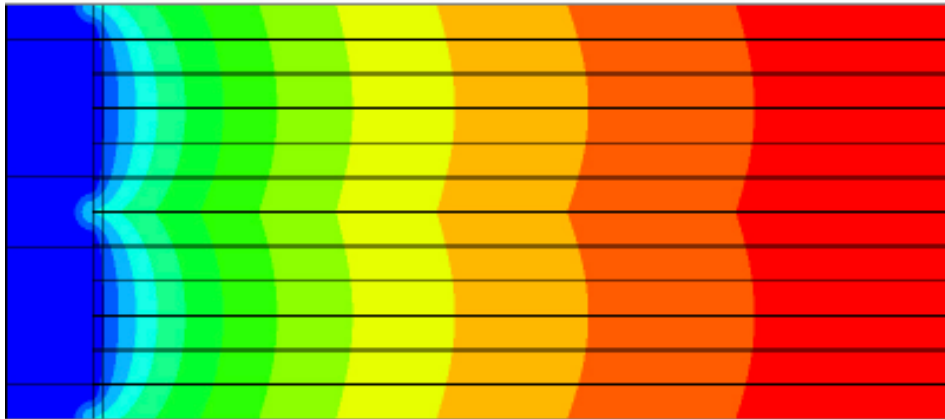
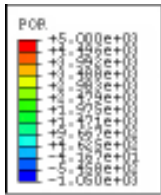


2 ODB: tunnel_2d_sandwich_wal.odb ABAQUS/Standard 6.4-2 Sun Mar 21 18:58:38 Västereuropa, normalt
3
Step: Step-1
Increment: 60; Step Time = 1.3098E+09
Primary Var: POR

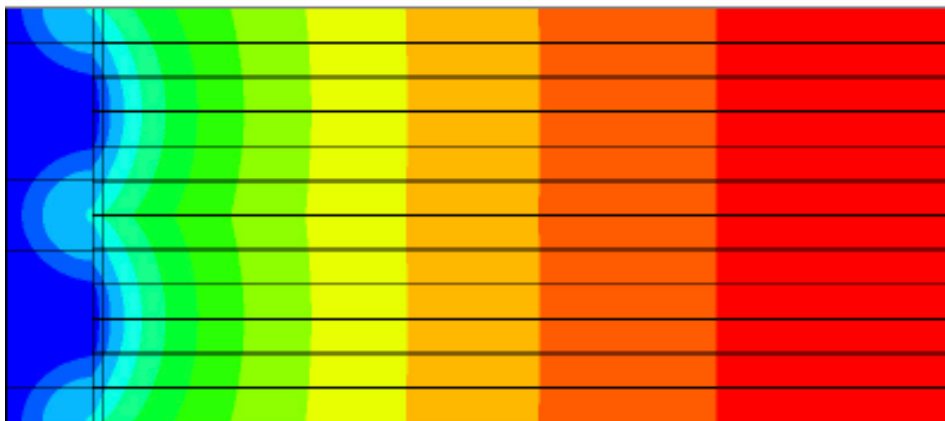


2 ODB: tunnel_2d_sandwich_wal.odb ABAQUS/Standard 6.4-2 Sun Mar 21 18:58:38 Västereuropa, normalt
3
Step: Step-1
Increment: 90; Step Time = 7.3098E+09
Primary Var: POR

Figure 5-11. Primary case of sandwich backfill with fracture distance 24 m and fracture transmissivity $5 \cdot 10^{-9} \text{ m/s}^2$ (a1). Water pressure (kPa) in the rock and backfill after 41 years (upper) and 231 years.



2
 COB: tunnel_2d_ac3.odb ABAQUS/Standard 6.4-2 Wed Apr 07 10:29:16 Västerås, sönnartid 2004
 3
 Step: Step-1
 Increment 50| Step Time = 1.3005E+07
 Primary Var: POR



2
 COB: tunnel_2d_ac3.odb ABAQUS/Standard 6.4-2 Wed Apr 07 10:29:16 Västerås, sönnartid 2004
 3
 Step: Step-1
 Increment 110| Step Time = 1.4124E+08
 Primary Var: POR

Figure 5-12. Primary case of 30/70 backfill with fracture distance 6 m and a low fracture transmissivity ($5 \cdot 10^{-11}$ m/s²) (ac3). Water pressure (kPa) in the rock and backfill after 0.4 years (upper) and 4.5 years.

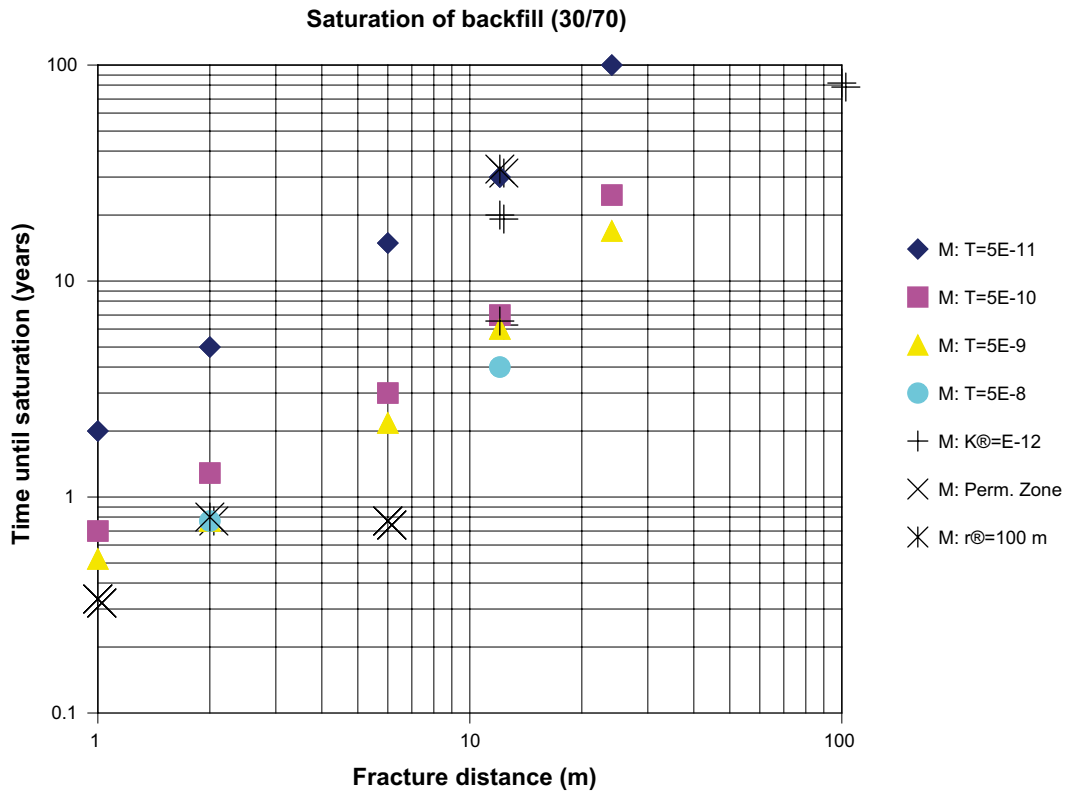


Figure 5-13. Summary of results from calculations on 30/70 backfill. The secondary variations correspond to high transmissivity ($T=5 \cdot 10^{-8}$ m/s²), high matrix hydraulic conductivity ($K_r=10^{-12}$ m/s), a highly permeable zone between the backfill and rock and a long distance to the hydraulic boundary ($r_r = 100$ m). The calculations with $K_r=10^{-12}$ at the fracture distance 12 m have been done with two different fracture transmissivities ($5 \cdot 10^{-10}$ and $5 \cdot 10^{-11}$ m²/s).

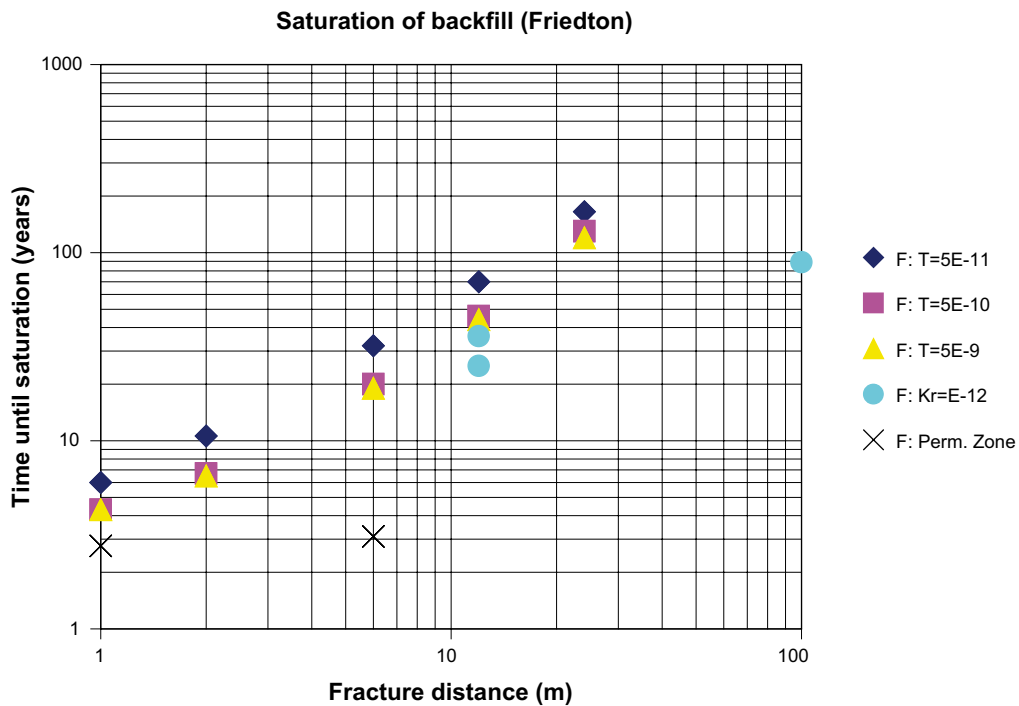


Figure 5-14. Summary of results from calculations on Friedland Clay. The secondary variations correspond to high matrix hydraulic conductivity ($K_r=10^{-12}$) and a highly permeable zone between the backfill and rock. The calculations with $K_r=10^{-12}$ at the fracture distance 12 m have been done with two different fracture transmissivities ($5 \cdot 10^{-10}$ and $5 \cdot 10^{-11}$).

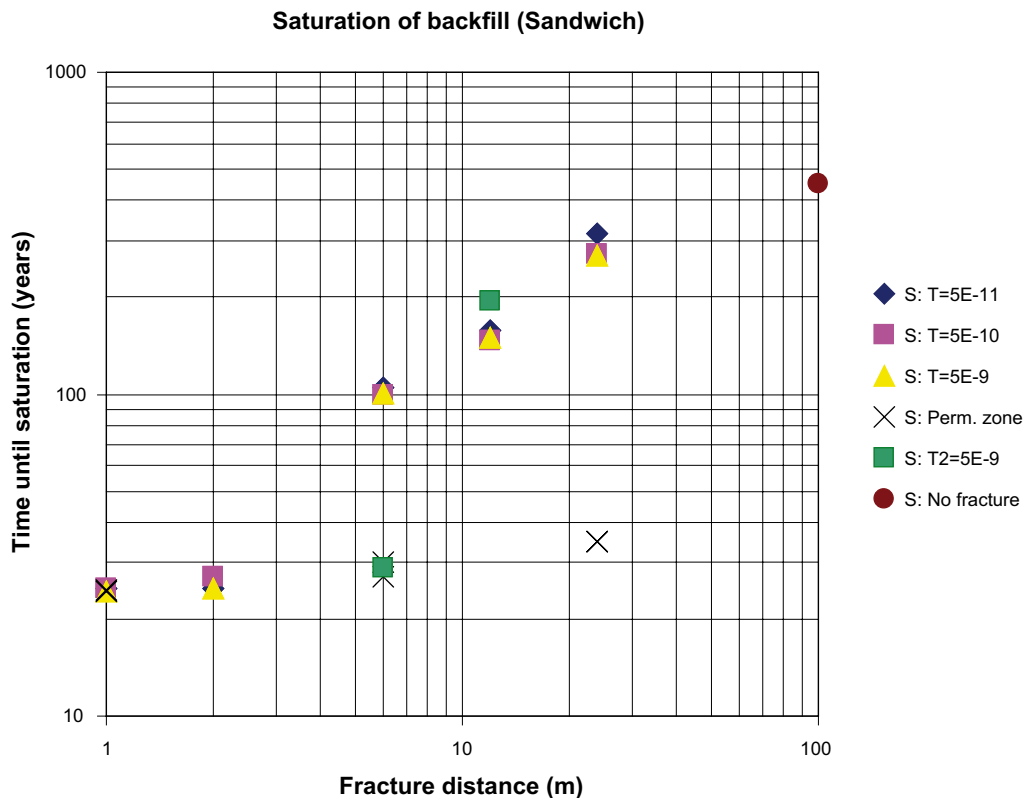


Figure 5-15. Summary of results from calculations on the sandwich backfill. The secondary variation corresponds to a highly permeable zone between the backfill and rock. The case $T_2 = 5 \cdot 10^{-9} \text{ m/s}^2$ imply that fractures only intersect the crushed rock part in opposite to the standard case that had all fractures intersecting the bentonite part.

Influence of a permeable zone between the rock and backfill

Most calculations show that the water pressure builds up to a very high level in the interface between the fracture and the backfill in most cases (see Section 5.4.2) due to the much higher hydraulic conductivity of the fracture than of the backfill. The high water pressure yields a very high hydraulic gradient in the backfill and since the swelling pressure of the backfill generally is much lower, a probable result will be piping between the rock and the backfill. This piping may continue as long as there is a high pressure and a high gradient and may thus probably cover a large part of the rock/backfill interface. In order to investigate the influence of this possible effect a number of additional calculations have been done (aa1-p to ac3-p).

As expected the effect of this phenomenon is rather strong. See e.g. Friedland Clay with the fracture distance 6 m where the time to saturation is reduced from about 20 to 3 years. The influence is even stronger for the sandwich concept, for which the time to saturation seems to be 25–35 years irrespective of the fracture frequency or transmissivity

5.5 Conclusions

A large number of calculations of the wetting of the tunnel backfill with primary variations of fracture frequency, fracture transmissivity and backfill type and secondary variations of the rock matrix hydraulic conductivity, the distance to the water supplying boundary and the existence of a highly permeable zone at the rock surface have been done. The following conclusions of these calculations can be made:

The time to complete saturation varies according to these calculations from 0.5 years for 30/70 backfill and 1 m between fractures to more than 150 years for Friedland Clay and 24 m between the fractures (300 years for the sandwich backfill).

The influence of backfill type on the wetting rate is strong due to the difference in hydraulic conductivity of the different backfill types, which seems to control the wetting rate. The difference in time to full saturation of Friedland Clay is about 10 times longer than for 30/70 backfill.

The influence of fracture frequency is strong since very little water is transported in the rock matrix at the hydraulic conductivity 10^{-13} m/s. The time to full saturation is almost proportional to the fracture distance.

The influence of transmissivity is insignificant except for the combination of the lowest transmissivity ($T = 10^{-11}$ m/s²) and 30/70 backfill, since the transmissivity is high enough compared to the hydraulic conductivity of the backfill to yield a high water pressure in the fracture/backfill interface and the water inflow thus hindered by the backfill and not by the fracture.

The influence of high matrix permeability (10^{-12} m/s instead of 10^{-13} m/s) is not very strong for the 30/70 and Friedland Clay backfill since the average hydraulic conductivity including the fractures is not affected very much and the hydraulic conductivity of the backfills are still much higher than the hydraulic conductivity of the rock matrix.

Matrix hydraulic conductivity 10^{-12} m/s and no fractures yielded about 80 years to full saturation for both 30/70 and Friedland Clay due to that the rock determines the inflow in those cases.

The influence of the distance to water supplying rock boundary is not very strong between 25 and 100 m (a factor of 1.5).

There is a strong risk of piping between the rock and the backfill due to the early water pressure build-up in the fractures. When the effect of such piping is simulated with a highly permeable zone the time to full saturation is reduced very much and the influence of fracture frequency is strongly reduced. Saturation seems to be reached within about one year for 30/70 and within about 10 years for Friedland Clay.

Note that in situ compacted Friedland clay with low density is assumed. If pre-compacted blocks are used the density will be higher, the hydraulic conductivity lower and the time to full saturation considerably longer.

6 Code_Bright analysis of trapped air in backfill

6.1 General

The influence by trapped air in the backfill on the water saturation process was analysed with Code_Bright version 2.2, which is a finite element code for thermo-hydro-mechanical analysis in geological media CIMNE 2002 /3-4/. Code_Bright handles standard two-phase flow of gas and liquid in porous materials. The two-phase flow model considers advective transport of gas in the unsaturated state, diffusion of dissolved gas in the saturated state and dissolution of gas into the liquid phase.

The modelling principle used here was to analyse a number of 1D, axially symmetric models, which included a backfilled tunnel and a portion of host rock (see Figure 6-1). At the model's outer boundary, a hydraulic boundary condition was set and the water supply to the backfill was varied by varying the rock permeability. The rock was kept saturated, thus the air hosted in the initially unsaturated backfill had to escape by diffusion through the rock. In addition to the models where the gas pressure was solved for, models with a constant gas pressure assumption were also analysed.

6.2 Initial- and boundary conditions

In Table 6-1, the initial conditions are presented. At the model outer boundary, the liquid pressure P_l was set at 5 MPa and the gas pressure P_g at 0.1 MPa. (Figure 6-1). The temperature in rock and backfill was kept constant at 15°C.

6.3 Governing equations and parameter values

In Table 6-2 and 6-3, the hydraulic material properties used are presented. The measured suction-retention data are shown in Figure 6-2 along with the Van Genuchten fit used in the calculation.

Table 6-1. Initial conditions.

	e_0	S_{r0}	P_{l0} [MPa]	P_{g0} [MPa]
Backfill	0.57	0.58	-0.95	0.1
Rock	0.005	1	0.1	0.1

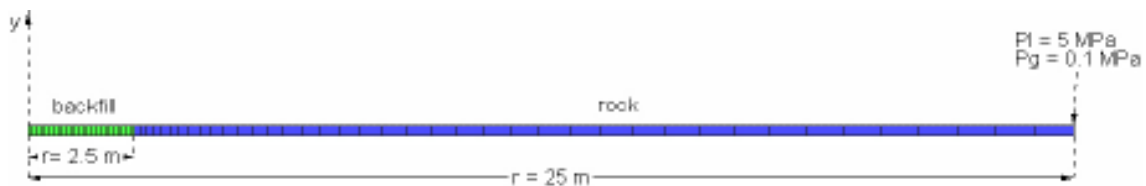


Figure 6-1. Model geometry, element mesh and hydraulic boundary conditions.

Table 6-2. Retention properties.

Material	Law (Van Genuchten)	P0 [MPa]	λ	Pm [MPa]	λm
Backfill	$S_r = \left\{ 1 + \left(\frac{P_g - P}{P_0} \right)^{\frac{1}{1-\lambda}} \right\}^{-\lambda} \left\{ 1 - \frac{P_g - P}{P_m} \right\}^{\lambda_m}$	0.1087	0.19	800	1.1
Rock	$S_r = \left\{ 1 + \left(\frac{P_g - P}{P_0} \right)^{\frac{1}{1-\lambda}} \right\}^{-\lambda}$	4	0.56	–	–

Table 6-3. Hydraulic properties.

Material	Intrinsic permeability [m ²]	Liquid phase relative permeability $k_{rl} = S_r^{\delta_l}$	Gas phase relative permeability $k_{rg} = A(1 - S_r)^{\delta_g}$	
	k	δ_l	A	δ_g
Backfill	$5 \cdot 10^{-18}$	10	10^8	4
Rock	Three cases: $5 \cdot 10^{-16}$ $5 \cdot 10^{-18}$ 10^{-19}	0 ($k_{rl} = 1$)		

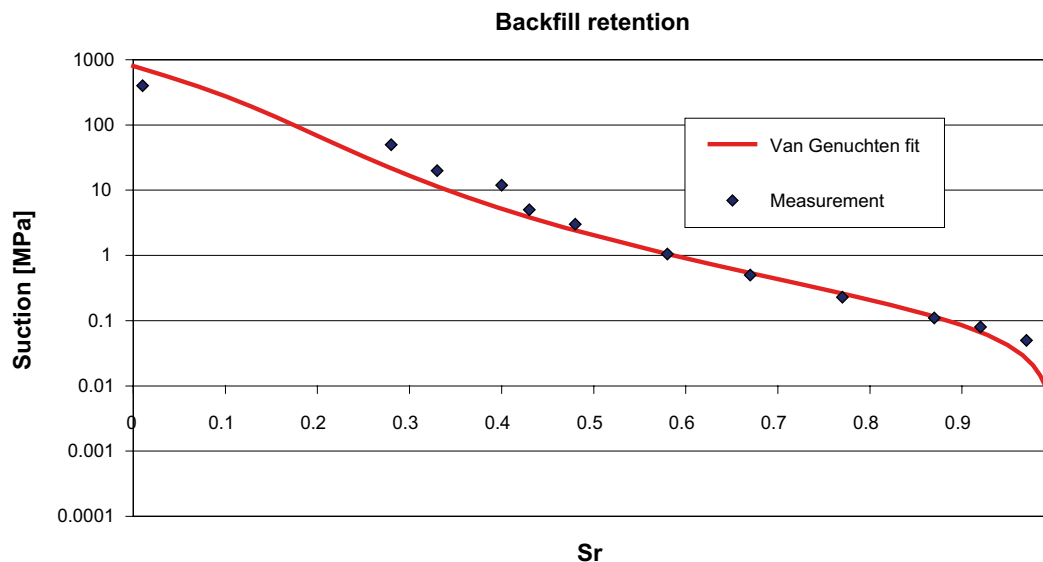


Figure 6-2. Measured backfill suction-saturation relation and corresponding Van Genuchten fit.

The Darcy flux q_α is given by Equation 6-1.

$$q_\alpha = -\frac{kk_{r\alpha}}{\mu_\alpha}(\nabla P_\alpha - \rho_\alpha \mathbf{g}) \quad (6-1)$$

where k is the intrinsic permeability and $k_{r\alpha}$, μ_α , P_α , ρ_α are the relative permeability, viscosity, pressure and density, respectively for the phase α .

Diffusion of dissolved gas is given by Equation 6-2.

$$\mathbf{i} = -(\phi\rho_l S_r D_m^g \mathbf{I}) \nabla \omega_l^g$$

$$D_m^g = D \exp \frac{-Q}{R(273.15 + T)} \quad (6-2)$$

where $D = 1.1 \cdot 10^{-4}$ m²/s, $Q = 24530$ J/mol and $R = 8.314$ J/molK. Values of Q and D are typical values for the process of diffusion of a solute into water. The solubility of gas in the liquid phase is controlled by Henry's law according to Equation 6-3.

$$\omega_l^g = \frac{P'_g M_g}{HM_w} \quad (6-3)$$

where ω_l^g is the mass fraction of dissolved gas in the liquid, P'_g is the gas pressure, $H = 10,000$ MPa is Henry's constant, M_g (0.02895 kg/mol) and M_w (0.018 kg/mol) are the molecular masses of air and water respectively. The gas pressure is computed by means of the law of ideal gases.

6.4 Models

Five different models were analysed. All the models had the same geometry, initial conditions and boundary conditions according to the description above. Three different values of the rock liquid permeability were used. In two of the models, the air pressure was assumed constant at 0.1 MPa (no trapped air). The models are presented in Table 6-4.

Table 6-4. Models analysed.

Model name	K_{rock} [m/s]	Comment
K5e-9	$5 \cdot 10^{-9}$	
K5e-11	$5 \cdot 10^{-11}$	
K1e-12	10^{-12}	
constP _g _K5e-9	$5 \cdot 10^{-9}$	Constant $P_g = 0.1$ MPa
constP _g _K1e-12	10^{-12}	Constant $P_g = 0.1$ MPa

6.5 Results

The results are presented as time development of liquid saturation, liquid pressure and gas pressure at different radial distances from the symmetry axis according to Figure 6-3. In Table 6-5, there is also a presentation of the times for reaching a saturation degree of 99% in the different models.

In general, the results seem to be reasonable. When the rock hydraulic conductivity is decreased, the water supply is impaired, which gives increased saturation time. For the two cases with the rock conductivities $5 \cdot 10^{-9}$ m/s and $5 \cdot 10^{-11}$ m/s, the water supply is enough to keep the rock completely saturated through the analysis. For the case with rock conductivity 10^{-12} m/s, there is a little desaturation at the rock wall due to lack of water (see Figures 6-4, 6-5, 6-6, 6-7 and 6-8).

The impact of the trapped gas is higher the higher the rock hydraulic conductivity. When the water supply from the rock is high, the trapped air is limiting the saturation speed. This is clearly shown in Figures 6-9 and 6-10, where the case with trapped air is compared with the constant air pressure case. The saturation time for the case with trapped air is about six times longer than in the constant gas pressure case. The air inside the backfill forms a “bubble”, which holds back the inflowing water. The gas pressure inside the “bubble” is as high as 5 MPa, which is the same as the water pressure at the model boundary. The only way in which gas can escape is by dissolution into the pore water and diffusion through the saturated backfill and rock. Thus, when the water supply is high, the saturation process is ruled by the gas diffusion rate.

Figures 6-11 to 6-13 show liquid pressure history plots while Figures 6-14 to 6-16 show gas pressure history plots

If the rock is tight and supplies little water, the effect of trapped air is very small. This can be seen in Figure 6-10. The saturation time for the case with constant gas pressure is almost as long as for the trapped air case. The water inflow into the backfill is so slow that the trapped air has time enough to escape by dissolution and diffusion. This is illustrated in Figure 6-16. The gas pressure in the backfill does not reach the maximum value of 5 MPa since the gas diffuses away fast enough to limit the pressure build up.

As mentioned above, the only way gas can escape through the saturated rock is by diffusion in the pore water. The diffusion is driven by dissolved gas mass fraction gradients. Thus it is clear that the gas content in the undisturbed rock has a great influence on the gas escape rate. In the calculations performed here, the gas pressure in the rock was set to 0.1 MPa. This is just an assumption. In a case with higher gas pressure in the rock, the saturation time would be increased.

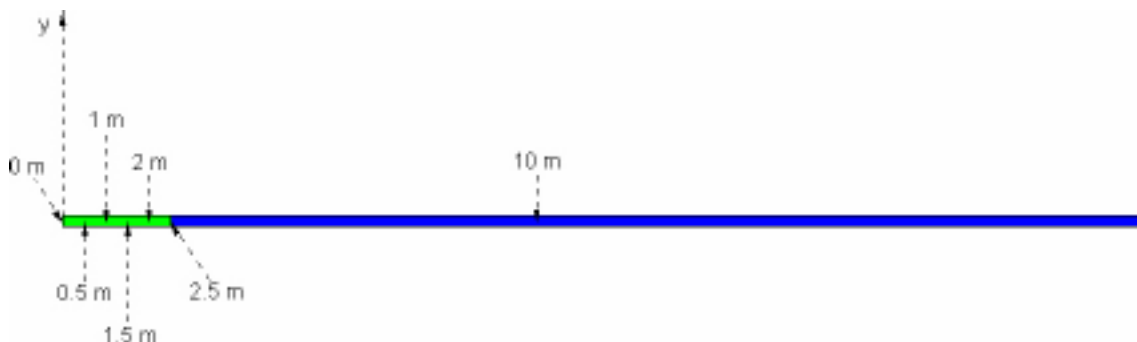


Figure 6-3. History points at different radial distances.

Table 6-5. Time for degree of saturation higher than 99%.

K_{rock} (m/s)	Time for saturation = 99% (years)	Comment
$5 \cdot 10^{-9}$	2.9	
$5 \cdot 10^{-11}$	4.3	
10^{-12}	78	
$5 \cdot 10^{-9}$	0.45	Constant $P_g = 0.1$ MPa
10^{-12}	75	Constant $P_g = 0.1$ MPa

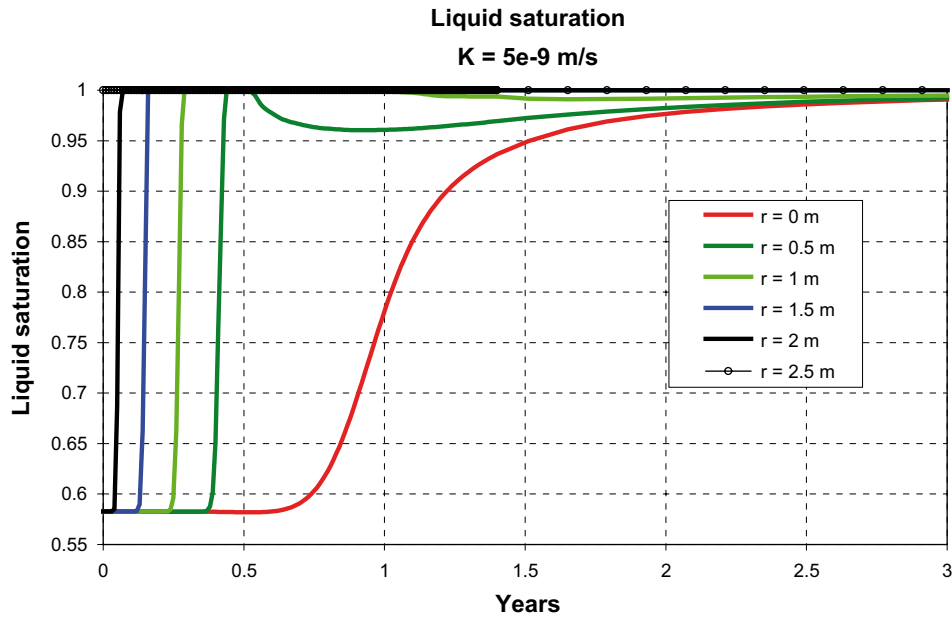


Figure 6-4. Rock hydraulic conductivity 10^9 m/s. Liquid saturation histories.

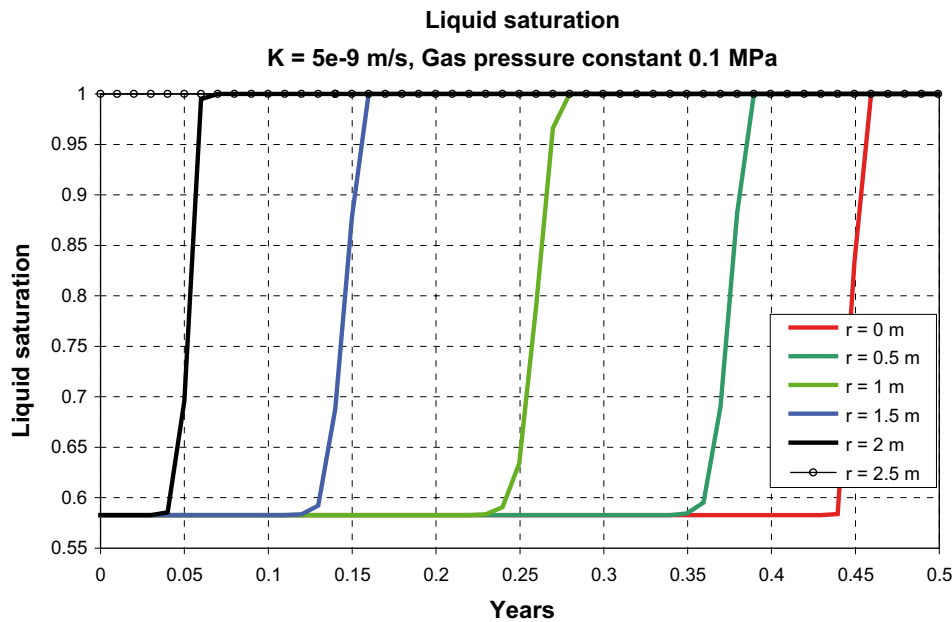


Figure 6-5. Rock hydraulic conductivity 10^9 m/s. Constant gas pressure assumed. Liquid saturation histories.

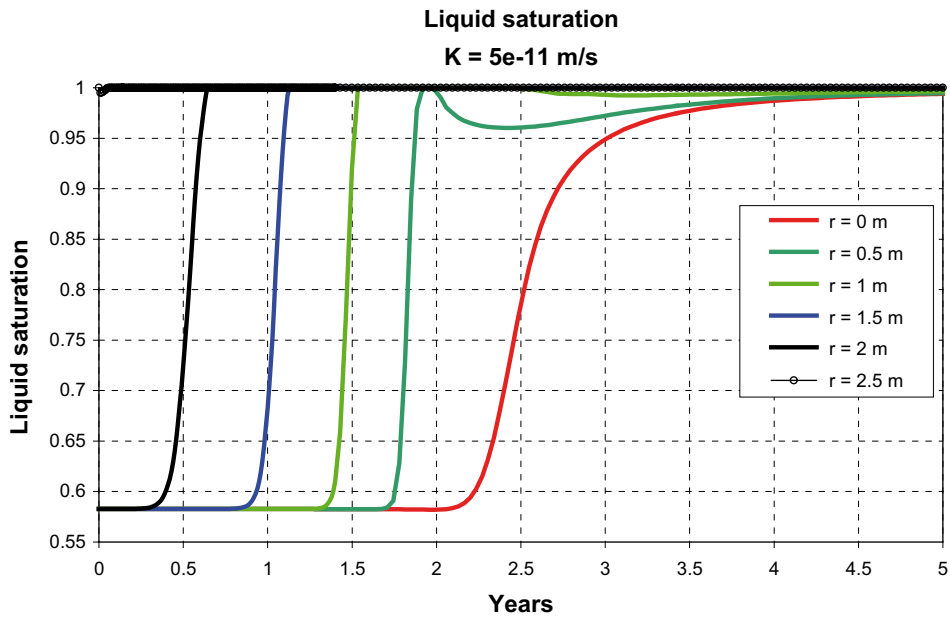


Figure 6-6. Rock hydraulic conductivity $5 \cdot 10^{-11}$ m/s. Liquid saturation histories.

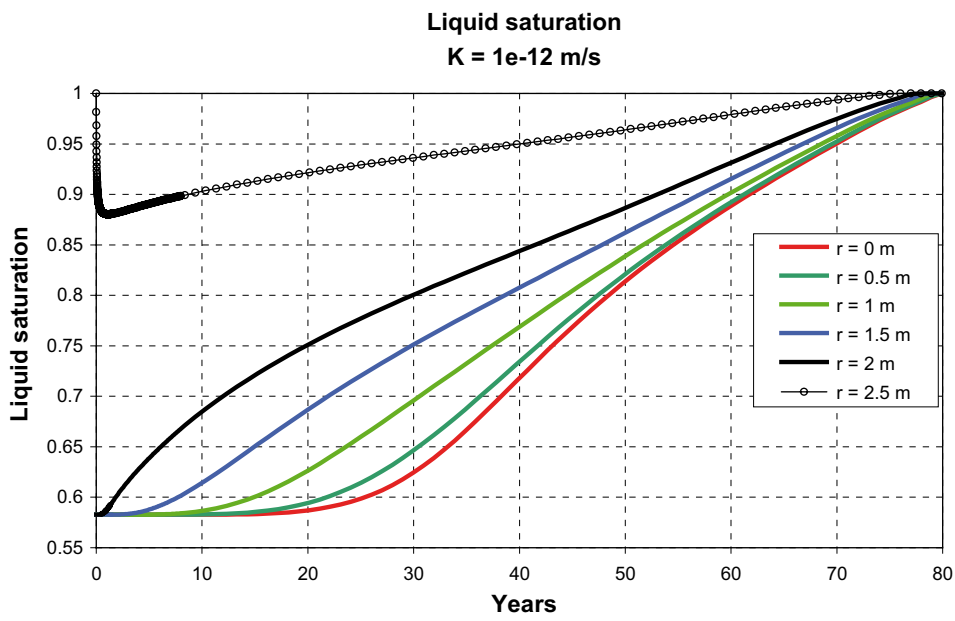


Figure 6-7. Rock hydraulic conductivity 10^{-12} m/s. Liquid saturation histories.

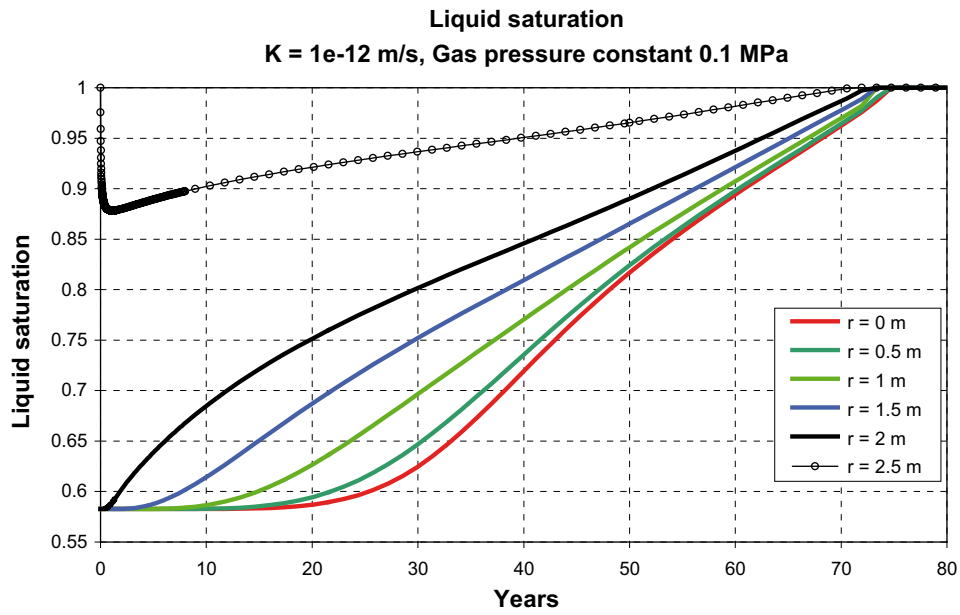


Figure 6-8. Rock hydraulic conductivity 10^{-12} m/s. Constant gas pressure assumed. Liquid saturation histories.

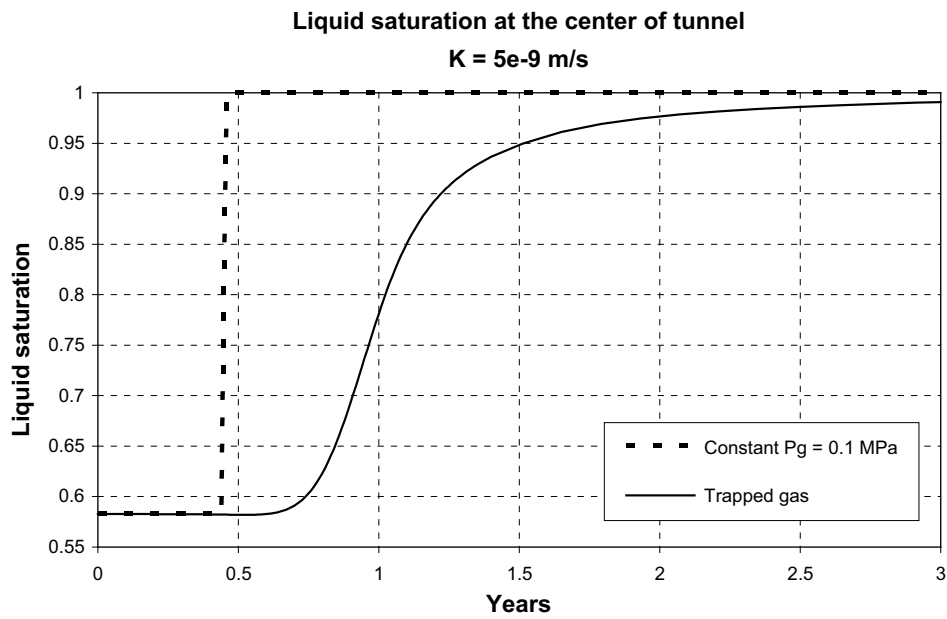


Figure 6-9. Saturation histories for the central part of the tunnel ($r = 0$ m) with rock hydraulic conductivity $5 \cdot 10^{-9}$ m/s. When the air in the backfill is considered trapped, the saturation time is increased considerably.

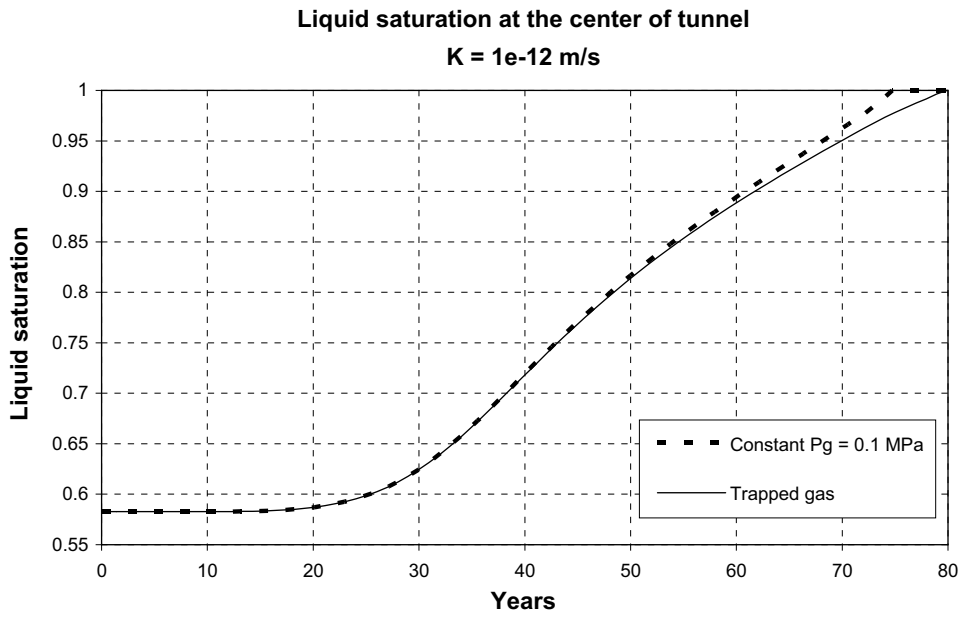


Figure 6-10. Saturation histories for the central part of the tunnel ($r = 0$ m) with rock hydraulic conductivity 10^{-12} m/s. Considering trapped air gives no significant difference in saturation time.

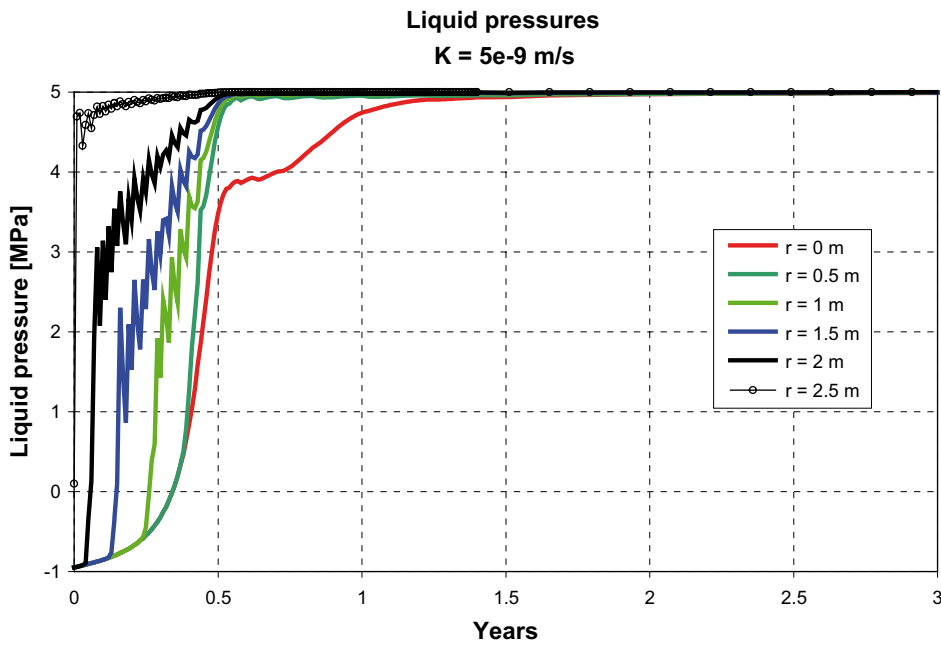


Figure 6-11. Rock hydraulic conductivity $5 \cdot 10^{-9}$ m/s. Liquid pressure histories.

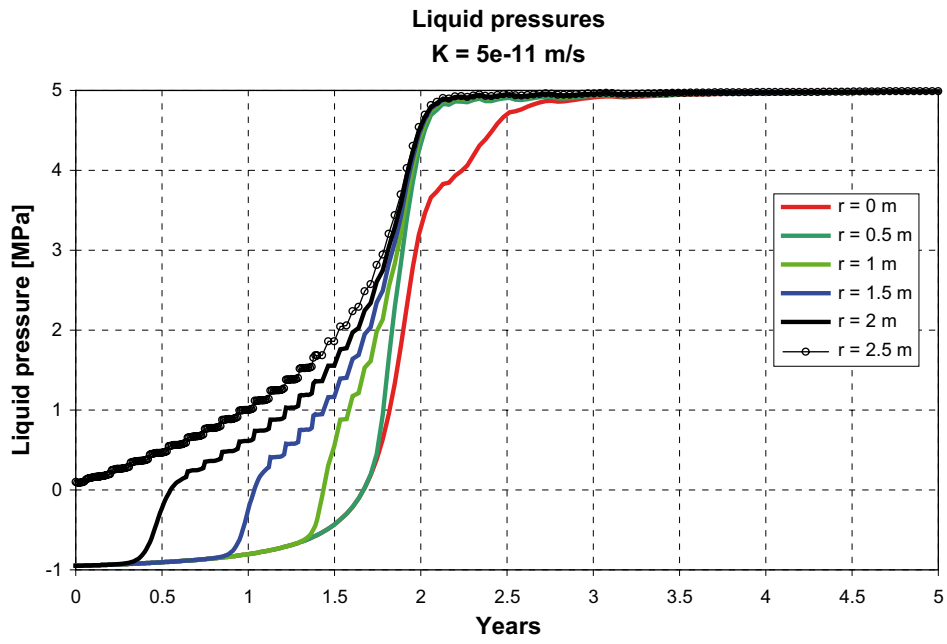


Figure 6-12. Rock hydraulic conductivity $5 \cdot 10^{-11}$ m/s. Liquid pressure histories.

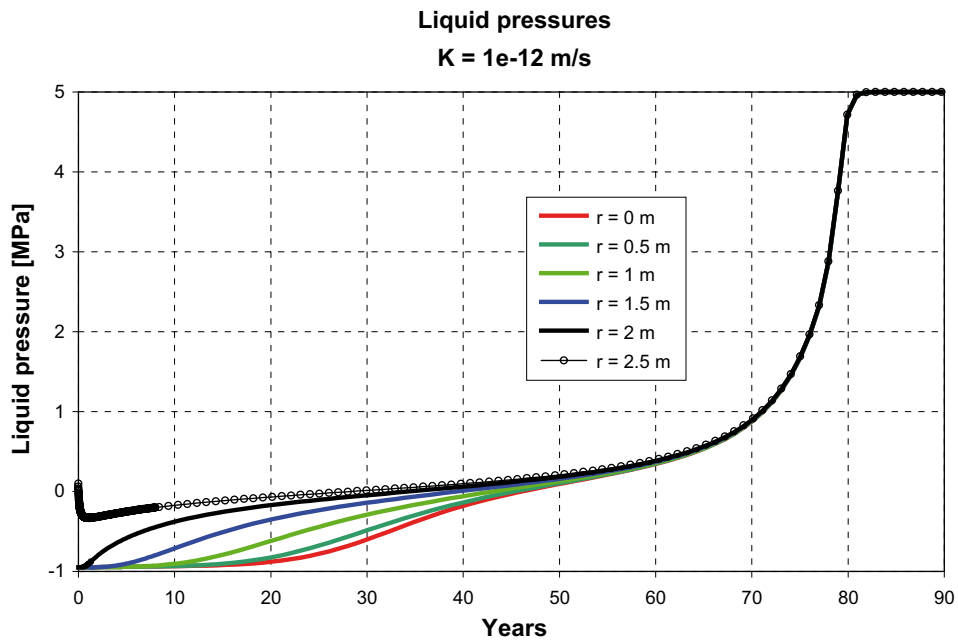


Figure 6-13. Rock hydraulic conductivity 10^{-12} m/s. Liquid pressure histories.

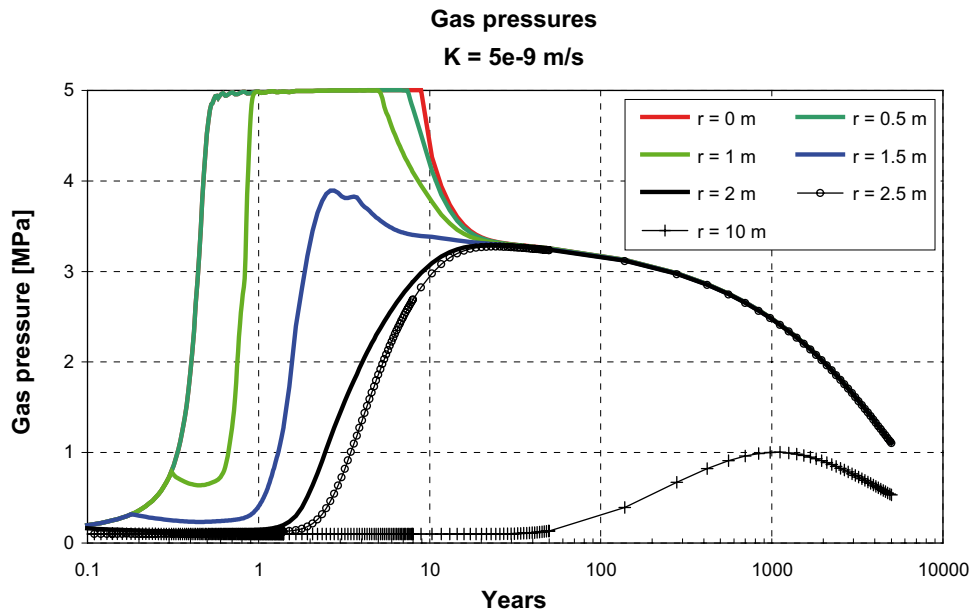


Figure 6-14. Rock hydraulic conductivity $5 \cdot 10^{-9}$ m/s. Gas pressure histories. The gas pressure inside the backfill reaches the boundary water pressure level.

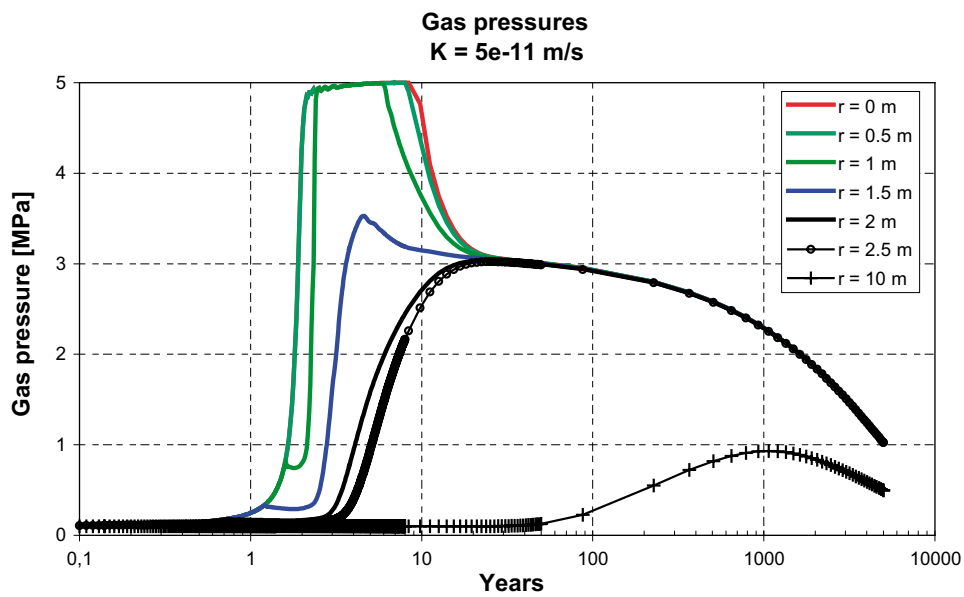


Figure 6-15. Rock hydraulic conductivity $5 \cdot 10^{-11}$ m/s. Gas pressure histories. The gas pressure inside the backfill reaches the boundary water pressure level.

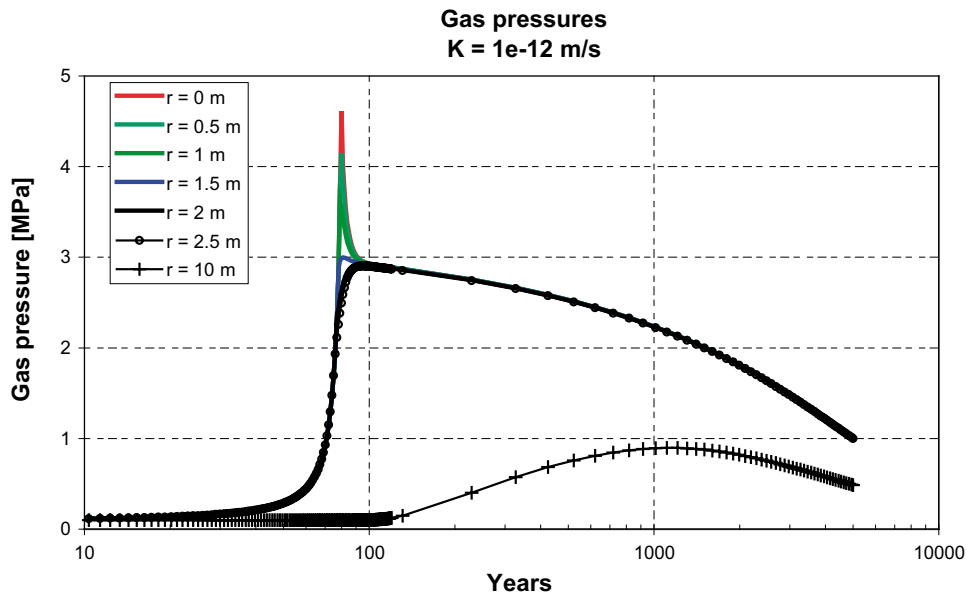


Figure 6-16. Rock hydraulic conductivity 10^{-12} m/s. Gas pressure histories.

6.6 Conclusions

The influence by trapped air on the saturation process in a backfilled tunnel has been analysed. Five 1D, axially symmetric models were run. Three different rock permeabilities were tried and in two of the models, a constant gas pressure was assumed (no trapped air). According to the results, the following conclusions can be drawn.

- If there are no escape routes for the air hosted in the initially unsaturated backfill others than through the host rock, the trapped air will have an impact on the saturation process. The trapped air forms a “bubble”, which holds back the inflowing water and delays the saturation. This effect is more important the more permeable the rock is. When the water supply from the rock is high, the gas diffusion rate will rule the water saturation process.
- Since the only way gas can escape is by being dissolved into the pore water and then diffuse away, the diffusion rate has a great importance for the saturation process. If the pore water in the undisturbed host rock contains much dissolved gas, the diffusion rate will be low with a corresponding low saturation rate. If the rock is saturated with gas, the backfill will not be water saturated.

7 3D-model of the tunnel and a deposition hole

7.1 General

The results and conclusions drawn from 2D calculations of the wetting of only the backfill and the wetting of the buffer through the backfill and the rock have been checked and supplemented by some 3D calculations. In these calculations the tunnel, the deposition hole and the rock with several fractures have been modelled in 3D. These calculations are rather extensive and generate large amount of results so only four calculations with different rock fracture properties were performed.

7.2 Geometry

The geometry is shown in Figures 7-1 and 7-2. The model is 55 m high, 3 m thick (in direction 1) and 15 m deep (in direction 3). All vertical boundaries are symmetry planes, which mean that it models a KBS-3V repository of infinite extension with 6 m distance between the deposition holes and 30 m distance between the deposition tunnels. Figure 7-1 shows the different property areas and Figure 7-2 shows the fractures and the disturbed zones surrounding the hole and the tunnel. Since the disturbed zones have been given the same properties as the intact rock these zones will not be further dealt with. There are one horizontal fracture and four vertical fractures with a thickness of 2 cm (except the two fractures that form the vertical boundaries, which are 1 cm thick due to the symmetry conditions). The fractures are either given the same properties as the host rock and are thus not activated or given properties that yield a specified transmissivity.

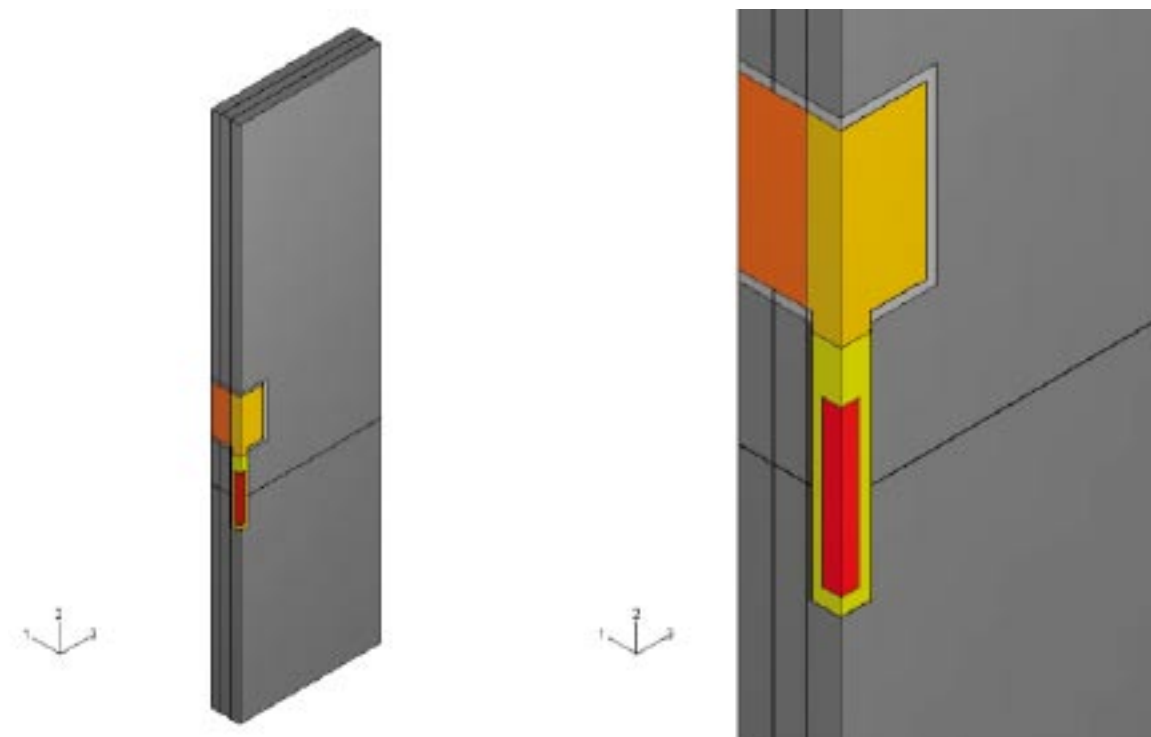


Figure 7-1. 3D model. All vertical boundaries are symmetry planes.
Grey: rock. Yellow: buffer. Orange-coloured: backfill. Red: canister.

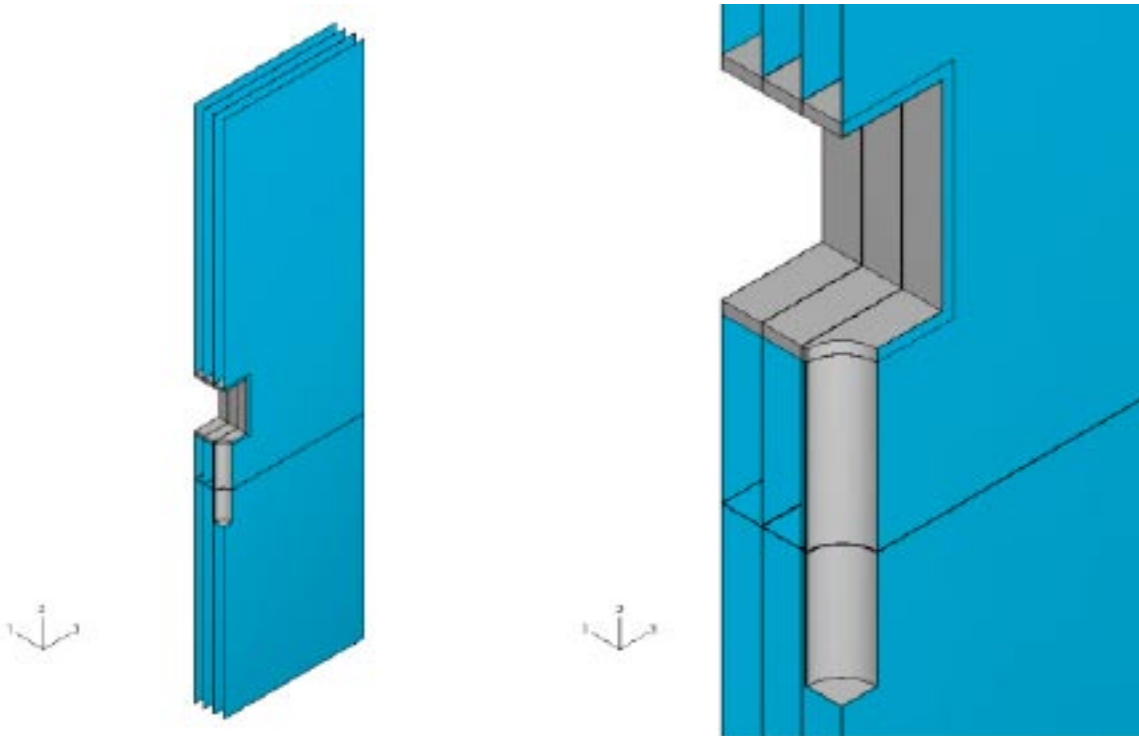


Figure 7-2. Fracture configuration. Blue: fractures. Grey: EDZ (not activated).

7.3 Material properties and initial conditions

7.3.1 General

The materials of the model have in principle been given the same properties as the basic cases in the previously reported calculations (Section 3-5). Also the initial and boundary conditions are the same except for the buffer, which for the entire buffer material has been given the properties of buffer 2, which is the inner 25 cm of the buffer in the calculations described in Chapter 4. The 10 cm zone with completely water saturated buffer that was assumed for the periphery has thus been changed to have the same initial conditions as the rest of the buffer. The reason for this change is that in the old calculations the pellets filled slot was assumed to be artificially filled with water, but experiences from the tests in Äspö HRL have shown that it is favourable to leave the slot unfilled so in the new 3D calculations described in this chapter the slot has been assumed to be unfilled.

7.3.2 Buffer material

The reference bentonite MX-80 has been applied as buffer material and the properties described in Section 3.3 have been used.

- dry density: $\rho_d = 1,670 \text{ kg/m}^3$ and
- water ratio: $w = 0.17$

which yield

$$e_0 = 0.77 \text{ (void ratio)}$$

$$S_{r0} = 0.61 \text{ (degree of saturation)}$$

$$u_0 = -31,000 \text{ kPa (pore pressure)}$$

$$p_0 = 18\,910 \text{ kPa (average effective stress)}$$

The initial temperature is

$$T_0 = 12^\circ$$

7.3.3 Backfill material

A mixture of 30% bentonite and 70% crushed rock has been used as backfill material with the hydraulic properties described in Section 5.3.3. In addition the following mechanical and thermal properties were applied:

Mechanical

$$E = 30 \text{ MPa}$$

$$\nu = 0.3$$

Thermal

$$\lambda = 1.5 \text{ W/m, K}$$

$$c = 1,200 \text{ Ws/kg, K}$$

$$\rho = 2,000 \text{ kg/m}^3 \text{ (bulk density)}$$

The initial conditions are the same i.e.

- dry density: $\rho_d = 1,700 \text{ kg/m}^3$ and
- water ratio: $w = 0.1$

which yield

$$e_0 = 0.57$$

$$S_{r0} = 0.58 \text{ (degree of saturation)}$$

$$u_0 = -1,050 \text{ kPa (pore water pressure)}$$

$$p_0 = 609 \text{ kPa (average effective stress)}$$

$$T_0 = 12^\circ$$

7.3.4 Rock

Hydraulic

The hydraulic conductivity of the rock matrix (and EDZ) is

$$K = 10^{-13} \text{ m/s.}$$

The transmissivity of the activated fractures is

$$T = 5 \cdot 10^{-10} \text{ m}^2/\text{s},$$

which means that for the fracture aperture 2 cm the hydraulic conductivity is $K = 2.5 \cdot 10^{-8} \text{ m/s}$. The corresponding inflow at the geometry used will be about 0.02 l/min per fracture into the open tunnel and about 0.01 l/min per fracture into the open deposition hole.

The rock is modeled to be unsaturated in case of a high suction with the retention curve according to Table 7-1 (see also Figure 3-2).

Table 7-1. Retention curve of the rock with the pore pressure u as a function of the degree of saturation S_r

S_r	u (kPa)
0.01	-20,000
0.1	-10,000
0.2	-9,000
0.3	-8,000
0.4	-7,000
0.5	-6,000
0.6	-5,000
0.7	-4,000
0.8	-3,000
0.9	-2,000
0.99	-1,000
1.0	0

Mechanical

For all rock parts:

$$E = 1,850 \text{ MPa}$$

$$\nu = 0.3$$

Thermal

For all rock parts:

$$\lambda = 3.0 \text{ W/m, K}$$

$$c = 800 \text{ Ws/kg, K}$$

$$\rho = 2,600 \text{ kg/m}^3$$

The hydraulic and mechanical initial conditions are determined by the results of the first step of the calculation, which models the mechanical and hydraulic steady state situation after excavation of the drifts and deposition holes but before installation of buffer and backfill.

$$T_{\theta} = 12^{\circ}$$

7.3.5 Canister

The canister is modelled as a hydraulically impermeable solid with the following mechanical and thermal properties:

$$E = 2.1 \cdot 10^5 \text{ MPa}$$

$$\nu = 0.3$$

$$\rho = 7,000 \text{ kg/m}^3$$

$$\lambda = 200 \text{ W/m, K}$$

$$c = 400 \text{ Ws/kg, K}$$

The power generation in the canister has been modelled with the reference initial power 1,050 W and a power decay with time according to Equation 7-1 /1-1/.

$$P(t) = P_0[c_1 \exp(0.02t) + c_2 \exp(0.002t) + c_3 \exp(0.0002t)] \quad (7-1)$$

where

$P(t)$ = canister power (W)

t = time (years)

P_0 = canister power at deposition = 1,680 W

$c_1 = 0.769$

$c_2 = 0.163$

$c_3 = 0.067$

7.4 Boundary conditions

The outer vertical boundaries of the rock are modelled as symmetry planes, which mean that the model is laterally infinite.

The following boundary conditions are applied to the two outer horizontal rock boundaries:

- Hydraulic: Upper boundary $u = 5,300$ kPa. Lower boundary $u = 4,750$ kPa.
- Thermal: Fixed temperature $T = 12$ °C with a heat transfer coefficient of $h = 10$ W/m², K.
- Mechanical: Vertical displacements locked.

The inner boundaries of the rock to the open tunnel and deposition hole before backfilling are mechanically free and hydraulically applied with a pore water pressure of $u = 0$.

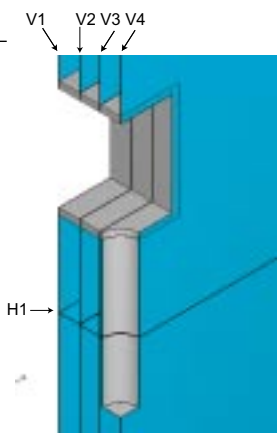
7.5 Calculations

7.5.1 General

Four calculations have been done with different fractures activated but otherwise identical models and calculation sequence as shown in Table 7-2. The activated fractures are fed with water primarily from the upper and lower horizontal boundaries, which act as large fractured zones. The horizontal fracture H1 must thus be fed via the vertical fractures so Case1 with no vertical fracture activated corresponds closely to fracture free rock.

Table 7-2. Overview of performed calculations.

Calculation	Activated fractures	Comment
Case1	H1	Fed with water by the rock matrix
Case2	All	
Case3	V1	
Case4	V1 and H1	H1 fed with water by V1



In cases 1 and 4 all nodes were mechanically locked in order to reduce the calculation time. This yields a small but obvious influence on the wetting history as shown by the comparison between cases 3 and 4 in Section 7.6.6.

7.5.2 Calculation sequence

The calculations were performed in the following steps.

1. Hydraulic and mechanical equilibrium established with empty tunnel and deposition hole.
2. Installation of buffer, canister and backfill.
3. Transient temperature calculation with power generation according to Equation 7-1 and with applied initial conditions of the hydro-mechanical variables.
4. Transient hydro-mechanical calculation with applied temperature according to the results of the temperature calculation.
5. New temperature calculation with the hydro-mechanical variables according to the results of the hydro-mechanical calculation.
6. Comparison of temperature results from the latest temperature calculations.
7. If temperature result disagree the steps are repeated from step 3, otherwise the calculation is complete.

Usually 2–3 hydro-mechanical calculations were performed.

7.6 Results

7.6.1 General

Huge amounts of results are generated. In order to structure the results two types of reporting are done.

1. Contour plots. A variable is plotted with contour lines in a section of the model at a specified time.
2. History plots at scan-lines. A variable is plotted as a function of time along a specified path. The paths used are shown in Figure 7-3.

History plots have only been used for the buffer and the backfill.

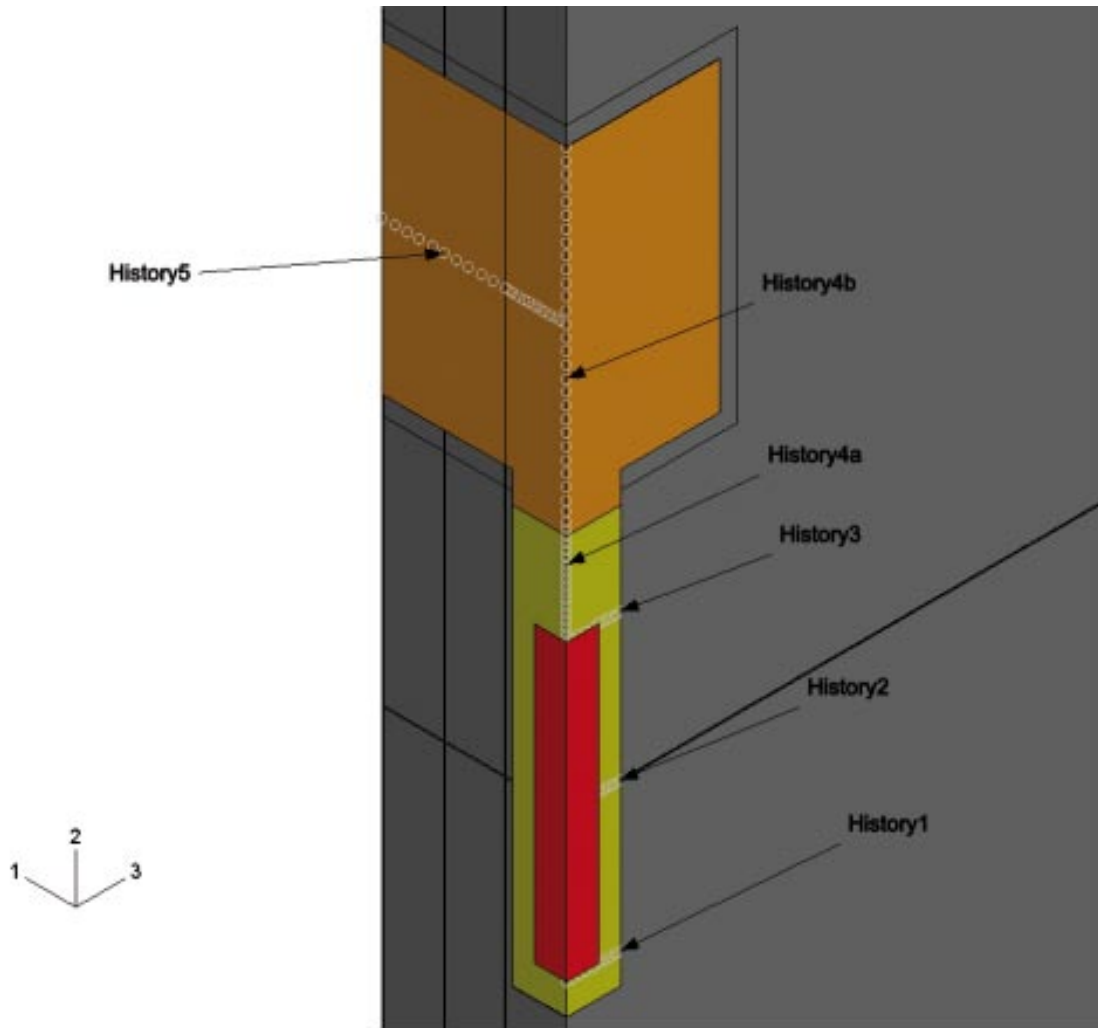


Figure 7-3. Scanlines (paths) used for the history plots.

7.6.2 Summary of results

The results are summarized in Table 7-3. The table shows the time to reach 99% degree of saturation in the buffer at mid-height of the canister, in the entire buffer and in the entire backfill. The column telling the time to 99% saturation of the entire buffer is comparable to column 8 in Table 4-1.

Case 4 yielding 16 years to 99% saturation of the buffer corresponds about to calculation Stress2_3b1_oa in Table 4-1b, which showed 12 years to 99% saturation. The difference is caused by the four main model differences:

1. Difference in initial conditions of the buffer since the 2D calculation assumes that the pellets filled slot was filled with water from start.
2. Difference in initial conditions of the backfill since the 2D calculation Stress2_3b1_oa assumed completely water saturated backfill from start.
3. Difference in hydraulic boundary conditions since the 2D model has a vertical hydraulic boundary surrounding the entire model while the 3D calculation only has a vertical boundary at one side (although closer to the deposition hole).
4. The 3D calculations have only one horizontal fracture while the 2D calculations have two. However the influence of the fracture intersecting the bottom of the deposition hole in the 2D calculations is insignificant on the wetting of the buffer on top of the canister.

Table 7-3. Summary of results. Time until 99% degree of saturation of buffer and backfill.

Case	Activated fractures	Time to 99% degree of saturation			Remarks
		Buffer, mid can.	All buffer	Backfill	
1	H1	62 years	570 years	1,100 years	Wetted through matrix
2	H1, V1–V4	2.4 years	8.6 years	1.0 year	
3	V1	14 years	15 years	3.8 years	
4	H1, V1	4.4 years	16 years	4.4 years	Main case

Case 3 yielding 15 years to saturation of the buffer corresponds about to calculation Stress_3b1_o in Table 4-1a with water saturated backfill from start yielding 99% saturation after 15 years and calculation Stress_3b1_or with no water supply from the backfill yielding 99% saturation after 26 years. Stress_3b1_o and Case 3 yield thus exactly the same time to saturation in spite of the difference in backfill initial conditions. The main reason is that the backfill gets water saturated already after 4 years in case 3 whereupon the conditions are similar. The other differences between the 2D and 3D calculations are thus of minor importance compared to the influence of wetting from the backfill.

The time to 99% saturation of the backfill for Cases 2 and 4 are comparable to Cases ab3 and ab5 of the backfill calculations shown in Table 5-2. Case ab3 with 6 m between the fractures yielded 3 years to saturation which thus can be compared to Case 4 with 4.4 years to 99% saturation. Case ab5 with 1 m between the fractures yielded 0.63 years to saturation which thus can be compared to Case 2 with 1 year to 99% saturation. The longer time for the 3D calculations are probably caused by the difference in hydraulic boundary, since the 3D model has water supply by only horizontal boundaries while the 2D model has water supply by a boundary surrounding the entire model.

7.6.3 Temperature

The temperature calculations have been done in an iterative way as described in Section 7.5.2. The first calculation is done with the initial conditions in the buffer and backfill prevailing during the entire evolution. The following calculations are done with the changed conditions and new thermal properties caused by the water uptake and redistribution. Figure 7-4 shows the final calculated temperature on the canister surface for all four cases and for the first calculation referred to as reference calculation with only initial conditions applied for comparison. The initial conditions yield higher temperature (94°C) due to the low thermal conductivity of the buffer before water uptake. The other cases yield very small difference in maximum temperature (89°C) but an obvious difference before the maximum is reached due to the difference in wetting history. Maximum temperature is reached after about 20 years.

Figure 7-5 shows example of temperature results for case 4. The temperature evolution in the buffer along scan-line 2 (mid-height canister) and the temperature distribution in the entire model after 16 years are shown.

7.6.4 Case 4, main case with two fractures

Case 4 includes two fractures and is used as the main case for these calculations.

Figure 7-6 shows the pore water pressure in the rock after 4 and 16 years. After 4 years there is a substantial negative pore water pressure around the deposition hole but not around the tunnel. The suction of the buffer sucks water from the rock and makes the rock unsaturated according to the retention curve. After 16 years almost the entire rock has returned to hydrostatic pressure except very close to the upper part of the deposition hole.

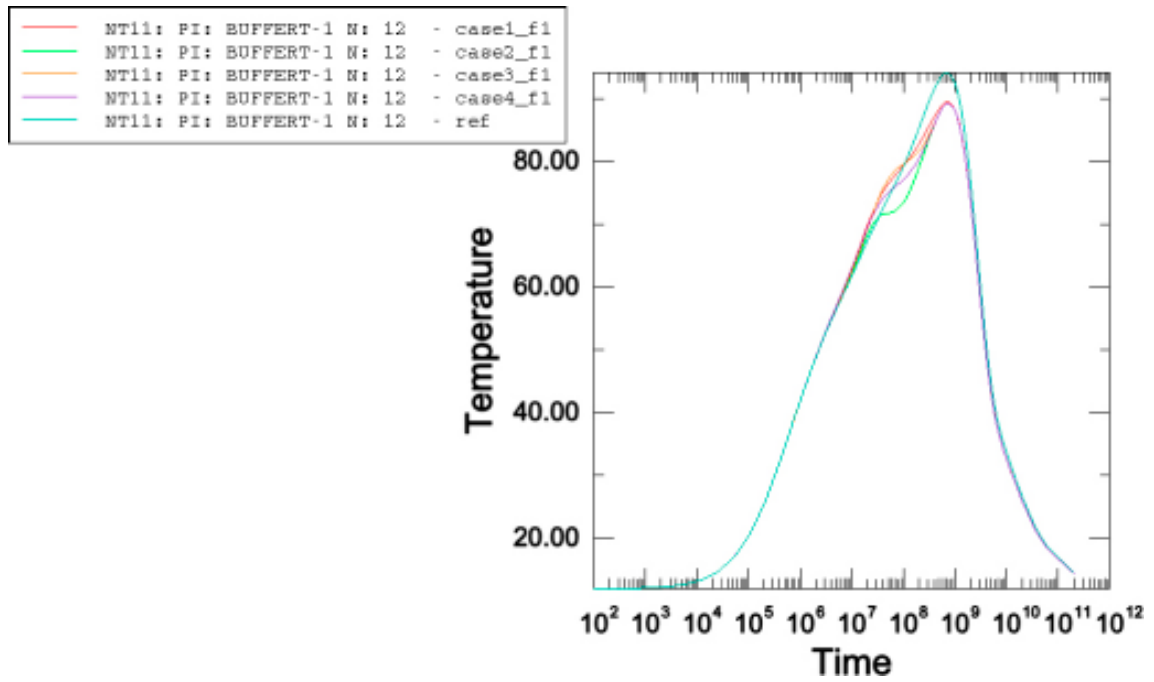


Figure 7-4. Evolution of the temperature on the canister surface mid-height canister for all cases + the reference case with initial conditions prevailing during the entire evolution. Time in seconds.

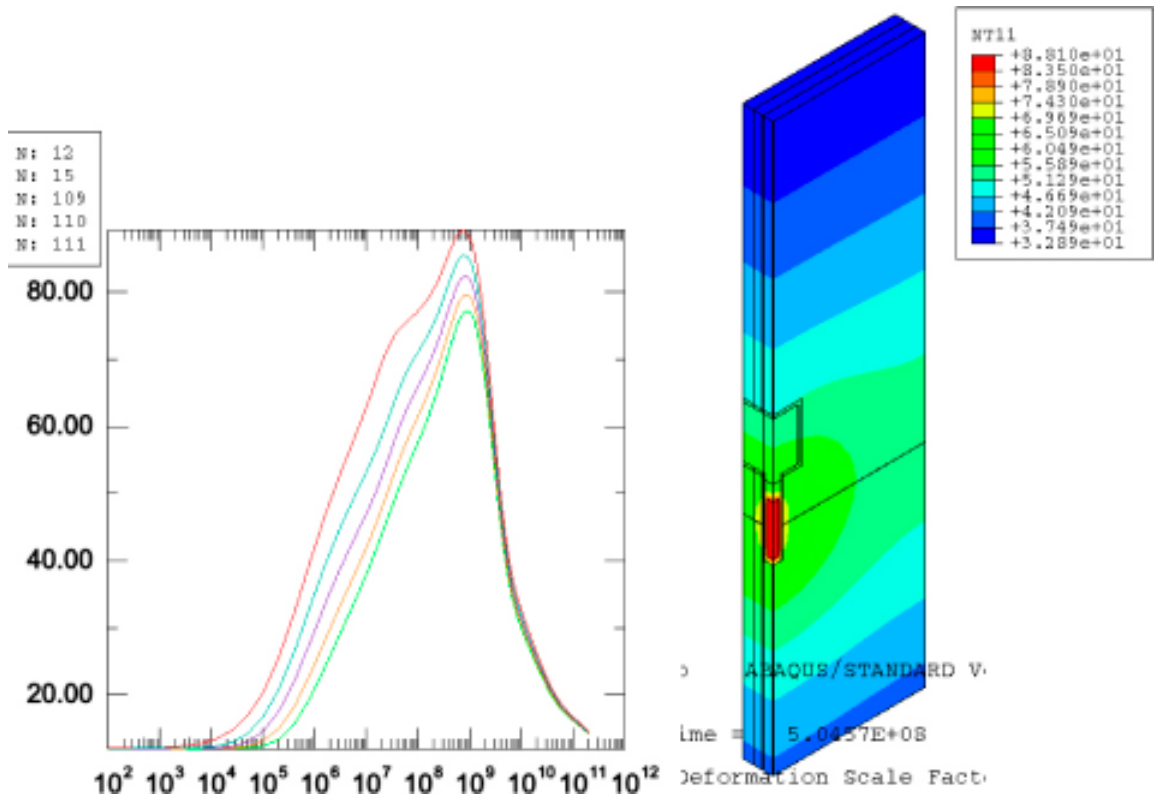
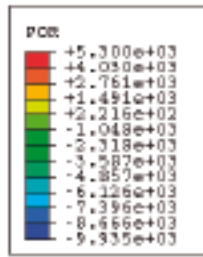


Figure 7-5. Temperature evolution in the buffer along scan line 2 and temperature distribution after 16 years (°C) for Case 4. Time in seconds

Case 4

Pore water pressure in the rock after 4 years (kPa)



Case 4

Pore water pressure in the rock after 16 years (kPa)

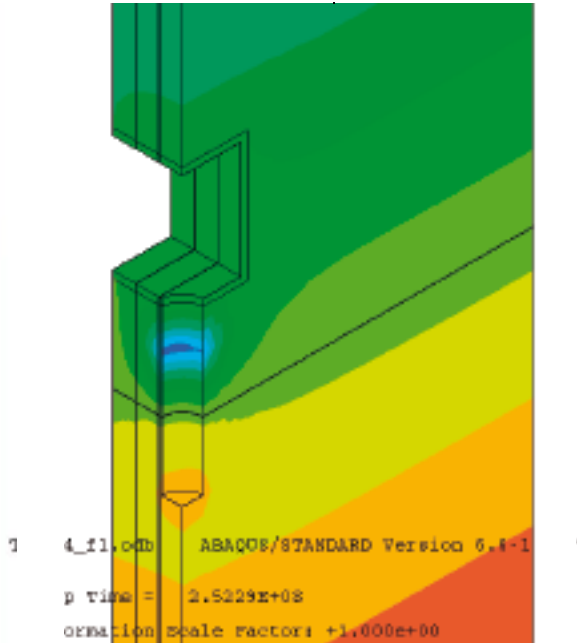
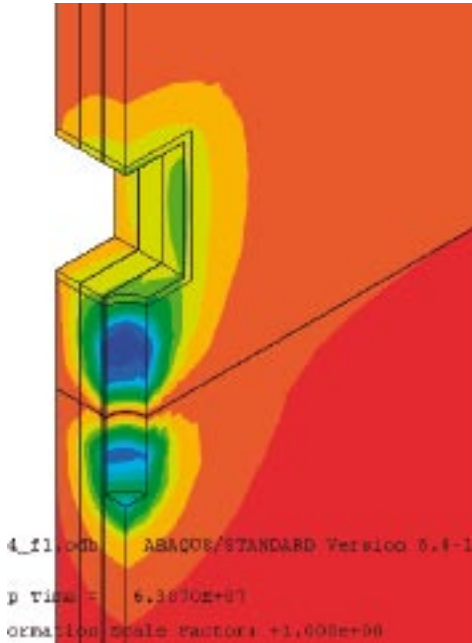
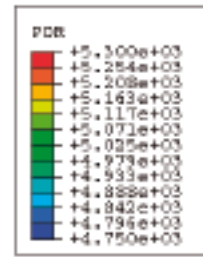


Figure 7-6. Pore water pressure in the rock after 4 and 16 years for case 4.

Figure 7-7 shows the degree of saturation in the buffer and backfill as a function of time for two scan-lines. Along scan-line 3 (on top of the canister) the degree of saturation is strongly reduced to almost 20% at radiuses smaller than the canister. After $4 \cdot 10^8$ seconds or about 13 years the buffer is completely water saturated in that section.

Figure 7-8 show the degree of saturation in the buffer and backfill in contour plots at 6 different times. There is an obvious drying of the buffer close to the canister especially at the end faces of the canister as well as wetting close to the rock fracture in the centre of the hole. There is also a wetting of the upper part of the buffer taking place from the backfill. The wetting of the backfill logically comes from the inner intersecting vertical fracture. The figure also shows that the wetting front of the backfill is steeper than the wetting front of the buffer since the zone of 90–99% degree of saturation (pink colour) is very narrow for the backfill.

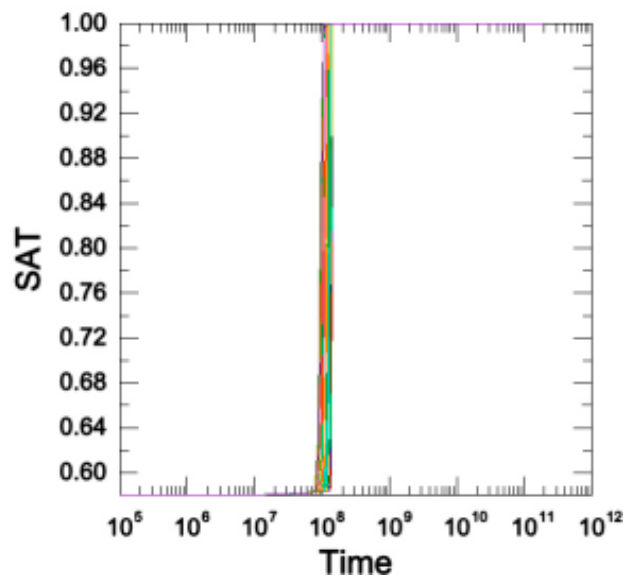
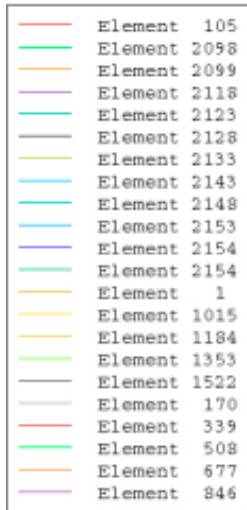
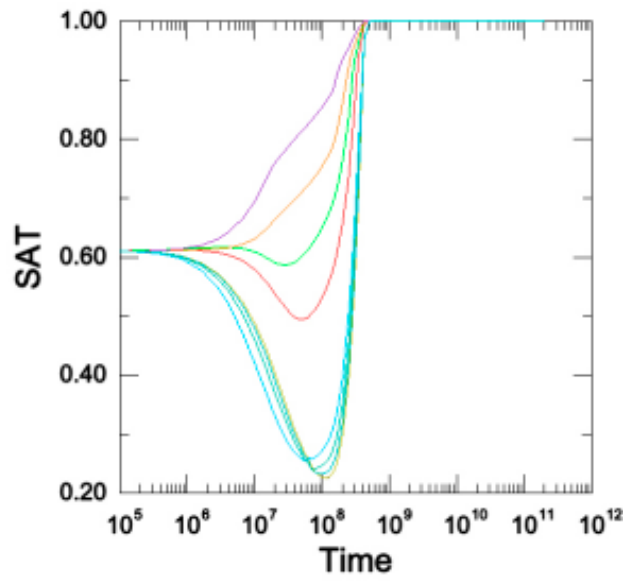
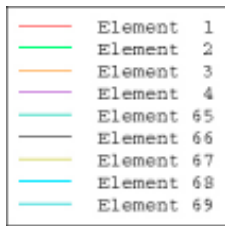


Figure 7-7. Case 4: History plots of the degree of saturation in the buffer at scan-line 3 (upper) and in the backfill at scan-line 5.

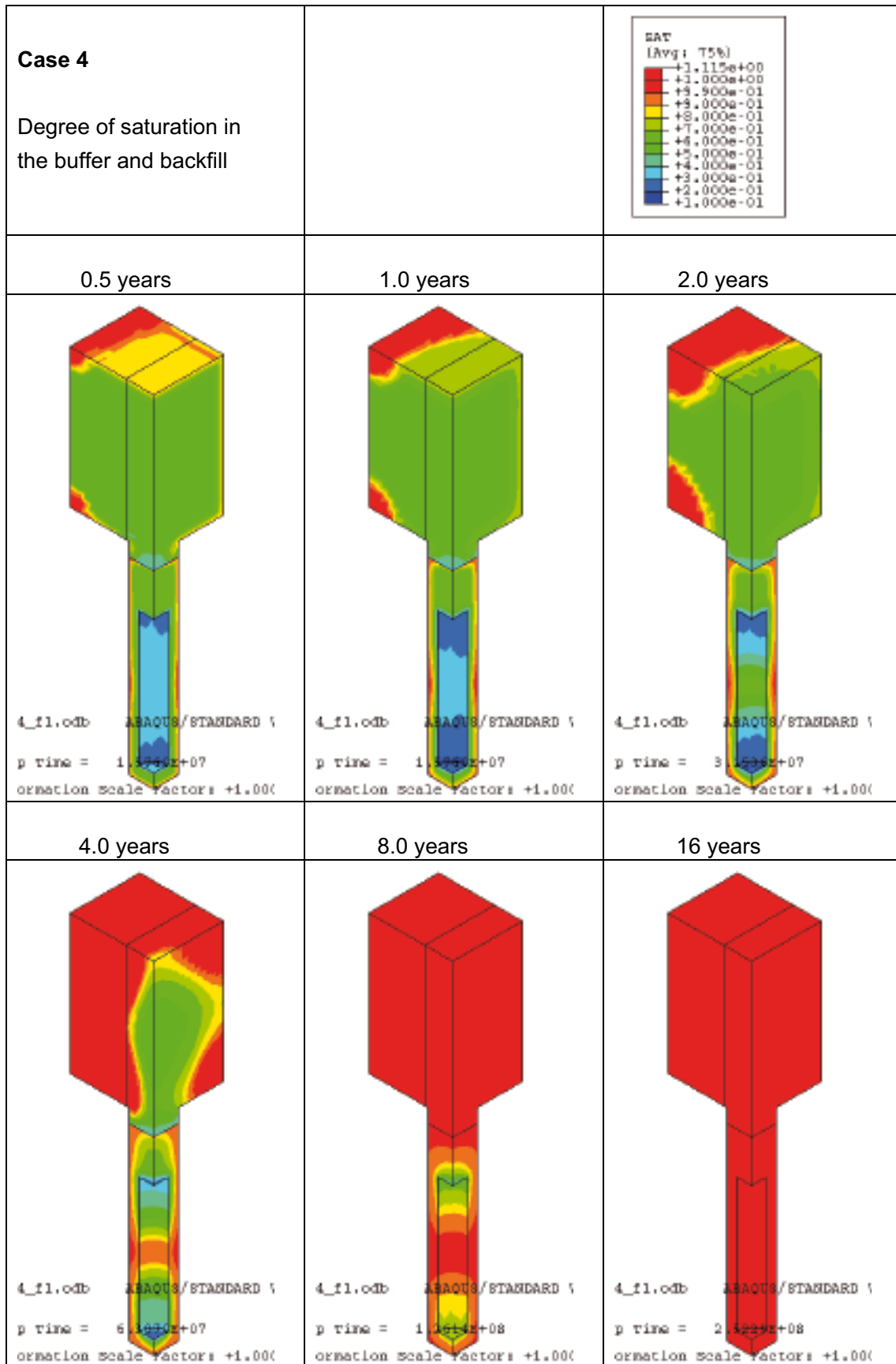


Figure 7-8. Case 4: Degree of saturation in the buffer and backfill after different times.

7.6.5 Cases 1–3

The degree of saturation is shown for the other three cases in Figures 7-9 to 7-16 with the same history and contour plots as case 4.

Case 3, only one vertical fracture

In case 3 only the vertical fracture is activated. The main difference to case 4, which has also a horizontal fracture, is logically a slower wetting of the central part of the buffer in case 3. The history plots in Figure 7-9 show little difference to case 4, but the saturation of the backfill seems to start earlier and have a slightly different history. This difference is also seen in the contour plots in Figure 7-10 where the backfill is completely saturated after 4 years in contrary to case 4. It is surprising that the saturation of the backfill goes slower when an additional fracture is activated. The explanation is that case 4 is calculated with locked displacements while the buffer and backfill are free to move in case 3. The swelling of the buffer causes a compression of the backfill above the deposition hole which yields a lower void ratio and a lower hydraulic conductivity since the hydraulic conductivity is modelled as a function of the void ratio. There is in average in the tunnel above the deposition hole a decrease in void ratio from 0.57 to 0.535, which yields a reduction in hydraulic conductivity with about 20%, which is enough to delay the wetting in the way shown in Figure 7-10. Case 3 was rerun with locked displacements in order to check this conclusion. The results were an identical wetting history of the backfill with case 4.

In addition the water pressure in the vertical fracture that causes the wetting of the backfill (very little water comes through the rock matrix) is lower when there is a horizontal fracture since some of the water from the vertical fracture is used to feed the horizontal fracture and the buffer material. Figure 7-11 shows the pore pressure distribution in the two fractures after 4 years. The pore pressure is higher in case 3 than in case 4 but the effect of this is smaller compared to the effect of the reduced hydraulic conductivity.

Case 2, all five fractures

In case 2 all five fractures are activated (Figures 7-12 and 7-13). The additional vertical fractures have an obvious and logical influence on the wetting rate of both the buffer and the backfill.

Case 1, only horizontal fracture with no water supply

In case 1 only the horizontal fracture is activated so the water has to be transported through the rock matrix to the horizontal fracture or directly to the barriers so the wetting is very slow as shown in Figures 7-14 to 7-16.

The wetting of the buffer is rather fast up to 10^9 seconds or about 32 years, when the entire buffer is saturated to almost 95%. The final 5% takes very long time to saturate and the entire buffer is 99% saturated after 570 years. The main reason for the extreme slow down is the strong de-saturation of the rock around the deposition hole, which reduces the hydraulic conductivity of the rock matrix substantially.

The wetting of the backfill is also very slow due to the large volume of water that has to pass the rock matrix before the backfill is saturated. There is also some de-saturation of the rock around the tunnel that slows down the wetting.

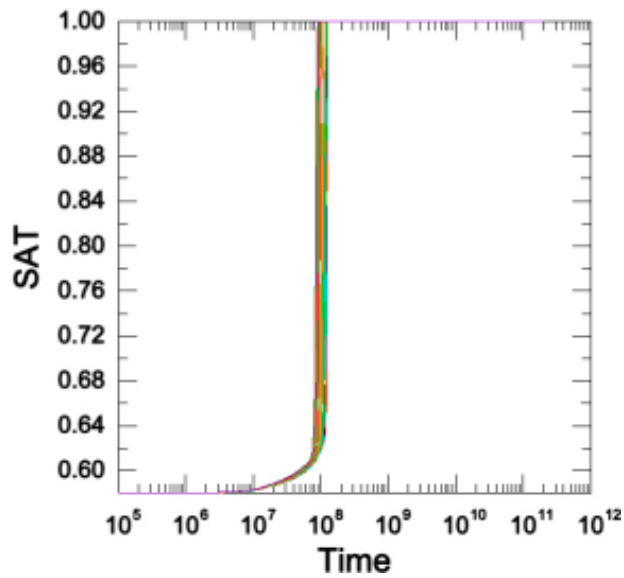
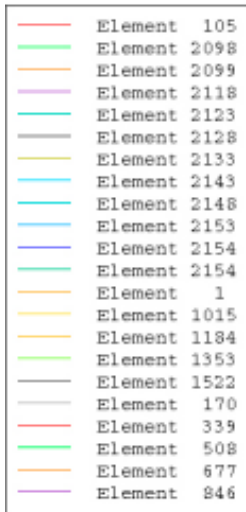
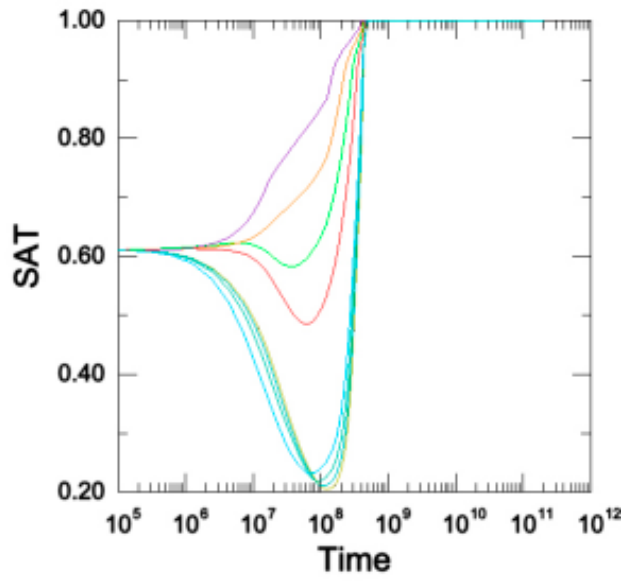
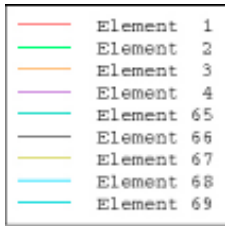


Figure 7-9. Case 3: History plots of the degree of saturation in the buffer at scan-line 3 (upper) and in the backfill at scan-line 5.

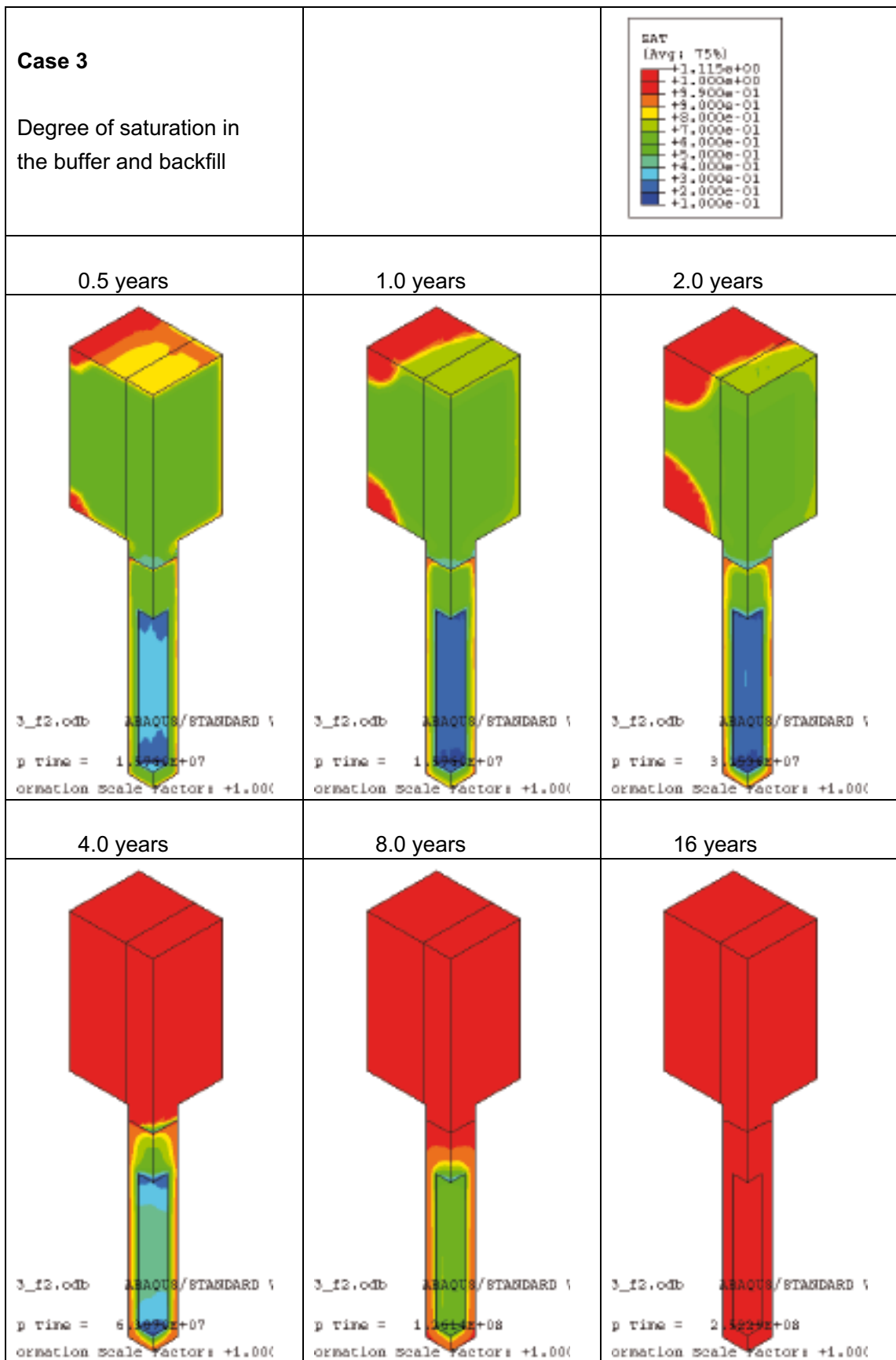


Figure 7-10. Case 3: Degree of saturation in the buffer and backfill after different times.

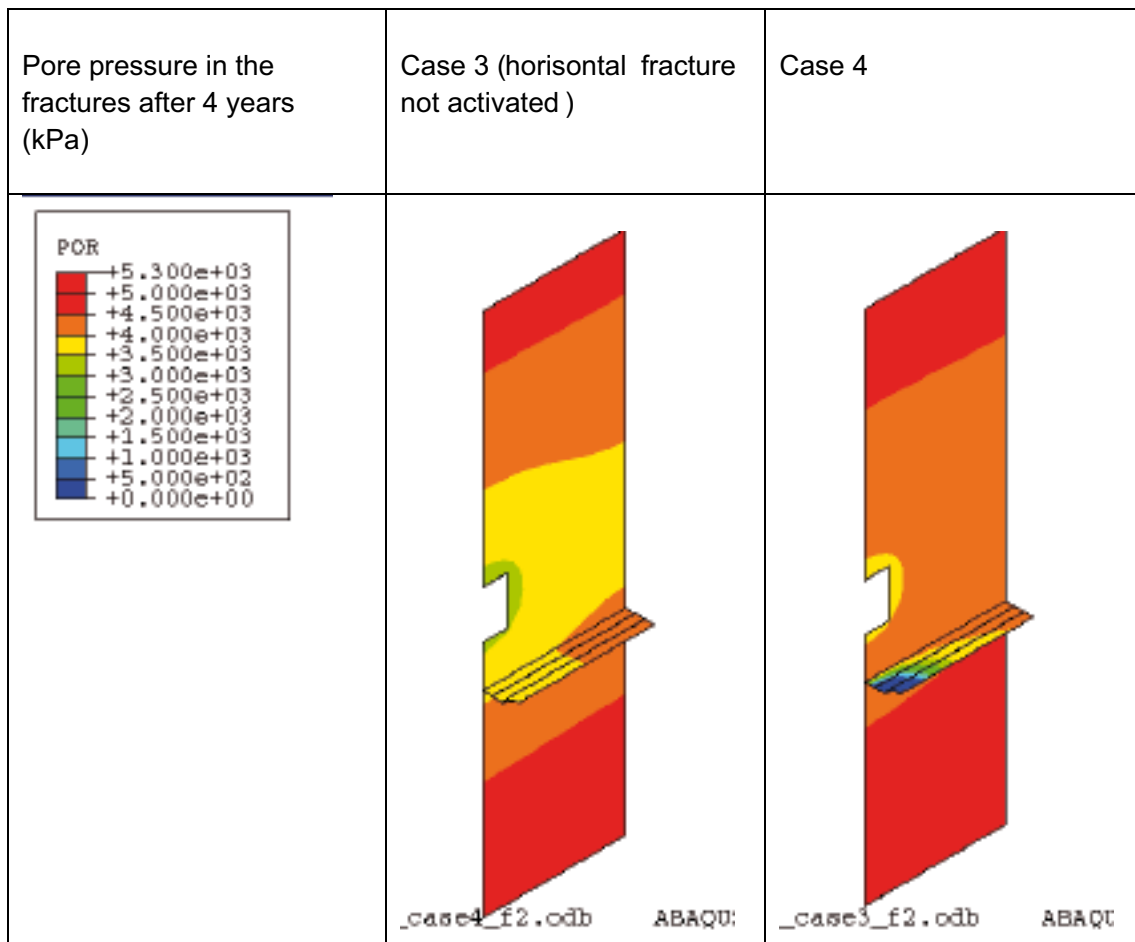


Figure 7-11. Pore pressure distribution in the fractures after 4 years in cases 3 and 4.

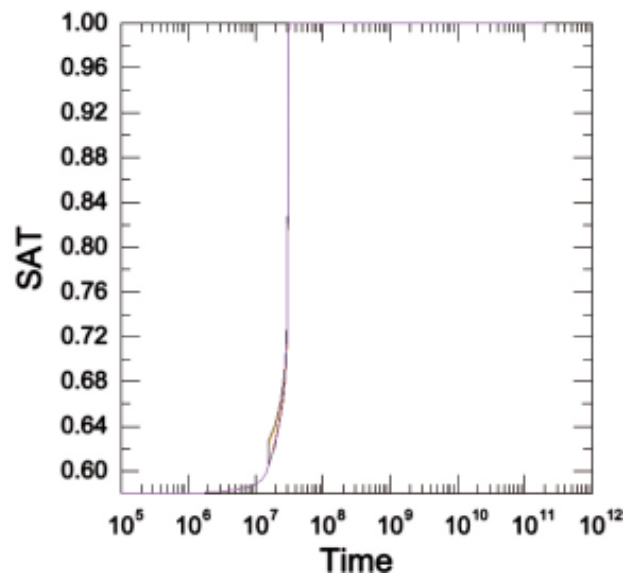
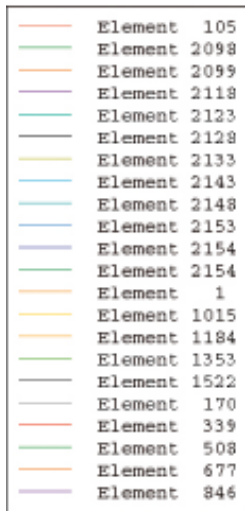
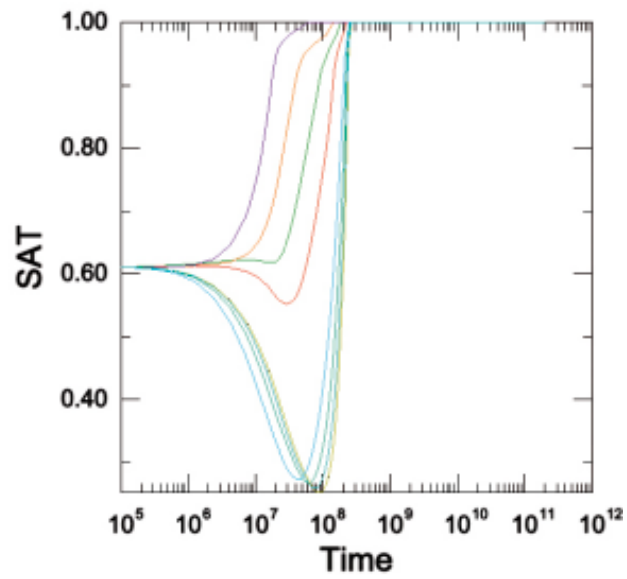
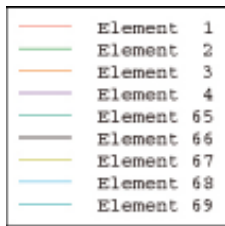


Figure 7-12. Case 2: History plots of the degree of saturation in the buffer at scan-line 3 (upper) and in the backfill at scan-line 5.

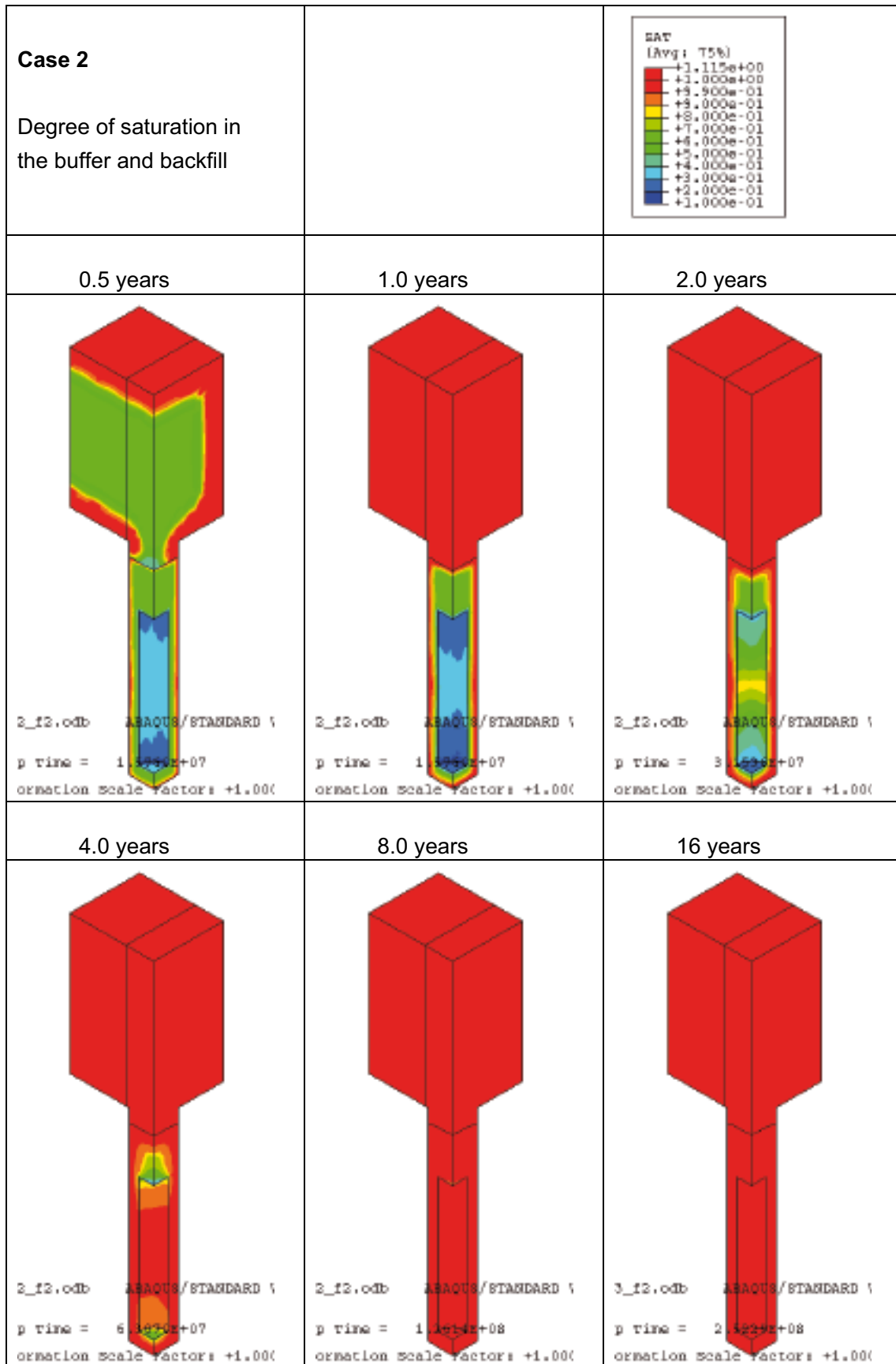


Figure 7-13. Case 2: Degree of saturation in the buffer and backfill after different times.

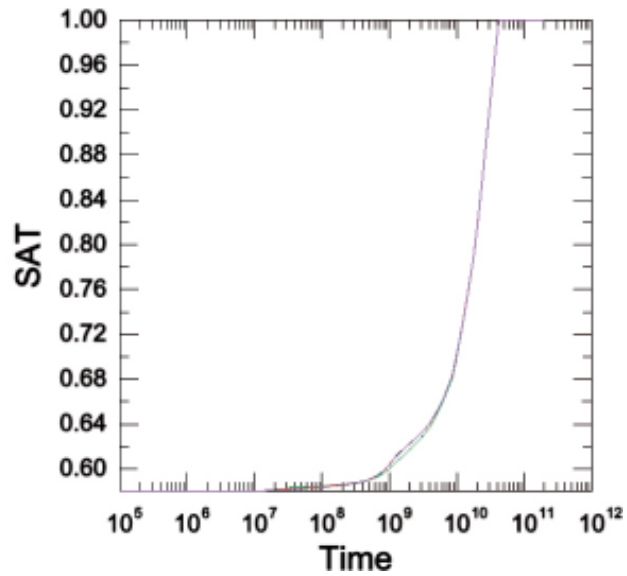
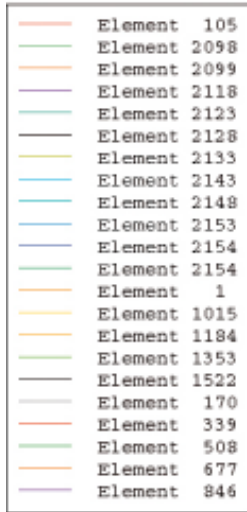
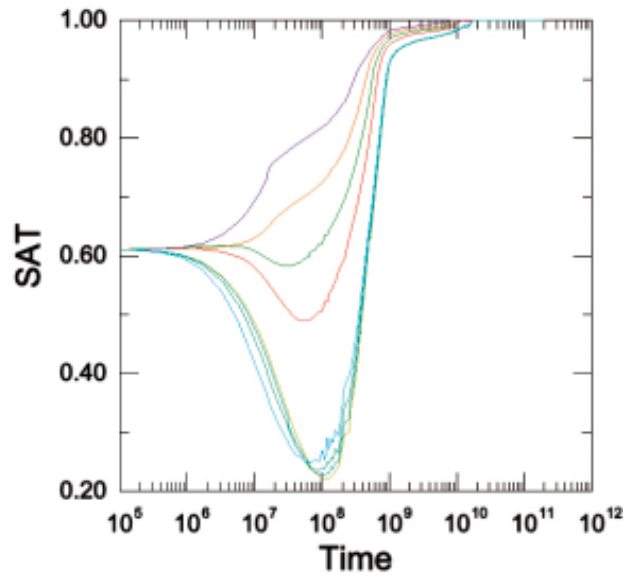
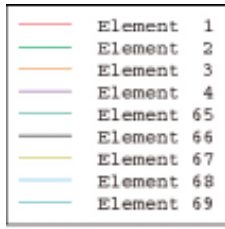


Figure 7-14. Case 1: History plots of the degree of saturation in the buffer at scan-line 3 (upper) and in the backfill at scan-line 5.

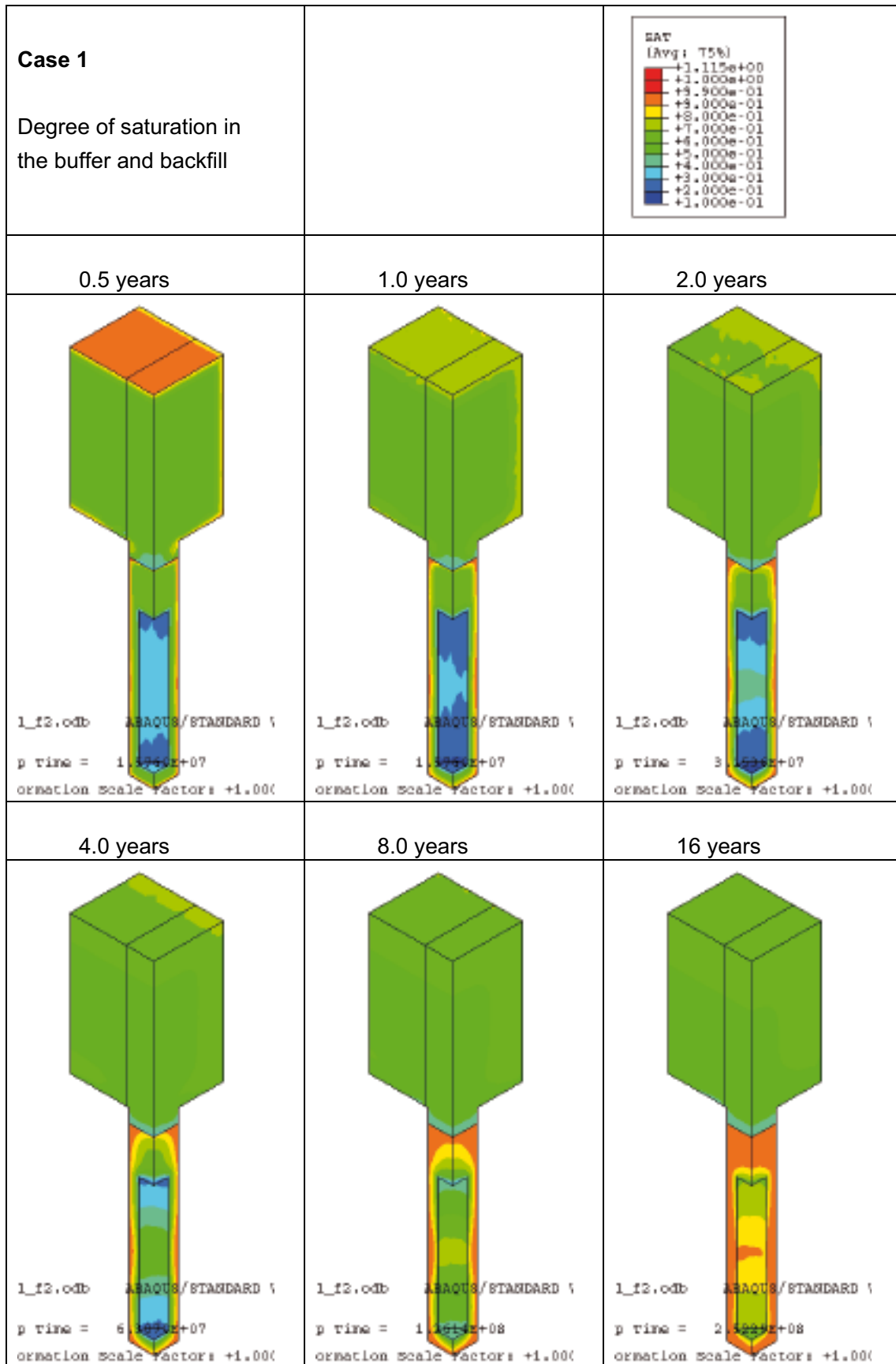


Figure 7-15. Case 1: Degree of saturation in the buffer and backfill after different times (0.5–16 years).

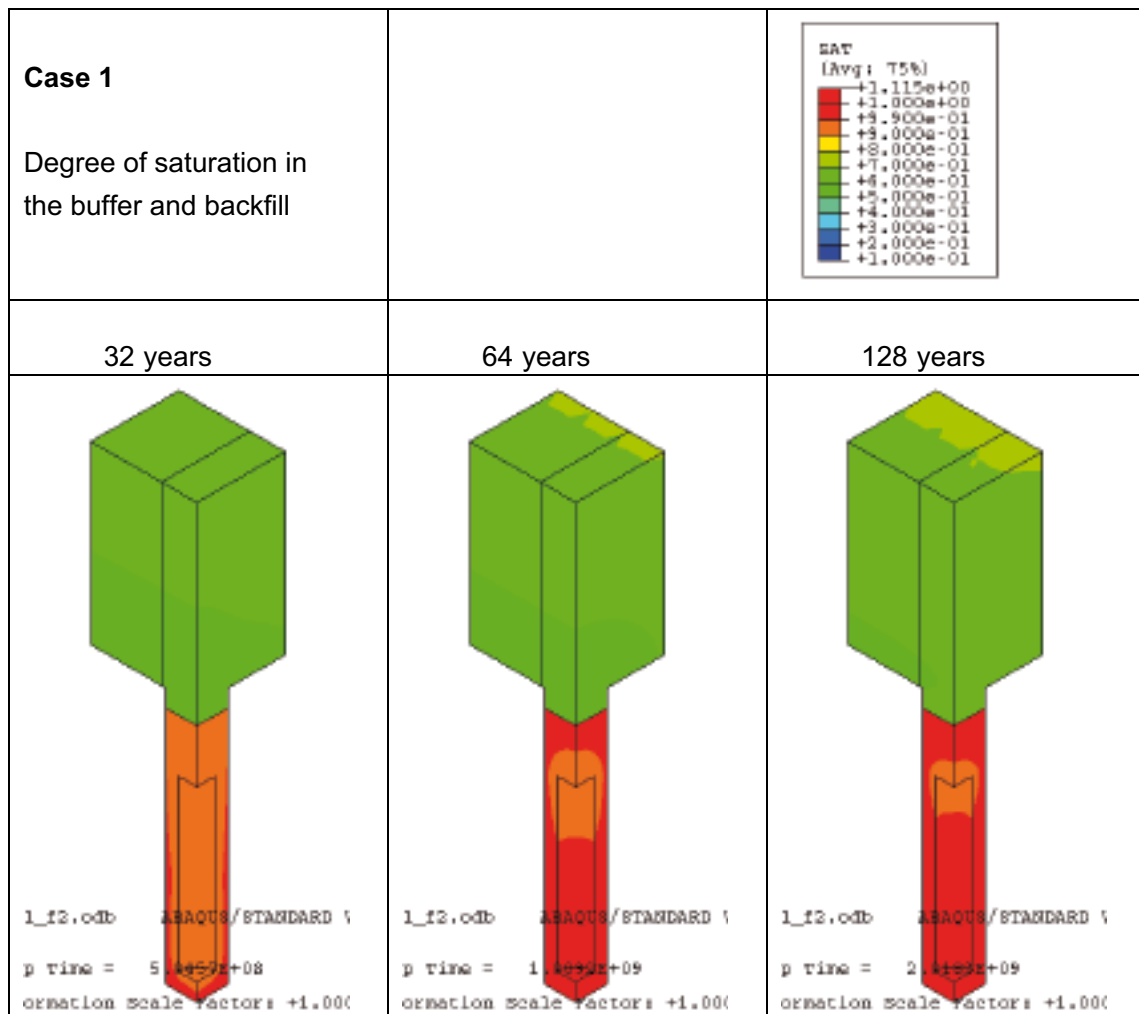


Figure 7-16. Case 1: Degree of saturation in the buffer and backfill after 32–128 years.

7.6.6 Mechanical results

The calculations also included mechanical response although all nodes were locked in cases 1 and 4 in order to reduce the calculation time. The mechanical results are not of primary interest for this study and will not be shown with exception of Figure 7-17, where the vertical displacements in the buffer and backfill for case 2 after full saturation are plotted in two contour plots with different displacement scales. The maximum upwards swelling is about 10 cm in the centre of the buffer/backfill interface. The figure also shows that almost the entire backfill is subjected to upwards swelling of more than 1 mm.

7.7 Conclusions

Four complete thermo-hydro-mechanical 3D modelling examples of the wetting of the buffer and backfill in a large repository have been done. The results show how the buffer, backfill, rock matrix and rock fractures interact during the wetting process. The results largely confirm the conclusions from the earlier 2D calculations. Using the low standard value for the hydraulic conductivity of the rock matrix (10^{-13} m/s) the influence of the wetting from the backfill is significant when there is no fracture intersecting the deposition hole close the upper lid of the canister.

Case 2

Displacements (m) after full saturation and homogenization

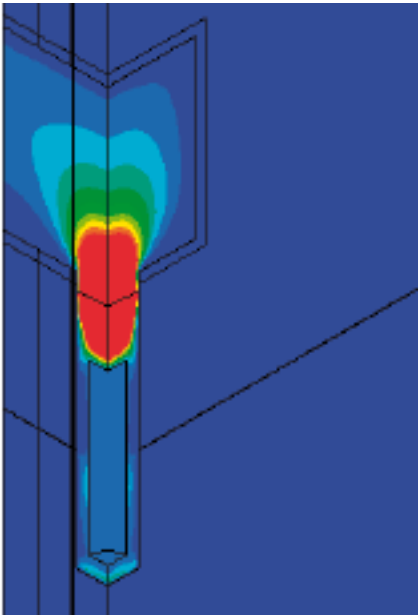
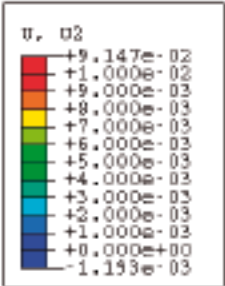
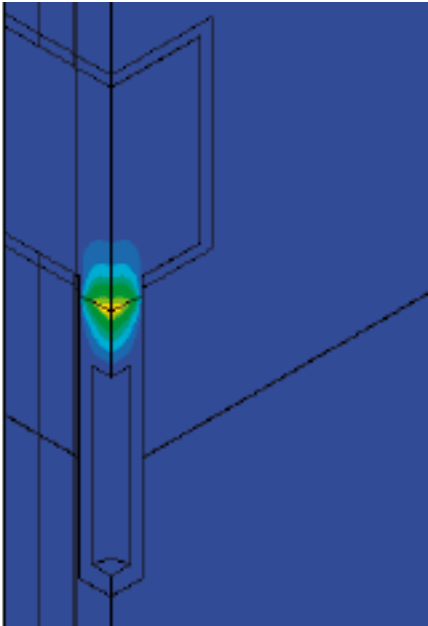
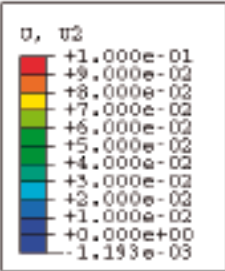


Figure 7-17. Displacements in the buffer and backfill after full saturation. Observe the difference in scale. 1 cm between contour lines in the upper figure and 1 mm between contour lines in the lower figure.

8 Comments and conclusions

The following set of calculations has been performed:

1. Investigation of the influence of the backfill properties and wetting conditions on the water saturation phase of the buffer with the old FEM-model used in earlier wetting calculations for SR-97. The old calculations have been updated regarding the influence of the backfill.
2. Influence of the rock conditions on the wetting phase of the backfill in the deposition tunnels for three different backfill types.
3. Influence of having entrapped air on the wetting phase of the backfill in the deposition tunnels. These calculations have been done with Code Bright with a material model that includes the air phase.
4. Finally complete hydraulic interaction between rock, buffer and backfill has been modelled with a 3D model that simulates an infinite repository intersected by rock fractures. Four rock fracture configurations have been modelled

The conclusions of each set of calculations are summarized at the final section of each chapter. The overall conclusions regarding the influence of the backfill conditions and saturation process on the wetting of the buffer will instead be discussed.

The first type of calculations shows that wetting from the backfill is only significant when the rock is rather dry. The saturation time of the buffer for a rock with a matrix hydraulic conductivity of 10^{-13} m/s is reduced with a factor of about 2 when water is freely available from the backfill compared to when no water is available. In reality the difference is even less in the case of 30/70 backfill since the initial water content of that backfill also feeds the buffer with water.

The difference between 30/70 and Friedland Clay is large regarding the possibility of the backfill to supply water mainly due to the difference in suction but partly also due to the difference in hydraulic conductivity.

Regarding 30/70 backfill the initial pore pressure is $-1,050$ kPa, which can be compared to $+5,000$ kPa when full saturation and full water pressure is acting. There is thus an assistance and wetting from the backfill even if it is not saturated. Thus, not even the combination of a deposition hole without intersecting fractures and a tunnel with strongly fractured rock will influence the wetting time of the buffer very much and not more than a factor 1.5–2. The extreme conditions with completely dry rock in the deposition hole and only the initial water in the backfill available (that took 2,000 years for equilibrium) will not occur since the 30/70 backfill will in all foreseen rock conditions be saturated within 100 years.

Regarding Friedland Clay the influence is stronger since the initial suction of the backfill is much higher and the backfill will not supply the buffer with water unless wetted by the rock. The backfill may even partly dry the buffer at very dry conditions since the time to a high degree of saturation and the resulting reduction in suction of the backfill may be more than 100 years. However, even for the extreme conditions with completely dry rock in the deposition hole the backfill will be wet enough within a couple of hundred years in order to prevent a far advanced drying of the buffer and instead lead to wetting.

The influence of entrapped gas is only important in respect of delaying the wetting when the rock is permeable and thus only when the backfill is saturated early. The influence of entrapped gas is thus not important for the wetting of the buffer. On the other hand this conclusion is only valid when very little gas is solved in the ground water.

The 3D calculations of four different fracture configurations show how the buffer, backfill, rock matrix and rock fractures interact during the wetting process. The results largely confirm the results from the earlier 2D calculations.

References

- /1-1/ **Börgesson L, Hernelind J, 1999.** Coupled thermo-hydro-mechanical calculations of the water saturation phase of a KBS3 deposition hole – influence of hydraulic rock properties on the water saturation phase. SKB TR-99-41. Svensk Kärnbränslehantering AB.
- /3-1/ ABAQUS manuals. ABAQUS Inc.
- /3-2/ **Börgesson L, Johannesson L E, Sandén T, Hernelind J, 1995.** Modelling of the physical behaviour of water saturated clay barriers. Laboratory tests, material models and finite element application. SKB Technical Report TR 95-20, Svensk Kärnbränslehantering AB..
- /3-3/ **Börgesson L, Fredriksson A, Johannesson L E, 1994.** Heat conductivity of buffer materials. SKB Technical Report TR 94-29. Svensk Kärnbränslehantering AB.
- /3-4/ **Cimne, 2002.** Code Bright. Ver. 2.2. Users manual. Departamento de Ingenieria del Terreno, Cartografica y Geofísica, UPC, Barcelona.
- /3-5/ **Olivella S A, Gens J, Carrera, E E Alonso, 1996.** Numerical formulation for a simulator (CODE_BRIGHT) for the coupled analysis of a saline media. Engineering Computations, 13, No. 7, pp 87–112.
- /5-1/ **Börgesson L, Hernelind J, 1998.** Preparatory modelling for the backfill and plug test – Scoping calculations of H-M processes. SKB ÄHRL International Progress Report IPR-99-11.
- /5-2/ **Börgesson L, Hernelind J, 2000.** Prototype Repository. Preliminary modelling of the water-saturation phase of the buffer and backfill materials. SKB ÄHRL IPR-00-11.
- /5-3/ **Johannesson L E, Börgesson L, 2002.** Laboratory tests on Friedland Clay. Friedland Clay as backfill material. Results of laboratory tests and swelling compression calculations. ÄHRL IPR-02-50.
- /5-4/ **Johannesson L E, Nilsson U, 2006.** Geotechnical behaviour of candidate backfill materials for the deep repository. Laboratory tests and calculations for determining the performance of the backfill. SKB report in print.